1-1-2006

Vehicle dynamics controller for a hybrid electric vehicle.

Edward Won Kyun Oh
University of Windsor

VEHICLE DYNAMICS CONTROLLER

FOR

A HYBRID ELECTRIC VEHICLE

by

Edward Won Kyun Oh

A Thesis
Submitted to the Faculty of Graduate Studies and Research
Through the Department of Mechanical,
Automotive, and Materials Engineering in
Partial Fulfillment of the Requirements for the
Degree of Master of Applied Science at the
University of Windsor

Windsor, Ontario, Canada
2006

© 2006 Edward W.K. Oh

Library and
Archives Canada

Published Heritage
Branch

395 Wellington Street
Ottawa ON K1A 0N4
Canada

Bibliothèque et
Archives Canada

Direction du
Patrimoine de l'édition

395, rue Wellington
Ottawa ON K1A 0N4
Canada

NOTICE:
The author has granted a non-
exclusive license allowing Library
and Archives Canada to reproduce,
publish, archive, preserve, conserve,
communicate to the public by
telecommunication or on the Internet,
loan, distribute and sell theses
worldwide, for commercial or non-
commercial purposes, in microform,
paper, electronic and/or any other
formats.

The author retains copyright
ownership and moral rights in
this thesis. Neither the thesis
nor substantial extracts from it
may be printed or otherwise
reproduced without the author's
permission.

AVIS:
L'auteur a accordé une licence non exclusive
permettant à la Bibliothèque et Archives
Canada de reproduire, publier, archiver,
sauvegarder, conserver, transmettre au public
par télécommunication ou par l'Internet, prêter,
distribuer et vendre des thèses partout dans
le monde, à des fins commerciales ou autres,
sur support microforme, papier, électronique
et/ou autres formats.

L'auteur conserve la propriété du droit d'auteur
et des droits moraux qui protège cette thèse.
Ni la thèse ni des extraits substantiels de
celle-ci ne doivent être imprimés ou autrement
reproduits sans son autorisation.

In compliance with the Canadian
Privacy Act some supporting
forms may have been removed
from this thesis.

While these forms may be included
in the document page count,
their removal does not represent
any loss of content from the
thesis.

Conformément à la loi canadienne
sur la protection de la vie privée,
quelques formulaires secondaires
ont été enlevés de cette thèse.

Bien que ces formulaires
aient inclus dans la pagination,
il n'y aura aucun contenu manquant.

Canada

ABSTRACT

In hybrid electric vehicles, when an uncontrolled electric motor torque is applied in regenerative braking or torque-assist accelerating, vehicle instability may occur from the loss of tire forces due to the road friction conditions. This can result in the loss of vehicle steer-ability and/or the lost traction in driving situations. The research objective is safely integrating the hybrid system operations of a prototype design, in order to achieve the safe lateral dynamic behaviour for various driving conditions.

By developing a vehicle dynamics controller (VDC) which employs the linear bicycle model as its estimator, the objective was achieved. Vehicle dynamics co-simulation was conducted to analyze the prototype's non-linear vehicle response while validating the linear controller performance. Implementation design of VDC entailing the X-by-wire, data acquisition, and microcontroller technology was considered. The developed VDC reduces the driver's steer control effort and prevents the incipient vehicle instability in all driving conditions.

iii

To my parents who have taught me to explore, observe, and discover without boundaries.
And to my brother, Andrew.

ACKNOWLEDGEMENTS

TABLE OF CONTENTS

LIST OF TABLES

LIST OF FIGURES

NOTATION

Label	Description
$\vec{a}$	resultant acceleration
A	front wheel base distance from centre of gravity of vehicle
a_x	acceleration along x-axis, in a body fixed system
a_y	acceleration along y-axis, in a body fixed system
a_{y_CarSim}	*CarSim* simulation result of acceleration along y-axis, in a body fixed system
$a_{y\_measured}$	measured acceleration along y-axis, in a body fixed system
$a_{y\_nominal}$	nominal acceleration along y-axis, in a body fixed system
a_{y_Ratio}	ratio of lateral acceleration comparison along y-axis, in a body fixed system
ABS	anti-lock braking system
AC	alternating current
AWD	all wheel drive system
B	rear wheel base distance from centre of gravity of vehicle
C_α	tire cornering coefficient
C_D	coefficient of drag
C_f	front tire cornering coefficient
C_r	rear tire cornering coefficient
CAN	controller area network
CD	charge depleting
CG	centre of gravity
CS	charge sustaining
CW	clockwise direction
CCW	counter-clockwise direction
DAQ	data acquisition system
DSP	digital signal processor
ECU	electronic control unit
ESC	electronic stability control
EM	electric machine
f_n ; n = 1,2,3 ...	input current frequency
F	force
$\vec{F}$	resultant force vector
F_f	forces of front two tires
F_r	forces of rear two tires
F_x	force along x-axis, in a body fixed system

F_y	force along y-axis, in a body fixed system
F_z	force along z-axis, in a body fixed system
G	gravitational acceleration unit
HEV	hybrid electric vehicle
I_{zz}	moment of inertia along z-axis, in a body fixed system
ICE	internal combustion engine
ISO	international standard organization
L1, R1, L2, R2	front-left, front-right, rear-left, rear-right
M	mass
M_{y_brk}	brake moment applied at a wheel
M_z	moment along z-axis, in a body fixed system
OEM	original equipment manufacturer
P	rotational velocity along x-axis, in a fixed body system
PCI	programmable communication interface
Q	rotational velocity along y-axis, in a fixed body system
$\dot{r}$	rotational acceleration along z-axis, in a body fixed system
R	rotational velocity along z-axis, in a body fixed system
r_d	dynamic effective rolling radius of tire
$r_{measured}$	measured rotational velocity along z-axis, in a body fixed system
SAE	society of automotive engineers
SOC	state of charge
T, τ	torque
T_{EM}	torque of electric machine
TCS	traction control system
u	linear velocity along x-axis, in a body fixed system
$\dot{v}$	linear acceleration along y-axis, in a body fixed system
V	linear velocity along y-axis, in a body fixed system
VDC	vehicle dynamics controller
α	tire slip angle, rotational acceleration
α_f	front tire slip angle
α_r	rear tire slip angle
$\dot{\beta}$	rate of change of body slip angle along z-axis, in a body fixed system
B	body slip angle along z-axis, in a body fixed system
β_{BM}	body slip angle of bicycle model along z-axis, in a body fixed system
β_{CarSim}	body slip angle of *CarSim* simulation model along z-axis, in a body fixed system
δ_f	front wheel steer angle
δ_r	rear wheel steer angle
δ_{SW}	steering wheel angle
δ_{Wheel}	wheel steer angle
Λ	wheelslip ratio
M	Coulomb coefficient of friction, micro
Σ	summation symbol

Ω	rotational velocity
ω_{EM}; n = 1,2,3 ...	rotational velocity of electric machine rotor
ω_{sn}; n=1,2,3 ...	synchronous rotational velocity of electric machine rotor

CHAPTER 1

INTRODUCTION

1.1 AUTO21 Project E03 Executive Summary

AUTO21, a part of Network of Centres of Excellence (NCE), is a Canadian government and industry funded research organization head-quartered at the University of Windsor. Currently there are over 40 AUTO21 projects that are active across Canada and Project E03 is a part of Theme E- Design Process, where its main focus is developing Highly Qualified Personnel (HQP) for automotive industry. Another part of the mandate is to involve industry sponsors to increase the project profile with technical relevancy.

AUTO21 Project E03 involves three Canadian universities (University of Windsor, University of Waterloo and University of British Columbia) collaborating on "Regenerative Braking Technology using Ultracapacitors for Hybrid Electric Vehicles". The following table summarizes the research team breakdown.

1

Table 1.1 Project E03 research personnel and focus breakdown

	U of Windsor	U of Waterloo	UBC
Graduate Students	E. Oh, N. Nantais R. Rieveley S. Draca (All Mechanical)	S. Samborsky (Mechanical) C. Mendes (Mechanical) Dr. M. Marei (Electrical) M. Wei (Electrical)	K. Wicks (Electrical)
Focuses	Vehicle dynamics control/ Vehicle hybridization/ Data Acquisition	Hybrid system control and energy management/ Regenerative braking integration/ Power electronics and control	Switch Reluctance Motor (SRM) development for rear drivetrain hybridization

A preliminary hybrid component design was completed via *ADVISOR* simulation and a 1/100th scale hybrid system bench testing was validated. [1] DAIMLERCHRYSLER Canada has donated a test-bench vehicle (*Pacifica*) for the hybrid prototype development. For Phase I project development, the team is working on hybridizing the *Pacifica* with an AC induction motor (front drivetrain) and ultracapacitor pack. For Phase II, a switch-reluctance motor (rear drivetrain) and battery pack implementation is planned.

1.2 Research Motivation

The research goal is to develop an active safety system for the prototype hybrid electric vehicle that was converted from a production *Chrysler Pacifica*. Depending on the powertrain and drivetrain configurations of a hybrid vehicle, the hybrid system operation may adversely affect the vehicle stability. In the case of a parallel hybrid system, where an electric motor is connected through the drivetrain, it requires safely integrating the regenerative braking function with the anti-lock braking system in order to achieve optimal braking performance. As well, the drive torque assist function needs to be controlled in order to prevent wheelspin caused by the excessive torque output of the hybrid system. Consequently, in this system, a supervisory

control system is necessary to provide unobtrusive hybrid operations during various vehicle manoeuvres in order to maintain the vehicle stability.

1.3 Thesis Synthesis

A hybrid electric vehicle (HEV) drivetrain can have unique effects on the vehicle dynamics, rooted in its component design/schematic layout. As the electric motor provides both additional driving and braking torques to the existing internal combustion engine (ICE) and brake system, it becomes a secondary control system of the vehicle powertrain and brake system. The location of the motor with respect to the path of torque delivery is the determinant in affecting the vehicle dynamics, both in handling and ride. Pre-transaxle or post-transaxle location of the electric motor (from the drivetrain perspective) has distinct functional effects to the overall system (vehicle).

The challenge with the hybrid *Pacifica* prototype design is that the electric motor is placed behind the transaxle so the motor torque is delivered from after the front transaxle. Therefore, the electric motor torque is equally shared by the front two wheels via half-shafts. This means that whenever the electric motor is activated, the drive or braking torque is equally transmitted by the front two wheels simultaneously. This creates an undesirable phenomenon where wheel traction control is impossible at low-μ conditions (low traction) during the electric motor activation.

Wheel traction is what delivers the drive torque from the powertrain or brake torque from the brake system to the road. When the wheel traction is lost at a wheel, the longitudinal and lateral force at the tire are reduced to the tire's limit and the driver's steer input is no longer effective for vehicle steering. This is represented by spinning wheels in acceleration or skidding wheels in braking in which case the vehicle does not move forward or slow down with any steer-

3

ability. In the case of the proposed prototype design, the regenerative braking (charge sustaining function) mode or the drive torque assist (charge depleting function) mode of the hybrid operation introduces the vehicle instability if the hybrid operation is not controlled.

This is the reason why the anti-lock braking system (ABS), traction control system (TCS), and electronic stability control (which uses both ABS and TCS) systems are developed to help maintain vehicle stability on conventional vehicles. Since the individual wheel braking is not possible by the inherent design, the underlying principle of this thesis is developing a system which controls the regenerative braking and drive torque assist functions of the hybrid system while maintaining the vehicle stability.

The main system design concept is derived from conventional original equipment manufacturer (OEM) system architectures. BOSCH's vehicle dynamics control (VDC[1]) system is the first to be introduced in the industry and it has been used by many automobile OEM's since the early 1990's. [2] An active supervisory controller is needed to ensure the vehicle brakes safely with the ABS function while maximizing the charge sustaining efficiency by allowing regenerative braking at all possible situations. The same controller can be utilized to control drive torque assist (charge depleting) to help accelerating the vehicle per driver request while ensuring the vehicle stability. This can be achieved by using various motion sensors and a feedback control system programmed on a microcontroller. These sensors are incorporated to monitor the overall vehicle behaviour and the driver's intent in operating the vehicle. Then, the controller can allow electric motor torque delivery for both braking and accelerating when it is safe to activate, based on its calculations. The developed VDC employs nominal acceleration $(a_{y\_nominal})$ and Body Slip Angle (β) control methods using the bicycle model explained in Chapter 2.

---

[1] The term "Vehicle Dynamics Control" system is a generic one used by BOSCH®. The SAE convention refers to the same system as Electronic Stability Control (ESC) system.

4

1.4 Research Outline

The research objective was to develop a vehicle dynamics controller through co-simulation, for controlling the hybrid system function (regenerative braking and drive torque assist) of the prototype design to maintain vehicle stability in various driving conditions. The objective is achieved for the prototype hybrid *Pacifica* through the following study.

The prototype hybrid *Pacifica* is simulated as a multi-DOF vehicle incorporating a non-linear tire model in the vehicle dynamics software *CarSim* to analyze its stability response in general. Furthermore, the effects of regenerative braking in vehicle stability are investigated. By simulating the prototype vehicle with its actual vehicle parameters, the realistic lateral vehicle dynamics behaviour is analyzed for safety limits applicable to the prototype vehicle. Using the threshold limits, a vehicle dynamics controller is developed in *Simulink* via co-simulation.

In co-simulation, the "bicycle model" is investigated as the reference component of the controller design. The bicycle model's ability to process the driver's intent for the vehicle path calculation is verified and the overall controller design was conducted based on the threshold limits of the bicycle model response in controlling the hybrid system function of the prototype.

Iterative vehicle dynamics simulations of various driving conditions are conducted in order to verify the robust controller performance. The validated vehicle dynamics controller design is implemented on PIC 18F458 μ-controller for the system implementation. A comprehensive data acquisition sensor system architecture is designed to function with the developed VDC on the prototype hybrid *Pacifica*.

CHAPTER 2

LITERATURE REVIEW & BACKGROUND

2.1 Literature Review

Although the concept of modern hybrid electric vehicle has been developed since 1970's, the first mass-production of hybrid electric vehicle was achieved in 1999[2]. [3] Therefore, only limited technical information of relevancy in vehicle dynamics control for hybrid electric vehicles was available when this study was commenced.

However, the concept of vehicle dynamics control has been developed in 1995 by van Zanten et al. of the Robert BOSCH Corporation by using a "β-method" (body slip angle control) in controlling the lateral vehicle stability on their vehicle dynamics controller. [4] Using the bicycle model, the "β-method" calculates the body slip angle of the vehicle and controls the hydraulic brake system of the individual wheel in order to maintain the vehicle yaw moment balance. [4 & 5]

Panagiotidis et al. developed a regenerative braking simulation model incorporating a wheel lock-up avoidance algorithm by using a co-simulation method. The authors focused on developing a simulation model that controls the amount of regenerative braking torque in

---

[2] Honda Insight was the first mass-produced hybrid electric vehicle.

proportion to the hydraulic braking torque in order to achieve the maximum regenerative braking efficiency. [6]

Khatun et al. investigated controlling the wheel slip for electric vehicle operation in order to study the anti-lock braking system (ABS) and traction control system (TCS) for electric vehicles. [7] Mi et al. developed an iterative learning control of ABS for electric and hybrid electric vehicles using a wheel slip control and a vehicle speed forward speed observer in order to allow regenerative braking to mimic the ABS function in assisting vehicle stability in braking. [8]

Hori developed a vehicle dynamics control system for an electric vehicle by installing a separate electric motor to each wheel of a four-wheel vehicle. Yaw rate and body slip angle control methods were developed by controlling the individual electric motor torque output. [9] Soga et al. of Toyota Motor Corporation developed a vehicle stability control system which uses the same concept as the BOSCH's vehicle dynamics control system for a hybrid electric vehicle which utilized the industry-first brake-by-wire system. [10]

This study focused on developing a vehicle dynamics controller that controls the hybrid electric system function for a specific prototype hybrid electric vehicle. The developed controller employs the bicycle model to estimate the vehicle body slip angle for stability control while comparing the driver's intended vehicle path to the actual one. Wheel slip control method was also employed to optimize the brake and traction torque of the electric motor in maintaining the lateral vehicle stability.

2.2 Hybrid Electric Vehicles

2.2.1 Definition of HEV

Hybrid electric vehicles (HEV) employ two different sources of propulsion- an internal combustion engine (ICE) and an electric machine[3] (EM). ICE is used as a primary propulsion source using gasoline as fuel (sometimes diesel is used). The EM is used as a secondary propulsion source, and switches its function to an electric generator to create electricity which is stored to power the electric motor later. Therefore, in the hybrid system, the ICE consumes less fuel, thus reducing emissions. Electricity generation is achieved by "regenerative braking" which recaptures the propulsion energy spent by fuel from the vehicular kinetic energy. The following explains the regenerative braking concept.

Typically, an automobile is slowed down by applying brakes to its rotating wheels via friction force (disc or drum brakes). In this phenomenon, the kinetic energy of the moving vehicle is dissipated primarily as heat energy caused by friction between the brake rotor and brake caliper pad; and in case of drum brakes, between the inner drum lining and brake shoe. When brakes are applied, the brake rotors of rotating wheels (powered by the vehicular kinetic energy) are essentially "grabbed" by brake calipers. The friction force between the brake rotor and the brake calipers is what causes the braking moment about the centre of rotating wheel that brakes the rotating wheel, hence decelerating the vehicle. The friction force between the brake rotor and the brake caliper creates a tremendous amount of heat energy as the rotors can heat-up up to 800 °C. [11] This large amount of heat energy transferred from kinetic energy is rejected to the environment in conventional braking systems.

---

[3] Electric motor/generator is referred to as an electric machine (EM). By motor control, EM can function as either a motor or generator. [12]

8
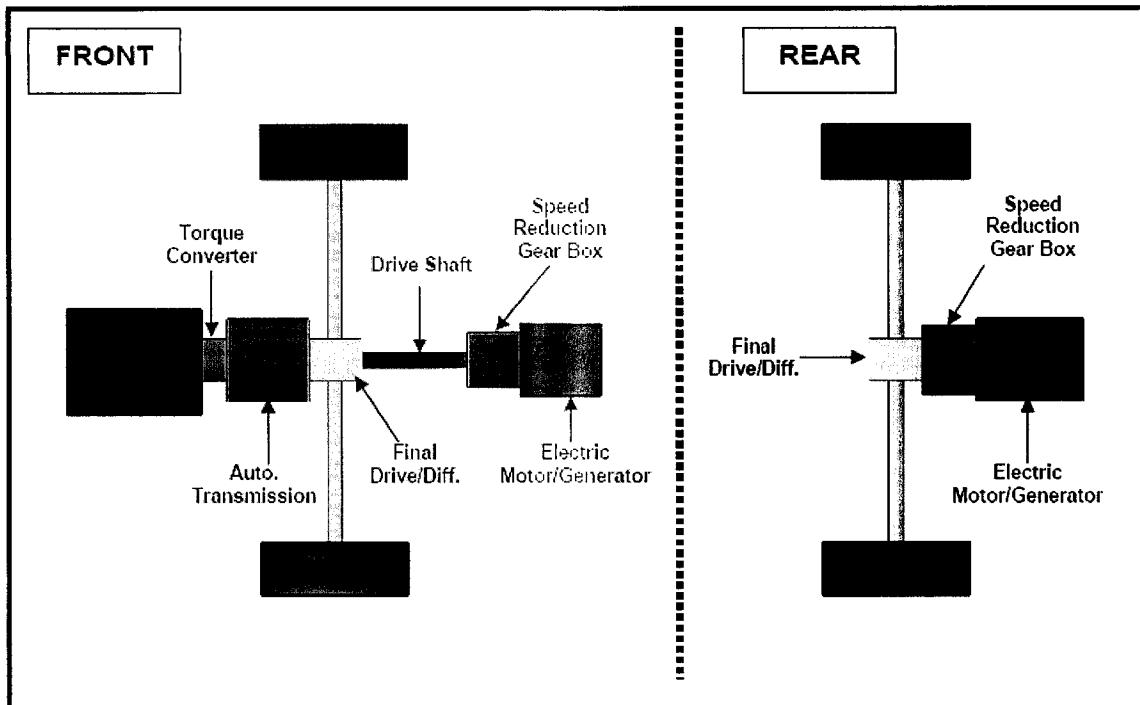
Figure 2.1 Schematic drawing of prototype hybrid Pacifica

In hybrid electric and electric vehicles, the aforementioned wasted energy is captured by regenerative braking by using the electric motor as a generator. In the above figure, the electric motor is connected to the drivetrain through a drive shaft. When regenerative braking is activated, the electric motor functions as a generator commanded by the motor controller of the hybrid system. The rotor of electric motor is spun through the drive shaft which is connected to the rotating wheels. Spinning of the rotor enables the electro-magnetic field excitation for generating electricity. In doing so, the vehicular kinetic energy is transformed as electricity and as a result, the vehicle brakes. This created electricity is then stored in an energy storage system[4] which powers the electric motor when additional propulsion power is requested for driving. Since the otherwise wasted energy is captured to do work, hybrid electric vehicles are more fuel efficient than the conventional vehicles, resulting less fuel consumption and emissions. Additional braking in hybrid electric vehicles is achieved by the regular hydraulic brakes as in conventional cars.

---

[4] For the prototype hybrid *Pacifica*, ultracapacitors are used as energy storage system. The details of the system can be found in [1]

9

2.2.2 Charge Sustaining (CS) and Charge Depleting (CD) Operation Theory

The term, charge sustaining (CS) operation, refers to the regenerative braking and charge depleting (CD) operation refers to the drive torque assist function of the hybrid electric vehicle. The idea of CS operation is that the vehicular kinetic energy of moving vehicle created by the ICE power is recaptured. The regenerated energy is used to recharge the energy storage system of an EV or HEV. In the case where the state of charge (SOC) is full, regenerative braking is no longer possible. For this reason, EVs and HEVs are equipped with the mechanical brake system which can also perform ABS braking. The vehicle hybrid master controller decides the amount of braking needed from the mechanical system based on the braking command of the driver, SOC, and vehicle velocity. Regenerative braking can increase the range of such equipped vehicles by about 10 to 15%. [12 & 13]

Since the prototype hybrid *Pacifica* uses the AC induction motor as its secondary drivetrain, the following is used to explain the operation of induction machines. The induction machine works as a generator when it is operated with a negative slip, i.e., the synchronous speed is less than the motor speed $\omega_{EM} > \omega_s$. Negative slip makes the electromagnetic torque negative during regeneration or generation mode of the EM. In the negative slip operational mode, voltages and currents induced in the rotor bars are of opposite polarity compared to those in the positive slip mode. As a result, electromagnetic torque acts on the rotor to oppose the rotor rotation. This is how regenerative braking decelerates the vehicle.

10
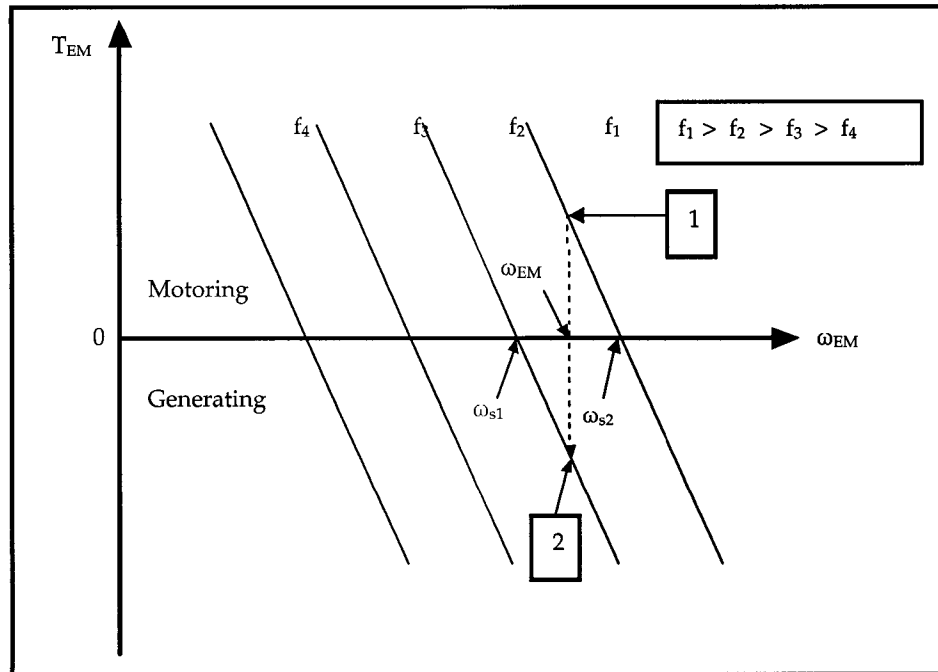
Figure 2.2 Transition from Motoring to Generating using a four quadrant drive

The motor drives for EVs always use four-quadrant drives, hence the electric motor is controlled by the drive to deliver positive or negative torque at positive or negative speed. The transition from motoring to regeneration can be explained with the help of Figure 2.2. The linear segments of the induction motor torque-speed curves for several operating frequencies are shown in the above and the curves are extended in the negative torque region to show the regeneration characteristics.

When the vehicle is moving forward by the positive induction motor torque, assume that the steady-state operating point of the EM is at point 1 as the driver commands regenerative braking. The hybrid system master controller immediately changes the motor drive frequency from f_1 to f_2 resulting the condition, $\omega_{s2} > \omega_{s1}$. The operating point shifts to point 2 immediately since the motor speed cannot change instantaneously due to the rotor inertia. At point 2, the slip and the electromagnetic torque are negative and this enables the EM to generate electricity. As a result, the vehicle will decelerate as long as the driver commands regenerative braking.

11

When the motor speed decreases below the synchronous speed, the operating frequency also needs to be changed to a lower value in order to maintain the generating operation mode. The power electronics system is responsible for establishing the shifted linear torque-speed curves with different synchronous speeds for the induction EM at different frequencies. This is achieved by changing the frequency of the input voltage of the drive circuit. The regenerative braking mode will continue as long as the vehicle kinetic energy is available and the driver commands the regenerative braking function.

2.3 Design Configurations of Hybrid Electric Vehicle

There are two main design configurations of hybrid systems. Currently, series and parallel system configurations are actively researched and developed in today's automotive industry.

2.3.1 Series Hybrid System

In the series hybrid the mechanical output of the internal combustion engine is used to generate electrical power by means of a sizeable alternator-rectifier arrangement similar to that used in a conventional car [13] The electric motor is directly connected to the ICE so it runs at its optimum operating speed range to power the electric motor as generator and by default, there is no mechanical transfer of power from ICE to drivetrain. The ICE generated electricity and regenerative braking charges the electric energy storage system, a battery/ultracapacitor pack.

Pros:

- ICE runs continuously at the optimal efficiency level for fuel consumption and emissions.

Cons:

- Limited propulsion power output as the electric motors have lower power to weight ratio compared to the ICE

12

• Requires a sizeable alternator/rectifier as a mandatory system component.

2.3.2 Parallel Hybrid System

In the parallel hybrid system, the electric motor can supply power in parallel with ICE through a shared gearbox of drivetrain. Electricity generation is only available through regenerative braking. Multiple electric motors can be installed to increase electricity generation at the cost of weight gain. An example is installing an electric motor on each front and rear drive axle of a vehicle.

Pros:

• Total system power output can be tailored for performance or efficiency.

• By adding an electric motor on the base ICE powertrain, total power output can be increased. (e.g. Lexus 400h)

• By installing a smaller ICE, electric motor can supplement the lack of power to match the performance of a bigger ICE powertrain. (e.g. Honda Insight)

Cons:

• ICE cannot operate at the set optimal efficiency level (Lower overall efficiency compared to the series hybrid system)

13

2.4 Vehicle Handling Dynamics and Tire Forces

2.4.1 Pneumatic Tire Force Generation

Pneumatic tires are vital components of any vehicle that generates longitudinal and lateral forces to allow vehicle manoeuvring. Since tires are made of rubber, they present a non-linear material behaviour reacting to forces generated from the tire-road interaction. For decades, efforts have been made to accurately model the tire behaviours but the rubber's non-linear property does not allow formulating an accurate mathematical model of its behaviours. Instead, experimental curve-fitting has been done for various tires to have a representative tire data used for vehicle dynamics simulation. Hans Pacejka developed the most widely used "Magic Formula Tyre Model" which employs trigonometric equations with various coefficients that represent the tire behaviour in various conditions. [14] Simulations performed using the Pacejka model have been proven to be accurate when compared to empirical data.

2.4.2 Longitudinal Tire Force (F_x)

When a driving or braking torque is applied to the wheel, a driving or braking traction force, F_x, is generated between the tire and the road surface. This is achieved through a longitudinal slip, which relates the angular velocity and the forward velocity of the wheel.
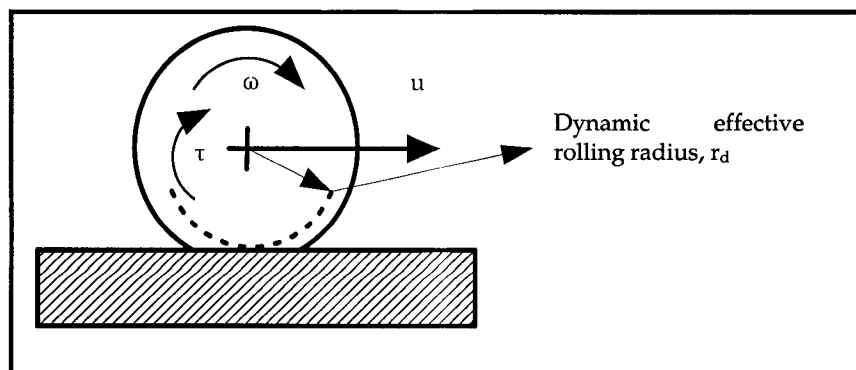
Figure 2.3 Rolling wheel with drive moment

14

A free-rolling tire of a dynamic effective rolling radius (r_d) has a relationship between the forward velocity (u) and the angular velocity (ω) in the form of:

$$u = r_d \omega \qquad \text{[Eq. 2.1]}$$

In Figure 2.3, a driving torque is shown as τ in the direction of wheel travel. A braking torque will have an opposite direction as to create a braking traction force in the wheel.

Braking slip occurs when the braking torque is applied to the wheel because its angular velocity is less than the free-rolling angular velocity. When the wheel locks, the angular velocity becomes zero. The relationship, referred to as longitudinal wheel-slip in braking (λ_B), is expressed as:

$$\lambda_B = \frac{(u - r_d \omega)}{u} \qquad \text{[Eq. 2.2]}$$

Driving slip (λ_D) is expressed differently due to the case of when u = 0 as:

$$\lambda_D = \frac{(r_d \omega - u)}{r \omega} \qquad \text{[Eq. 2.3]}$$

An assumption can be made (although not strictly true) that the longitudinal force (F_x) is proportional to the normal force (F_z) so that the longitudinal coefficient of friction (μ_x) can be defined as:

$$\mu_x = \frac{F_x}{F_z} \qquad \text{[Eq. 2.4]}$$

15

2.4.3 Lateral Tire Force (F_y)

In vehicle handling dynamics, lateral forces generated by tires are primarily important. Lateral tire forces allow lateral vehicle motion responding to driver's steering input, and provide the vehicle its ability to negotiate a turn. When a lateral force is applied to the wheel traveling with a forward velocity, a corresponding lateral force will arise in the contact patch between the tire and the road surface, due to friction. If the lateral force is small enough not to cause the tire to skid sideways on the surface, it will cause the wheel to deviate its direction from where it is pointed. This will induce a lateral velocity in addition to the wheel's forward velocity. Therefore the resultant velocity vector of the wheel will point in a different direction than the direction of the centre plane of the wheel. The angle between the wheel centreline and the direction of wheel travel is called the tire slip angle (α).
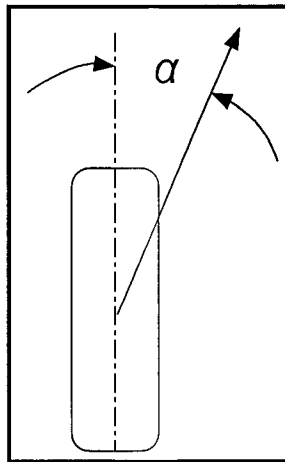
Figure 2.4 The tire slip angle (α) between a wheel centerline & the direction of wheel travel

In the vehicle stability analysis, a linearized model of the relation between the tire lateral force (F_y) and the slip angle (α) is commonly used as described by Equations 2.10 and 2.11. For small tire slip angles, a proportionality constant called, the cornering coefficient, C_α, can be defined as the slope of the line relating lateral force to slip angle. Although the slip angle is the main determinant of the side force, there are other characteristics such as camber angle of small influence and the driving and braking torque that can be of a significant influence.

16

2.4.4 Normal Tire Force (F$_z$)

Normal force acting on the tire allows the tire lateral force generation. The Coulomb friction model,

$$F_y = \mu F_z \qquad \text{[Eq. 2.5]}$$

is used to represent the lateral tire force. It is commonly assumed that the lateral tire force at a given slip angle is roughly proportional to the normal force. [15] The coefficient of friction depends on the road surface as well as on the tire material. Although tire side force and normal force is approximately proportional, this relationship is not entirely true and coefficient of friction decreases when the normal force becomes excessively large.

2.4.5 Combined Lateral and Longitudinal Forces (Friction Circle)

Tires generate lateral and longitudinal forces simultaneously as when a car is turning and braking or accelerating at the same time. This interaction can be described in plot called a Friction Circle [16] where the lateral force (F$_y$) and the longitudinal force (F$_x$) make up the axes. The idea is that the maximum tire forces are essentially limited to a circle in the F$_x$-F$_y$ plane assuming a constant normal force. The maximum lateral force is achieved when there is no longitudinal force. Conversely, the maximum longitudinal force is achieved when no lateral force is present.

17
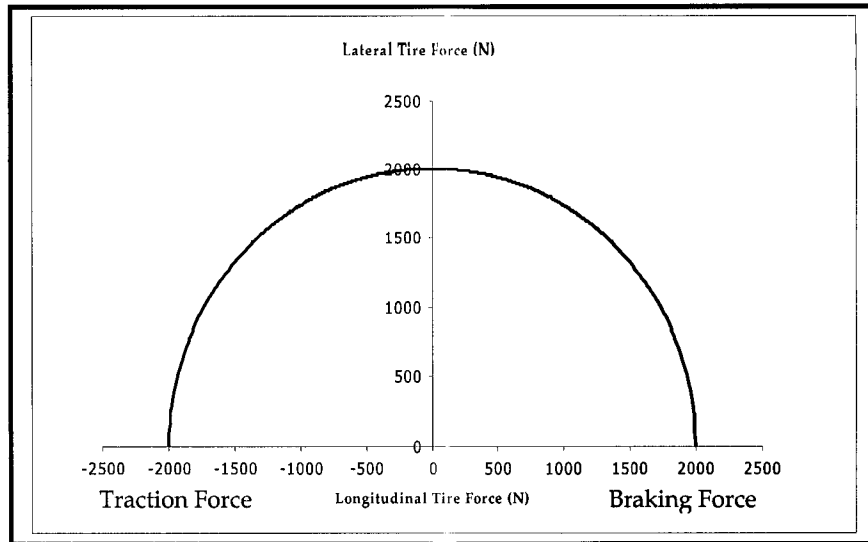
Figure 2.5 A typical friction circle containing lateral & longitudinal forces

At large slip angles or large longitudinal slips, the magnitude of the total force generated typically drops below its maximum value. By modulating the brake torque output, the longitudinal slip is minimized to generate maximum possible braking force. Therefore, the braking distance can actually be shorter with ABS brakes than the fully locked ordinary brakes. Under various road conditions where coefficient of friction and load transfer along the longitudinal (x) and lateral (y) axes vary, the traction level on each tire increases or decreases. The increased traction force of driven wheels cannot always be transferred into vehicle propulsion effectively and thus results in wheel spin.

The danger of wheel spin is that it further reduces the traction limit at that particular wheel. The unbalanced traction force in left and right wheel therefore causes an unwanted vehicle yawing moment about the z-axis of vehicle (CG). This presents potential instability in vehicle handling dynamics. In braking, the excessive braking torque induces wheel lock-up and it results in skidding of a particular wheel. The traction force of a skidding wheel is very low and causes non-effective braking at that wheel. Furthermore, in the case of steered wheels, vehicle steering becomes impossible as the lateral tire forces are minimized due to skidding and the vehicle cannot negotiate the driver's intended path. In this case, the vehicle will continue to

18

travel in the direction where the CG of the vehicle is heading, not to the direction where the steered wheels are pointed. Thus, the excessive torque provided to the braking wheels imposes potential instability in vehicle handling dynamics.

2.5 Bicycle Model Equations

The bicycle model is a classic model that has been widely used in the study of vehicle dynamics. Its name stems from the fact that the width of the two-track vehicle investigated is considered to be unimportant to the vehicle behaviour. Hence, two front tires are lumped together as one and so are the rear tires. It is a linear 2-DOF (lateral velocity & yaw rate) mathematical model derived from the Newton's Second Law:

$$\sum \vec{F} = m\vec{a}$$
[Eq. 2.6]

The bicycle model (Figure 2.6) is an integral component of the developed vehicle dynamics controller for the following reasons. Firstly, the body slip angle can be calculated using the model. The body slip angle, which is a control variable of the VDC system, cannot simply be measured by motion sensors. Secondly, using the bicycle model, the driver's intent in vehicle maneuvering (nominal path) can be calculated by the controller in various driving conditions. This nominal path is compared with the actual state/path of the vehicle to recognize the vehicle instability (if present), and necessary action is commanded by the controller to help maintain the vehicle stability.

2.5.1 Equation Derivations

In lateral dynamics of a vehicle, the lateral motion is stipulated by the lateral tire forces (F_f & F_r) developed at the contact patch. The lateral velocity (v) and yaw velocity (r) are the degrees of freedom in the mathematical model. The forward velocity (u) is assumed to be constant which further simplifies the equations. The properties of the vehicle are mass (m), yaw

19

moment of inertia (I_{zz}), and distances of the front and rear axles from the centre of the gravity of the vehicle (a & b). The cornering stiffnesses of the front and rear tires are denoted C_f and C_r, respectively. The steering angle of the front tire is δ_f.
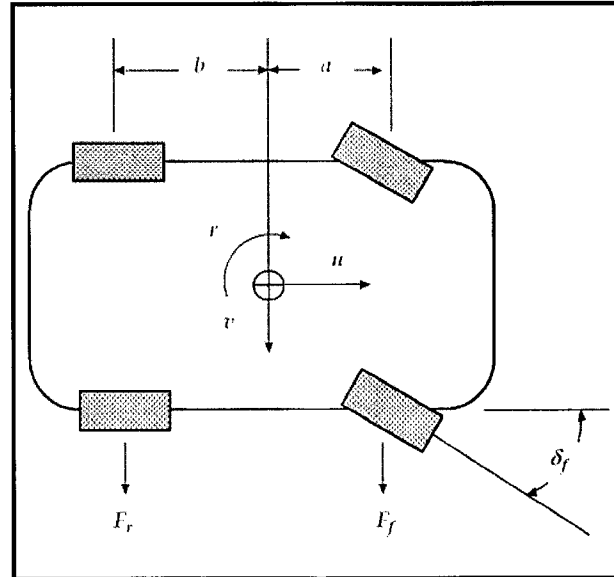
Figure 2.6 The bicycle model

By using Eq. 2.6 and using the velocities of the vehicle that are defined in a frame attached to the vehicle rotating with it, the following is obtained.

$$\sum F = F_f + F_r = m(\dot{v} + ru) \qquad \text{[Eq. 2.7]}$$

And from the moment equilibrium about the z-axis,

$$\sum M = I\alpha \qquad \text{[Eq. 2.8]}$$

it can be achieved that,

$$\sum M_z = I\dot{r} = aF_f - bF_r \qquad \text{[Eq. 2.9]}$$

Mostly, the lateral forces are developed from the misalignment, tire slip angle (α) and steer angle (δ) as shown in Fig. 2.7.

20
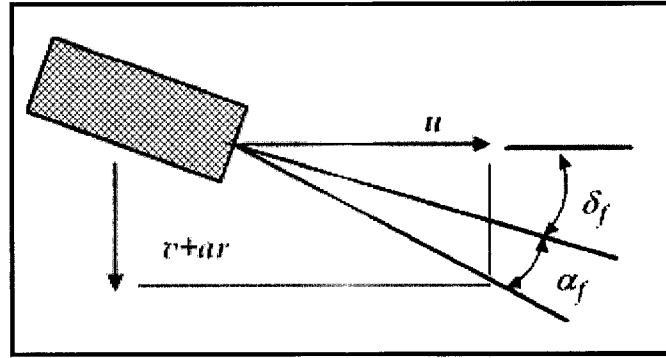
Figure 2.7 The tire slip angle (α)

In order to keep the linearity of the bicycle model, a simple linear function describing the lateral force as a function of α is developed as following:

$$F_f = -C_f \alpha_f$$

[Eq. 2.10]

$$F_r = -C_r \alpha_r$$

[Eq. 2.11]

In Figure 2.7, by using small angle approximation for the slip angles that are constrained kinematically by the vehicle velocity, the following equation is derived.

$$\alpha_f + \delta_f = \frac{v + ra}{u}$$

[Eq. 2.12]

And applying the same method, for the lumped rear tire, the following is obtained. Note that $\delta_r = 0$ at the rear tire unless rear wheel steering is applied.

$$\alpha_r + \delta_r = \frac{v - rb}{u}$$

[Eq. 2.13]

Substituting Eq. 2.10 & Eq. 2.11 into Eq. 2.12 & Eq. 2.13 respectively. The following equations are achieved.

$$F_f = C_f \delta_f - \frac{(v + ra)}{u} C_f$$

[Eq. 2.14]

$$F_r = -C_r \frac{(rb - v)}{u}$$

[Eq. 2.15]

21

Substituting the Eq. 2.12 & Eq. 2.13 into the lateral force equation of Eq. 2.7 and the moment equation of Eq. 2.9 and combining them into a matrix form, the following matrix equations is achieved. This the final form of the bicycle model describing the lateral dynamics of a vehicle.

$$\begin{bmatrix} m & 0 \\ 0 & I \end{bmatrix} \begin{Bmatrix} \dot{v} \\ \dot{r} \end{Bmatrix} + \begin{bmatrix} (c_f + c_r)/u & (ac_f - c_r)/u + mu \\ (ac_f - bc_{r)}/u & (a^2 c_f + b^2 c_r)/u \end{bmatrix} \begin{Bmatrix} v \\ r \end{Bmatrix} = \begin{bmatrix} c_f \\ ac_f \end{bmatrix} \{\delta_f\} \quad \text{[Eq. 2.16]}$$

It is of an interest to discuss the definition of body slip angle (β). As per SAE J670e standard, Sideslip Angle (body slip angle, β) is the angle between the traces on the X-Y plane of the vehicle x-axis and the vehicle velocity vector at some specified point in the vehicle. [17]
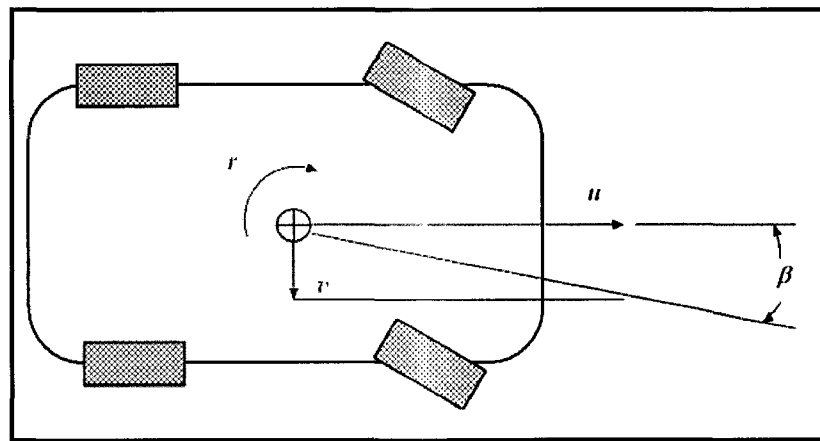
Figure 2.8   The body slip angle (β)

In low speed cornering where the lateral acceleration is low, the vehicle velocity vector will coincide with the vehicle x-axis. At higher speeds, the greater lateral acceleration will cause the velocity vector deviate from the vehicle x-axis. This is how the body slip angle is created.

2.6 Vehicle Dynamics Controller Concept

Since the emergence of ABS in late 1970's, advances have been made in controlling tire-road traction control to provide maximum longitudinal and lateral forces for the vehicle in motion. [18]

ABS braking modulates braking torque output by modulating brake line pressure in order to prevent wheel lock-up. [19 & 20] This allows maximum braking force at wheels. The traction control system (TCS) works in the same principle to provide maximum traction force at driven wheels. [19 & 20] The engine torque output is modulated by spark retardation or fuel cut-off. The production *Pacifica* is not equipped with TCS so individual wheel slip control is not possible for maintaining stability in acceleration. In the case of braking, ABS controls individual wheel braking to prevent wheel lock-up to avoid skidding but this cannot be achieved when regenerative braking is in effect.

More recently the concept of electronic stability control (ESC) was first developed by the BOSCH corporation in 1995, incorporating ABS and TCS technology. [2] It is an active safety system for road vehicles which controls the lateral dynamic vehicle motion in emergency situations. From the steering angle, the accelerator pedal position and the brake pressure, the driver's desired motion is derived while the actual vehicle motion is derived from the measured yaw rate and lateral acceleration.

The driver's inputs measured by the steering wheel angle, throttle position, brake position, and brake pressure sensors are used to calculate nominal behaviour of the vehicle by the nominal values of the controlled variables (driver's input). The actual behaviour of the vehicle is determined from longitudinal & lateral acceleration, yaw rate, and wheel rotation speed sensors (calculates vehicle forward speed). The nominal behaviour which is calculated by the bicycle

23

model is compared to the actual behaviour of the vehicle to determine the difference between the nominal and actual paths of the vehicle. In BOSCH's vehicle dynamics control system, if the actual vehicle path is beyond the safety limit, then the vehicle controller signals necessary actuation of brakes and/or engine torque retardation to keep the vehicle on safe path. This process effectively controls the yaw moment around the vehicle z-axis to cause appropriate yaw angle to the direction that the driver commands and effectively maintains the vehicle stability.
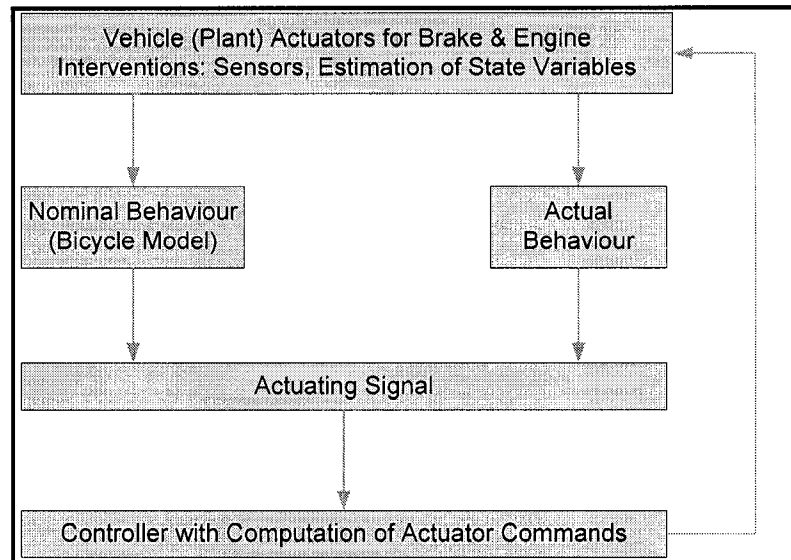
Figure 2.9 Fundamental control task of BOSCH VDC

In this study, the developed supervisory VDC controls the extra braking or acceleration torque output of the electric motor in lieu of individual wheel braking and/or engine torque retardation, based on the vehicle state variables of a_y and β. It will be a closed loop control system that continuously monitors the system behaviour and control the torque output when necessary.

2.7 Vehicle Dynamics Co-simulation Softwares Review: *CarSim & Matlab/Simulink*

CarSim is a software package for simulating and analyzing the behaviour of four-wheeled vehicles both with and without trailers. It works as a stand-alone program or as a *Simulink* plug-in and for this reason it is suitably fast and easy software for co-simulation with *Matlab* where the VDC using the bicycle model is created.

The VDC design is developed in the *Matlab/Simulink* environment. *Matlab* is used to develop the mathematical bicycle model for the prototype hybrid *Pacifica*. The developed mathematical model is converted into a *Simulink* block as a part (estimator) of the closed-loop design of VDC. A mathematical model of electric motor is developed to represent hybrid functions (regenerative braking & electric motor torque assist) of the prototype for simulation. The developed vehicle dynamics controller is interfaced with *CarSim* for co-simulation that is used to validate the controller design.

CHAPTER 3

HYBRID SYSTEM DESIGN & PERFORMANCE

3.1 *Chrysler Pacifica*

A 2004 *Chrysler Pacifica* production model is donated for the project by DAIMLERCHRYSLER of Canada.
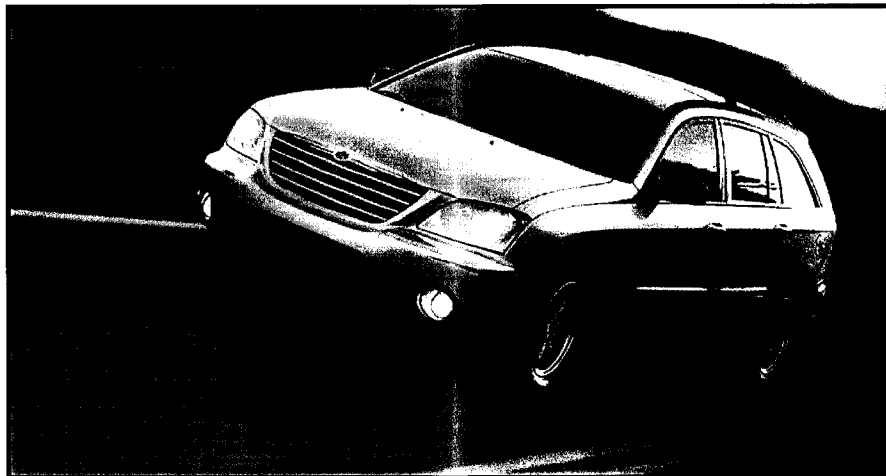
Figure 3.1 2004 Chrysler Pacifica AWD model (Courtesy of DAIMLERCHRYSLER Corp.)

The project objective is to produce a prototype hybrid electric *Pacifica* using an AC synchronous induction motor (SIEMENS 1PV5133-4WS20) as the secondary propulsion source and an ultracapacitor pack as an energy storage system. The 2004 production *Pacifica* AWD model has the following standard features of relevance.

26

	Table 3.1 2004 Chrysler Pacifica standard features
Powertrain	3.5L V6 engine: 184 KW (250 HP) @ 6,400 RPM & 339 N•m (250 lb•f) @ 4,000 RPM Four-Speed Automatic Transmission with Auto-Stick Fuel Efficiency: EPA Mileage Estimates: City = 7.23 Km/L; Highway = 9.35 Km/L
Weight	1993 Kg Weight Distribution- Front : Rear = 56% : 44%
Dimensions	Wheelbase: 2954.02 mm Track Width: 1676.40 mm for both front and rear
Chassis Control Features	Brakes- Power assisted 4-wheel disc, anti-lock with Electronic Variable Brake Proportioning Suspension: Load-leveling rear shock absorbers to maintain a consistent ride height when laden with cargo (4-wheel independent suspension, with MacPherson strut front and 5-link rear)

3.2 Prototype Hybrid Electric *Pacifica* Design

The prototype design is a post-transmission, parallel hybrid since the electric motor is installed separate from the engine to generate electricity. The following Figure 3.2 describes the Phase I design schematic. The electric motor (2) is located behind the front differential unit through the front torque coupler (speed-reduction gear box) (1). When the electric motor is activated, controlled by the driver input in the throttle or brake-by-wire system (9), the hybrid system controller (5) signals the electric motor actuation. If the command is for drive torque, the induction motor controller (4) controls the electric motor to produce positive torque. The motor is powered by the electric energy stored in the ultracapacitor bank (6) through the induction motor inverter (3). The positive torque created will be delivered to the front drivetrain via the front torque coupler to propel the vehicle forward.

27

1	Front Torque Coupler (gear box)	6	Ultracapacitor Bank
2	Front Drive AC Induction Motor	7	Cooling System
3	Induction Motor Inverter	8	Engine Control Unit (ECU)
4	Induction Motor Controller	9	Throttle-by-Wire & Brake-by-Wire Systems
5	Hybrid System Controller	10	Data Acquisition System
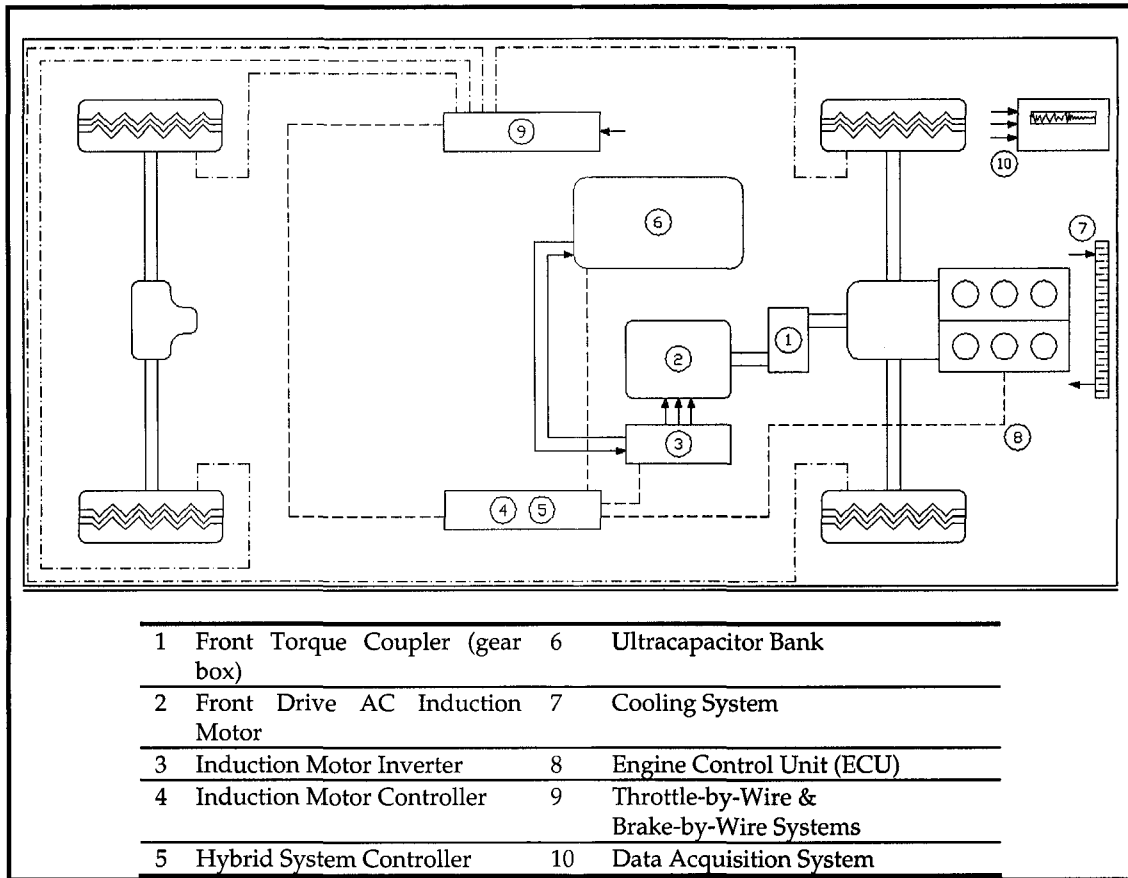
Figure 3.2 Phase I schematic design (Courtesy of S. Samborsky)

If the command is for brake torque, the induction motor controller (4) controls the electric motor to produce negative torque, in which the torque generation is provided by the vehicle kinetic energy transferred by the front drivetrain and through the front torque coupler. At this instance, electricity is created by the electric motor and it is relayed through the induction motor inverter to charge the ultracapacitor bank. The cooling system (7) maintains the operating temperatures for the electric motor, inverter, hybrid system controller, and torque coupler. These components require a separate, dedicated liquid cooling as the hybrid system operates with the range of 180 to 400 V (450 A) of electricity. The electric motor coupled with the gearbox, operates up to 12,000 rpm. The engine control unit (8) works in conjunction with the hybrid system controller in order to produce a modulated drive torque from the internal combustion engine for the system efficiency. Lastly, the data acquisition system (10) monitors all the system data

28

information necessary for the hybrid system operation as well as the VDC system developed in this study.

3.2.1 Prototype *Pacifica* Hybrid Powertrain (ICE & EM)

In addition to its stock internal combustion engine (ICE), the prototype powertrain has a 3-phase AC induction electric motor with a 67 KW peak power.

SIEMENS 1PV5133WS20 Motor	
Motor Type	3-Phase AC Induction
Peak Power	67 kW
Continuous Power	32 kW
Peak Torque	190 N-m
Speed Range	0 – 12,000 rpm
Input Bus Voltage	260 – 385 V
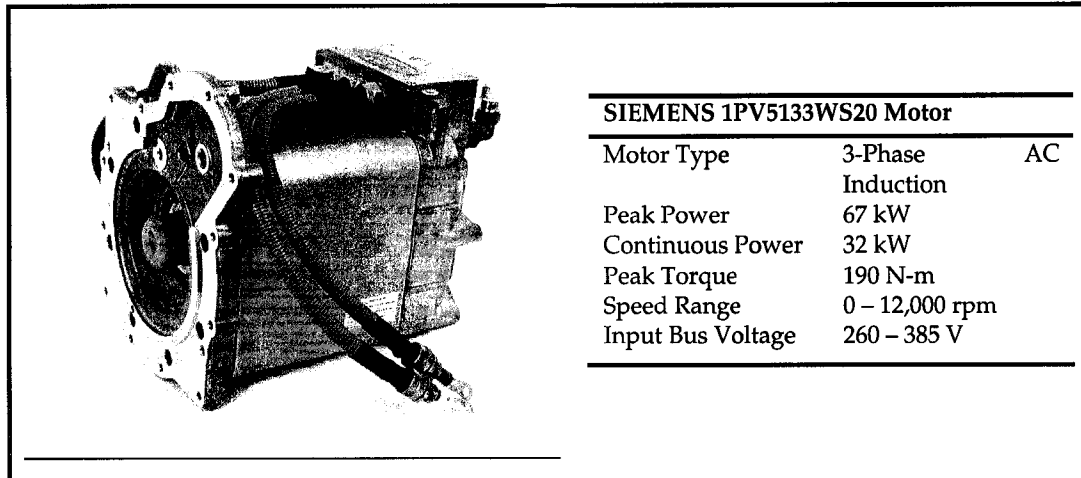
Figure 3.3 SIEMENS 1PV5133WS20 motor

The electric motor alone is a considerably powerful powertrain unit. Added to the stock 184 KW internal combustion engine, the hybrid powertrain system can produce an enhanced power output. However, due to its design nature, the electric motor has a very different performance curves compared to the standard ICE; therefore, the combined power output is not simply the sum of the two powertrain units. A detailed electric motor performance discussion is found in Section 3.3.

3.2.2 Prototype *Pacifica* Hybrid Drivetrain

The electric motor is integrated as a post-transmission powertrain component in the front drivetrain. As mentioned in the beginning of this section, the electric motor is directly connected to the gearbox (front torque coupler) which serves as a medium in order to:

29

- Transmit the electric motor torque to the front drivetrain to provide propulsion to the vehicle.

- Match the electric motor operation speed range of 0 to 12,000 rpm to the existing drivetrain operation speed range of 0 to 1083 rpm through gear ratio of 1.71 : 1 (automatic transaxle) and 6.52 : 1 (speed-reduction gear box).

In order to install the gearbox to the existing front drivetrain, the propeller shaft between the front and rear drivetrains is removed from the power transfer unit (PTU), depicted as (1) in Figure 3.4 of the automatic transaxle. (See Figures 3.4 & 3.6)

Fig. 1 AWD Driveline

1 - PTU FLANGE	6 - BEARING/SUPPORT
2 - PLUNGING CV JOINT	7 - REAR SEGMENT
3 - FRONT SEGMENT	8 - REAR DRIVELINE MODULE
4 - BEARING/SUPPORT	9 - RUBBER COUPLER
5 - CENTER SEGMENT	
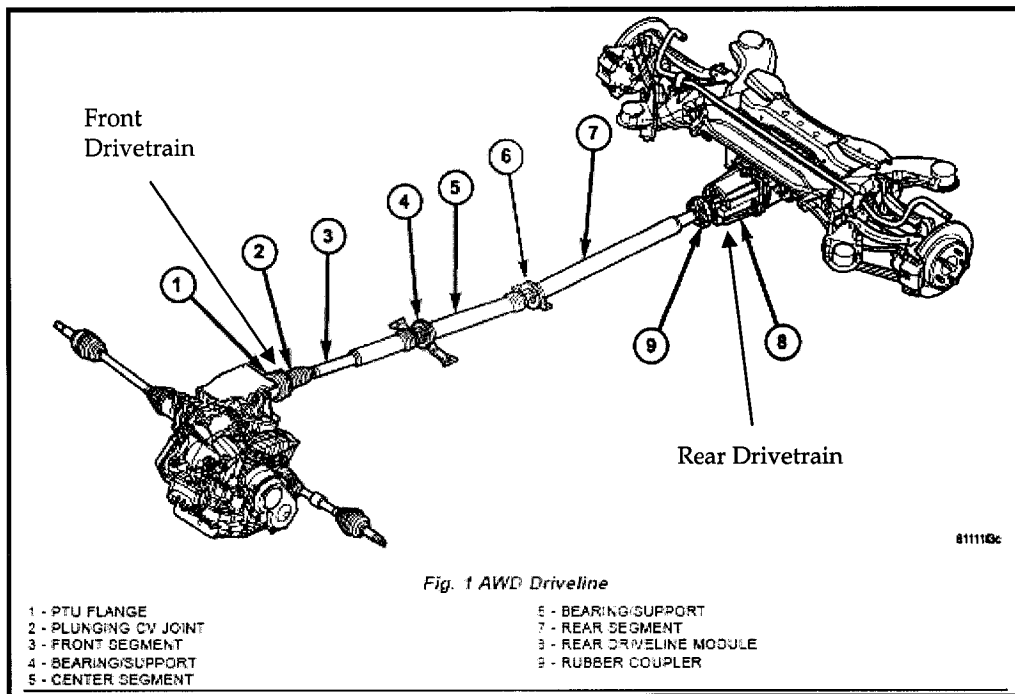
Figure 3.4 Pacifica AWD drivetrain schematic drawing (Courtesy of DAIMLERCHRYSLER Corp.)

30
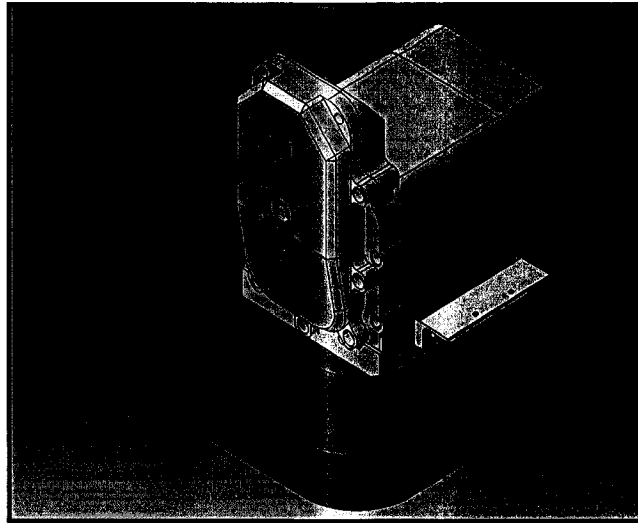
Figure 3.5 3D model of gearbox and electric motor assembly (Courtesy of S. Draca)

Fig. 4 Power Transfer Unit Lower Bolts
1 - POWER TRANSFER UNIT
2 - TRANSAXLE
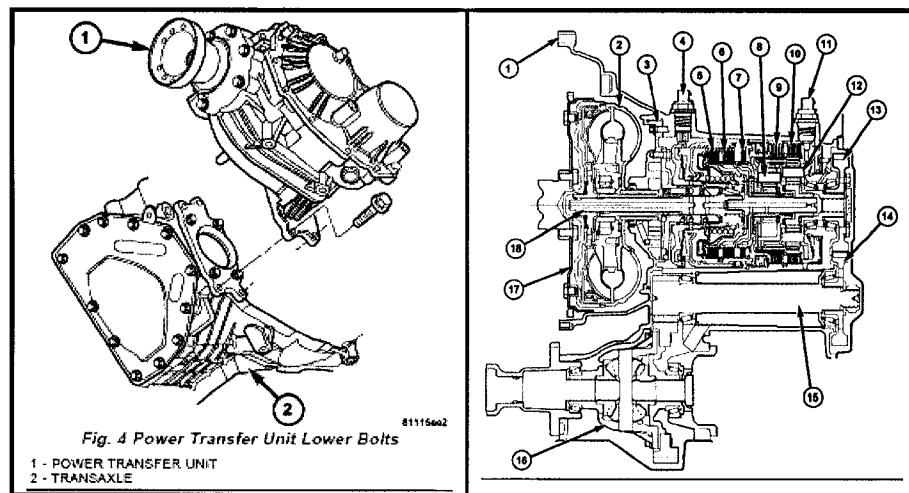
Figure 3.6 Drawings of PTU and 41AE/TE automatic transaxle (Courtesy of DAIMLERCHRYSLER Corp.)

The gearbox output shaft is connected to the PTU joint, and the input shaft of the gearbox is connected to the output shaft of the electric motor. The torque transmission is as follows. In drive torque delivery mode of the electric motor, the torque flow starts from the motor to gearbox to front differential (housed inside the automatic transaxle) to half-shafts which are connected to the front left and right wheels. In regenerative brake torque delivery mode, the same path as the drive torque is followed in the reversed order.

In the prototype design, no clutch system is used to engage/disengage the electric motor torque output to the front drivetrain. This design stipulates a permanently engaged electric

31

motor to the front drivetrain. A good analogy is the powertrain/drivetrain interaction of a manual transmission vehicle which has a front-engine mounted and front-wheel driven design. With a gear engaged, the engine torque produced (positive) is delivered to the drivetrain to propel the vehicle. When down-shifting to decelerate the vehicle, "engine braking" is done. This is achieved by the higher gear ratio (of selected low gear) and the rotational inertia of the engine and transmission components that act as negative torque delivered to the front drivetrain. At this point, the front left and right wheel produces the same negative torque output and "engine braking" cannot control individual braking as does the anti-lock braking system. When encountered by a slippery surface in engine braking, the driver applies brakes while disengaging the clutch to command a proper braking control to the vehicle. This allows the ABS braking to provide a safe deceleration performance.

Same as in the illustrated analogy, the torque generated by the electric motor is delivered equally to the left and right wheels whenever the motor is activated. In drive torque mode, the excessive positive torque can spin the front wheels when the tires exceed their traction limit, creating vehicle instability as the steer-ability is lost. Conversely, in brake torque mode, the excessive negative torque can lock-up the front wheels which will cause vehicle instability due to the loss of steer-ability. The research motivation of this study is rooted from this design constraint of the prototype hybrid vehicle.

3.3 SIEMENS Electric Motor Performance Analysis for Regenerative Braking and Drive Torque Assist Function

In order to accurately model the regenerative braking and drive torque assist function of the prototype *Pacifica* and study their effects, the electric motor performance is analyzed. The electric motor speed-reduction gear ratio and the drivetrain gear ratio are used to relate the vehicle speed and the motor power/torque output. The vehicle speed vs. motor power & torque

32

curves are obtained as a result. The achieved torque curve is used for analyzing the effects of regenerative braking on the prototype vehicle.

3.3.1 Statement of Assumption

Since the exact prototype hybrid system performance is yet to be tested and validated, the electric motor torque used in Sections 3.3.2 and 3.3.3 is an idealized value assuming a 100% efficiency in the hybrid power-electronics system. As well, it assumes that the state of charge (SOC) in the prototype ultracapacitor bank is at an ideal level to be able to provide a 100% excitation power for the induction motor and being able to absorb all the current produced by the electric motor for charging. This allows the design of an idealized prototype system, which can be scaled back appropriately when the prototype design is validated through testing.

As well, this exercise assumes a 100% drivetrain efficiency in torque transmission. This is because the accurate efficiency is unknown, and the study looks at the preliminary evaluation of the prototype design, with custom made components such as the speed-reduction gearbox. The actual efficiency can only be found from a direct measuring of the system performance, which is planned to be done in the Phase II of this project. Therefore, at this stage of the project, the ideal system performance calculation is a rather appropriate approach so that the measured data can be compared to the ideal system performance for the final evaluation.

3.3.2 SIEMENS Motor Performance Curves

The following motor performance data was obtained from the SIEMENS product specification information presented in Appendix A. The torque curves below essentially determine the regenerative and drive torque when commanded by the driver.
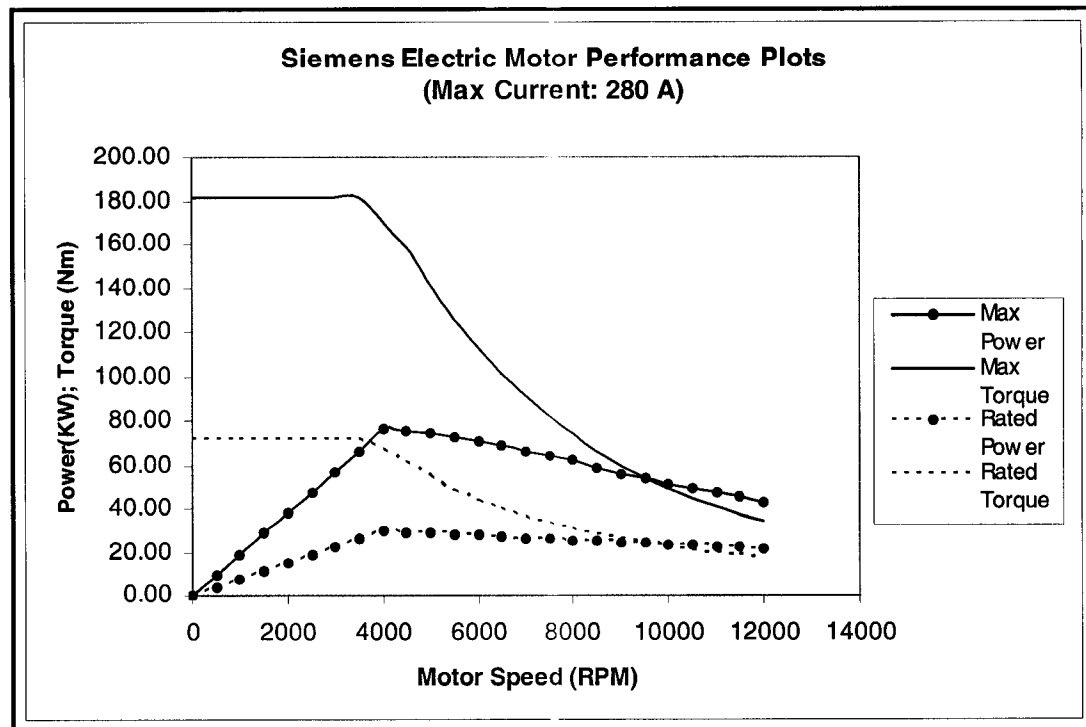
Figure 3.7 SIEMENS 1PV51334WS20 motor performance curves

3.3.3 Speed-Reduction Gearbox (Torque Coupler) Final Gear Ratio Selection

As the motor is permanently attached to the running drivetrain without a clutch device, the motor (rotor) continuously spins in all driving speed range. Therefore the maximum motor rpm (12,000 rpm) needs to be matched to the maximum vehicle design speed of 150 km/h. The final speed reduction gear ratio is designed to be 6.52 : 1 with the stock automatic transaxle gear ratio of 1.71 : 1. These gear ratios are multiplied together to the motor performance curves in order to calculate the actual motor torque and power delivered to the front two wheels of the prototype.

34

Siemens Electric Motor Performance @ Wheel
(Max Current: 280 A)
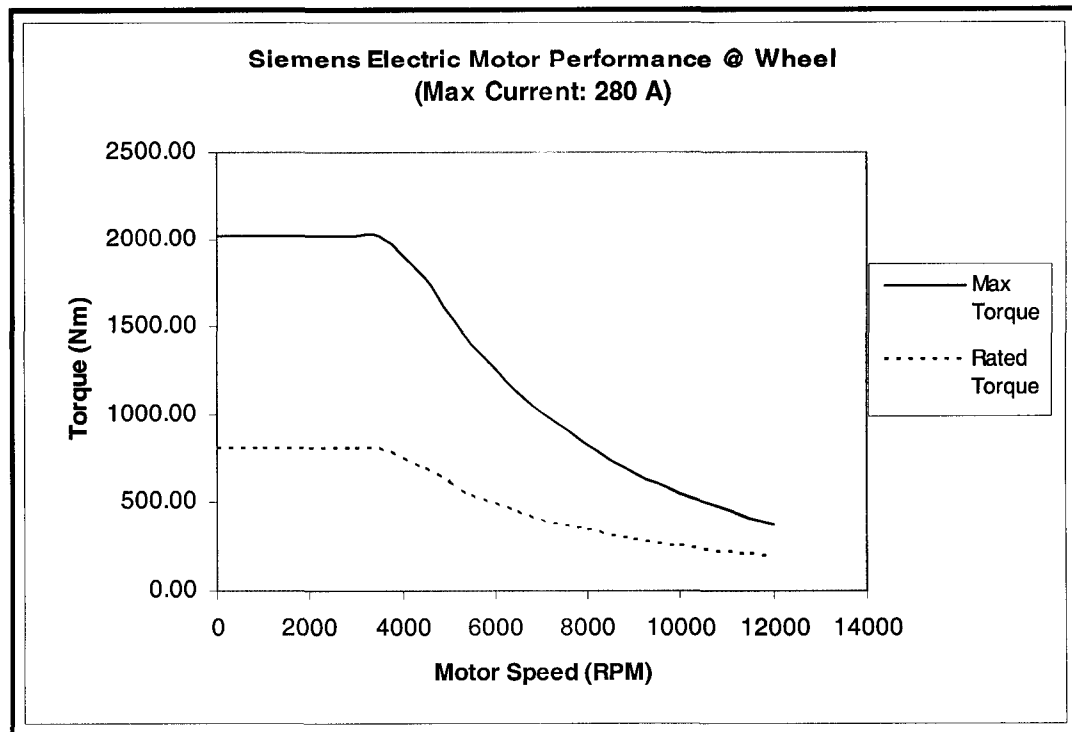
Figure 3.8 SIEMENS 1PV51334WS20 motor performance at the wheel

Over the vehicle speed range of 0 to 150 KPH, the above maximum torque can be generated in an idealized condition. The above torque curve is curve-fitted to obtain a polynomial function of 8th degree which is implemented in the electric motor torque calculator of the *Simulink* model discussed in Section 5.3.6.

3.4 Data Acquisition (DAQ) System for Hybrid *Pacifica*

The Figure 3.9 describes the overall hybrid system component interaction for operating the prototype vehicle. The DAQ system to be incorporated on the hybridized *Pacifica* enables hybrid CS & CD function (regenerative braking and motor assist) actuation by communicating driver's request to the hybrid system master controller, and monitoring the system characteristics for a safe and efficient operation. As well, a custom-design data acquisition system will allow the vehicle dynamics controller to asses the vehicle dynamics state and control the hybrid function appropriately for maintaining vehicle stability.

35

The prototype hybrid system employs the SIEMENS motor inverter and controller. Signal processing and data communication is done by the digital signal processor (DSP) onboard the motor inverter via controller area network (CAN) bus. MICROCHIP's PIC 18F458 microcontrollers are used for controlling throttle, brakes, energy management, and vehicle dynamics control system.
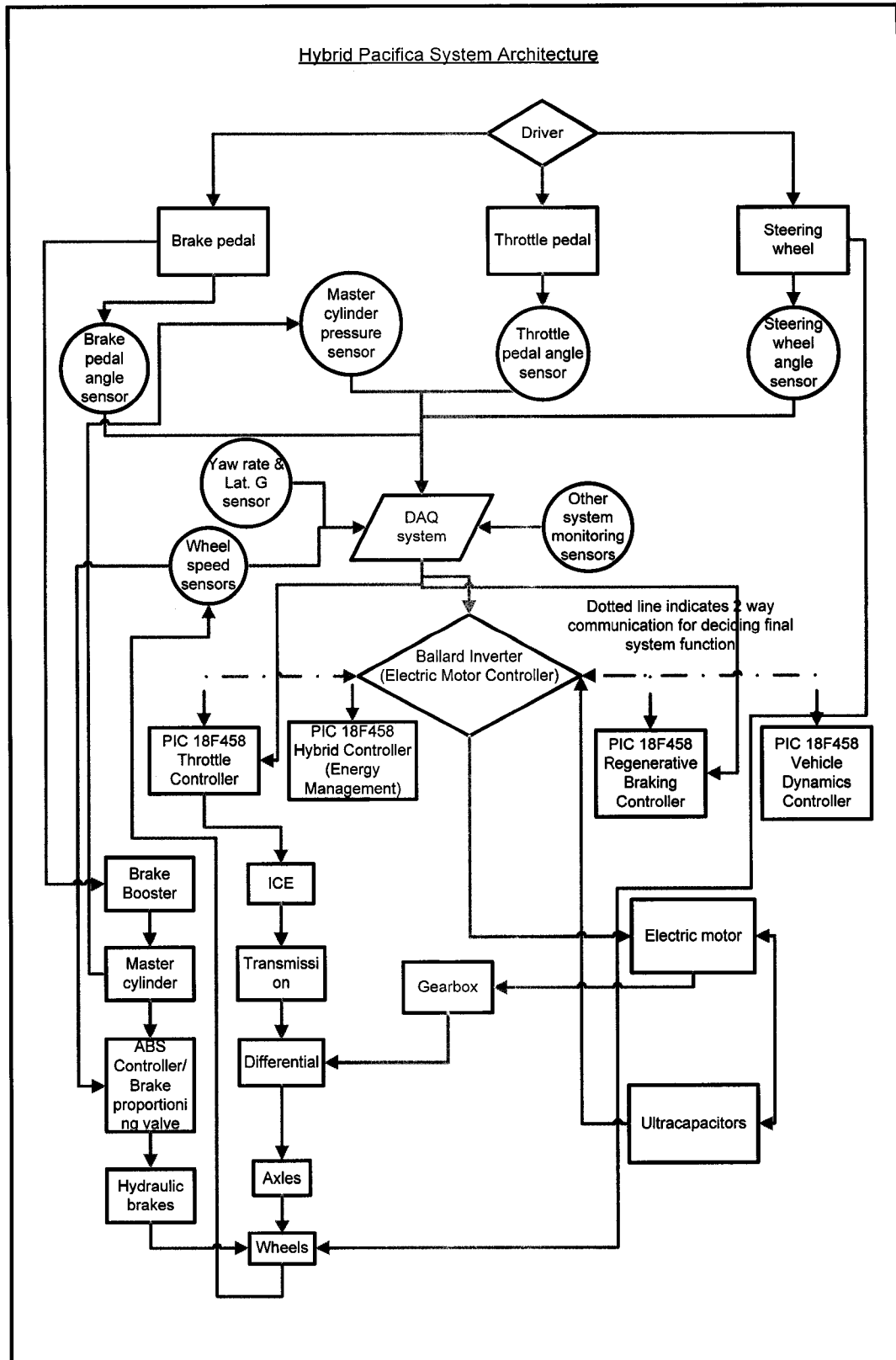
Figure 3.9 Hybrid Pacifica system architecture

37

The sensor data communication is done in two different environments. Custom sensors outlined in Appendix D will communicate via the controller area network (CAN) data bus which will be relayed to the master hybrid system controller. Stock sensors on *Pacifica* communicate via the programmable communication interface (PCI) data bus. The results are used for controlling the CS & CD functions of the hybrid system for maintaining the vehicle stability.

3.5 X-by-wire Technology

As controlling regenerative braking and motor assist function on the prototype is a crucial task which requires an integral controllability, the X-by-wire technology (brake & throttle) is implemented for the vehicle.

3.5.1 Brake-by-wire & *Pacifica* Stock Brake System

Chrysler Pacifica's stock brake system is the CONTINENTAL TEVES MARK 25 ABS system. It is a hydraulic operated friction brake system, using a diagonal split hydraulic system.[5] The system also features electronic variable brake proportioning (EVPB) to balance front-to-rear braking when brakes are applied in the partial braking range. The EVPB controls the braking force in the rear according to the front braking force to achieve an optimal braking performance (maintaining a near lock-up for maximum braking effect). [11] The stock brake system is designed and tested to the OEM specifications, meaning that the system is optimized for *Pacifica* to satisfy all government safety regulations. Therefore, modifying the brake system is a very critical task which requires an extensive design analysis, testing, and validation. [21]

The ideal braking system for the prototype hybrid is a fully integrated brake-by-wire system which would control both the regenerative braking and hydraulic braking seamlessly. Compared to a conventional hydraulic braking system, a brake-by-wire system has an electronic

---

[5] In the standard brake mode, the master cylinder primary circuit supplies pressure to the right front and left rear wheel brakes, and the secondary master cylinder circuit supplies pressure to the left front and right rear wheel brakes.

38

control unit that controls the hydraulics with an electric pump(s) to deliver brake line pressure independent of the pedal force when braking is commanded. An electronic pedal module with pedal angle sensor determines the driver's request by the pedal position and delivers the appropriate brake line pressure which actuates the hydraulic brake calipers for braking. In addition to providing an optimum braking behaviour, it is capable of realizing all required braking and stability assistance functions such as ABS, TCS, and ESC. [22]

However, implementing such a system is a considerable engineering task and requires necessary components customized for the *Pacifica* prototype (hydraulic pump unit, electronic controller unit, etc.). Most of all, developing an ABS algorithm to match the stock performance would also be a complex task[6]. Although this is the ideal and safer (if designed appropriately) *for controlling braking dynamics for the hybrid system, this system is not pursued for the scope* of this research. A brake-by-wire system that addresses the aforementioned issues is under investigation for future implementation in the vehicle.

3.5.1.1 Dual-Stage System: Electrical and Hydraulic

In the meantime, for its simplicity, the proposed design considered in this study is a "dual-stage" brake-by-wire system with a simulated pedal feel. It does not modify the CONTINENTAL TEVES ABS brake system and the regenerative braking is used as an independent, additional braking system by having two stages of braking pedal range. Stage I is a regenerative braking region and Stage II is a hydraulic braking region. The mechanical connection between the brake pedal and brake booster is decoupled to create an offset gap. This gap will be used for the regenerative braking pedal range. Once the pedal couples with the booster actuator rod, the hydraulic system is activated via driver's pedal force as is done conventionally. In order to alleviate the loose pedal phenomenon in Stage I, a torsional spring is

---

[6] ABS braking algorithm is proprietary technical information developed and kept by OEM brake and auto manufacturers.

integrated to the pedal lever. Inherently, there will be a two-stage (regenerative & hydraulic) pedal feel feedback; however, this may be advantageous in informing the driver in which braking that they are applying.

The *CTS 503 Adjustable Pedal Sensor* is equipped with two angular position sensors and is mounted on the pedal's rotational axis. The sensor signals are fed into the *LabJack* data acquisition terminal for the digital signal processor. The independent input signals are compared and processed to communicate the braking power request from the driver to the motor controller thus activating regenerative braking. In hydraulic braking range (Stage II), regenerative braking can still be activated ($T_{Total} = T_{Hydraulic} + T_{Regen}$) to provide requested braking power if necessary. The two sensor signals are compared with each other for the signal integrity and fault-detection as a safety check. If two signals deviate in a range exceeding a specified value, a system fault is signaled and regenerative braking function is suspended. Thus, the system will only work with the stock hydraulic system braking. The driver shall be alerted by a warning signal as the first stage braking (regenerative) is no longer available and the driver shall be trained to ignore the Stage I braking.

This presents a poor braking dynamics (drive-ability) and may be dangerous to untrained drivers. However, for the purpose of implementing a functional regenerative braking, the "dual-stage" system is deemed to be sufficient for the scope of this project. One very significant drawback of this design is the "loss" of braking in Stage I where regenerative braking is not activated due to the VDC intervention or due to the ultracapacitor[7] bank's SOC level being too high or low. A possible solution to avoid the loss of braking in Stage I is utilizing a resistor bank which will provide regenerative baking by allowing electric current generation. The current can be by-passed to the resistor bank where electric energy can be dissipated as heat. However, this still does not help the situation when SOC is too low to energize the generator function. Due

---

[7] Ultracapacitors are used for energy storage system in the Prototype *Pacifica.*

to the added complexity and weight of a resistor bank to the overall system, such system is not used in the design.

3.5.2 Throttle-by-wire

In a conventional system, the throttle valve is controlled by a cable attached to the throttle pedal. In a throttle-by-wire system, the mechanical connection is removed and in its place, position sensors are implemented to generate actuation signal according to the pedal angle. This signal triggers the electric actuator attached to the throttle body to control the throttle valve angle for desired power output. The benefits of these systems are such that transient (inefficient) phase of throttle operation is eliminated and the hybrid control system is "informed" for power demand and is able to generate the desired output by controlling engine and motor efficiently. A throttle-by-wire project is under investigation to be installed on the prototype hybrid *Pacifica*.

CHAPTER 4

VEHICLE MODELING FOR CO-SIMULATION

The vehicle simulation was done using the MECHANICAL SIMULATION CORPORATION's vehicle dynamics simulation software *CarSim 6.04*, along with MATHWORKS INC.'s *Matlab/Simulink* software where the vehicle dynamics controller was designed and developed through co-simulation. The MSC SOFTWARE's widely used *ADAMS/CAR* & *ADAMS/CONTROLS* softwares were given consideration for use. Due to *CarSim*'s better ability to interface with *Simulink* for co-simulation, it was decided to use *CarSim* for this study.

4.1 Vehicle Coordinate System

CarSim uses the ISO 8855 coordinate system that has X positive forward, Z positive up, and Y positive to the left-hand side of the vehicle. This is in contrast to the SAE J670e coordinate system, where Y is positive to the right and Z is positive down. It has six degrees of freedom along its three axes- translation along and rotation about each axis. Rotation about the X axis is roll (p); about the Y axis is pitch (q); and about the Z axis is yaw (r).

42
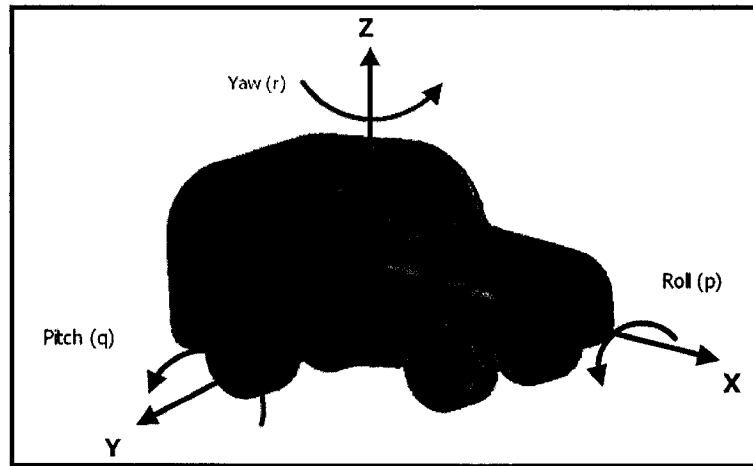
Figure 4.1 Vehicle coordinate system

4.2 Prototype Vehicle Modeling in *CarSim*

4.2.1 Vehicle Mass & Dimensional Properties

The prototype hybrid *Pacifica* is modeled in *CarSim* based on the stock *Pacifica* mass and dimensional properties. Major hybrid components such as the AC electric motor, motor inverter & controller, gearbox, motor cooling system, and ultracapacitor bank are modeled in the simulation model with the most accurate knowledge of mass and dimensions according to the current project development stage. The final prototype mass with the driver is determined to be 2325 Kg with a driver (80 Kg), motor and gear box assembly (88 Kg), and ultracapacitor bank (72 Kg). These mass properties are located in the *Pacifica* model at their design locations as show in Figure 4.2. The rest of hybrid component mass is applied at the vehicle CG. *CarSim* uses these properties to adjust the inertial properties and ride height of the vehicle, to simulate the vehicle with the loaded conditions.

43
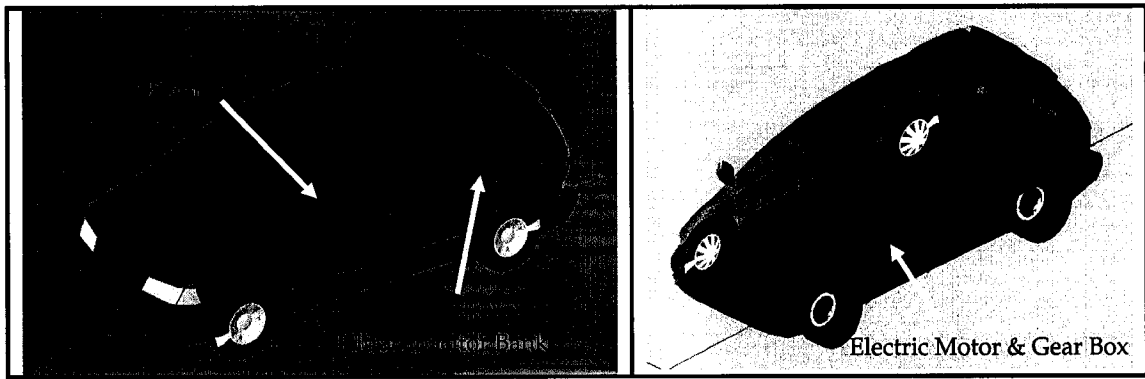
Figure 4.2 Hybrid Pacifica with driver & hybrid components

Inertia properties in roll, pitch, and yaw (I_{xx}, I_{yy}, and I_{zz}) were extrapolated from the National Highway Traffic Safety Administration (NHTSA) test data on the Static Stability Factor of the 2004 Chrysler *Pacifica* and similarly sized vehicles' inertia properties. [23] The detailed mass and dimensional values are provided in Appendix C.

4.2.2 Suspension Kinematics & Compliances

Suspension kinematics and compliances data are crucial properties of a vehicle suspension that represent the motion of the vehicle suspension, relative to the sprung mass. The accurate information of these data will simulate the vehicle in motion accurately for realistic results. Accurate measurement of such data requires a special suspension measurement fixture.

A satisfactory measurement of both front and rear suspension kinematics points of *Pacifica* was taken to produce representative kinematics curves for the simulation model. The points were measured by using strings, plumb bob, square, and a measuring tape. The measurement contains some known inaccuracy as some of the points were inaccessible to measure directly; however, such inaccuracy is negligible in this study. Steering kinematics was not measured but the rack and pinion steering assembly gear ratio of 17.8 : 1 is used in simulation. The wheels were left on the hub in order to maintain the ride height at normal loading condition. However, the resulting suspension properties would not cause significant error in the simulations.

44
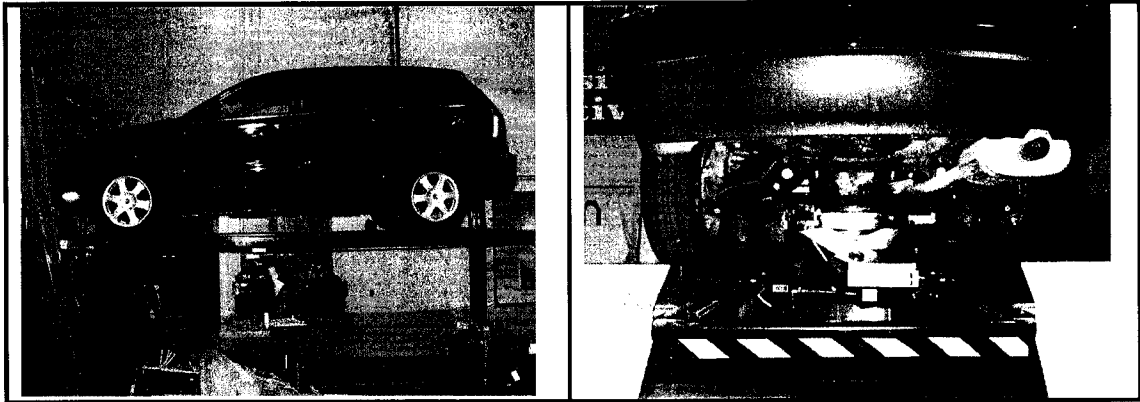
Figure 4.3 2004 Chrysler Pacifica AWD on hoist for kinematics measurement

Racing by the Numbers, a kinematics analysis program, is used to generate kinematics curves using the measured suspension hard-points data. Caster, Wheelbase Change, Camber, Toe, and Lateral Movement (scrub) kinematics curves are implemented in *CarSim* model.

Compliances data cannot be measured without a sophisticated and purpose-built measuring fixture. So the *CarSim* generic "Minivan" compliances data were adopted for simulation. As well, for suspension spring rate and damping, the generic *CarSim* "Minivan" data were used. These values are reasonable representations of the actual values since the production *Pacifica* shares similar dimensional and mass properties with minivans.

4.2.3 Tire Data

It is a well known fact that the virtual vehicle simulation results are largely dependent on the tire data used. This is because the tire is the medium for transferring vehicle forces with the road interaction. Because tire is made of rubber, its reaction to forces is non-linear, which makes it very difficult to define the characteristics. Often tire manufactures do not share the proprietary information. Studies have been done in an attempt to model tire characteristics for realistic simulation results. The most trusted method of simulating tire is by the use of "Magic Tire Model" developed by Hans Pacejka of Delft University in Netherlands. The "Magic Tire Model" is a set of interpolation equations that are derived from the empirical data of tire forces. *CarSim* is

45

able to handle Pacejka 5.2 tire model; however, the representative model for *Pacifica*'s tire data (Michelin Energy MXV4 Plus P235/65R17) was not available[8].

CarSim features "Internal Tire Model" which is derived from a various tire data which represents a generic behaviour of the selected tire class. The internal *CarSim* "Big SUV Tire" model with the effective rolling radius of 0.353 m was used for simulating *Pacifica*.

4.2.4 Aerodynamics Data

A coefficient of Drag (C_D) value of 0.355, a frontal area of 2.84 m², and a reference length of 2.954 m are used for the aerodynamic modeling of the prototype. These values account for the aerodynamic resistance to the vehicle at all speeds and the vehicle orientations.

4.2.5 Hybrid Powertrain & Drivetrain Modeling

As the hybrid drivetrain layout is of a special design, *CarSim* does not support hybrid powertrain configurations so it was created in the *Simulink* function block instead. In all simulations of this study, the vehicle model is set to maintain a certain speed to execute braking simulations. Therefore, exact engine output per throttle input is, in this case, irrelevant. As used in simulating regenerative braking torque, the same electric motor torque curve can be used to describe the additional torque output of the hybrid powertrain. Engine fuel map and power curves were obtained from Chrysler Technical Center (CTC). [24 & 25] SIEMENS electric motor performance curves were obtained from a SIEMENS publication source. However, the engine maps are not used in this study as the dynamic throttle input is not simulated.

As hybrid drive train layout is of a special design, *CarSim* does not support hybrid drivetrain configurations. Although it is not possible to create a simulation model with a hybrid drivetrain, it can be represented mathematically within vehicle input and output parameters.

---

[8] Delft-Tyre, the company that publishes Pacejka model information was contacted. Tire information for Goodyear 245/70/R16 which is similar to *Pacifica*'s tire, was available for purchase for US$1,450. Due to the high cost, the data was not purchased.

46

Within *Simulink*, the electric motor torque curve of Figure 3.8 is created using Eq. 5.9. The torque output values are directly linked to *CarSim* as a brake torque (My_brk) input to each of the front wheels. This torque is activated by brake command and applied to the vehicle along with the hydraulic braking torque. The *Simulink* power/drivetrain model is discussed in detail in Section 5.3.6.

4.3 *CarSim* & *Simulink* Co-simulation Interfacing

4.3.1 Hybrid *Pacifica* Bicycle Model Implementation in *Simulink*

The following vehicle parameters of Table 4.1 are implemented in the bicycle model used in the *Simulink* model which is verified to yield a realistic result in Chapter 6.

Table 4.1 Bicycle model parameter values for hybrid Pacifica

Mass (kg)	Izz (kgm²)	a (m)	b (m)	C_f (N/rad) for both tires	C_r (N/rad) for both tires
2325	4309.356	1.359	1.595	90756.8	96257.0

With the lack of tire data, the "cornering stiffness" coefficients were obtained by using curve-fit data of *CarSim*'s lateral tire force (F_y) and tire slip angle (α) output data. These are obtained from the Equations 2.10 and 2.11.

4.3.2 *CarSim* and *Simulink* Co-simulation Interfacing

The ultimate goal of implementing the bicycle model to the vehicle dynamics controller is to calculate the discrepancy between the driver's intended vehicle path and the vehicle's actual path and provide a controlled electric motor torque output to maintain the vehicle stability. In order to verify the bicycle model-based controller is a well-suited application for the purpose, the co-simulation method is chosen to validate the controller performance. Through iterative co-simulation, the VDC design is optimized for the control performance. It can be understood that the non-linear *CarSim* model represents the prototype hybrid *Pacifica* and the *Simulink* controller

47

model represents the actual microprocessor-based Vehicle Dynamics Controller implemented on the prototype.

As well, the co-simulation verifies the DAQ system design architecture that is to be implemented on the prototype. Lateral state variables: lateral acceleration, yaw rate, body slip angle, and the rate of body slip angle change are calculated from the *CarSim* model, these variables are extracted to be compared to the same variables of the bicycle model for validity.

Co-simulation allows running the same simulation in the two different software environments; therefore, eliminates the need of analyzing the simulations independently at a different time. Moreover, it enables interactively controlling the simulation parameters through the interface. In this study, the developed *Simulink* controller controls the CS and CD functions of the *CarSim* vehicle model based on the parameters supplied by *CarSim* in the simulation. The outcome is a VDC controller (*Simulink*) performance evaluation on the virtual prototype vehicle model (*CarSim*). Vehicle dynamics simulation in *CarSim* can be exported to the *Simulink* environment via the 'S-function' block. Using export variables of the 'S-function' block, the vehicular behaviour can be investigated by the *Simulink* simulation. The details are discussed in Chapter 5.

48

CHAPTER 5

VEHICLE DYNAMICS CONTROLLER

The primary objective of the conventional electronic stability control (ESC[9]) system is to provide vehicle stability and handling predictability by using microprocessors, vehicle motion sensors, and vehicle control actuators. This is achieved by recognizing the driver's intended path of vehicle travel and actively controlling the vehicle motion to guide the vehicle following the driver's commanded path without causing vehicle instability. The driver's intended path can be calculated by using the steering input and vehicle speed input (brake/throttle) and the vehicle motion control can be done by actuating vehicle subsystems: such as a brake system or the engine.

The very important and major difference between the conventional ESC and the developed vehicle dynamics controller (VDC) is as follows. "The electronic stability program (ESP) is a system that relies on the vehicle's braking system as a tool for "steering" the vehicle." [20] In other words, appropriate braking at the individual wheel(s) is activated independently to balance the yaw moment of the vehicle about the z-axis in order to maintain the vehicle stability. On the contrary, the VDC cannot command independent braking to control the yaw moment of

---

[9] Electronic Stability Control (ESC) is an SAE conventional term.

49

the prototype vehicle due to the inherent system design[10]. It monitors the vehicle dynamic states

and only allows the electric motor's braking (or driving) torque when such torque will not

disturb the vehicle yaw moment. As well, it eliminates the regenerative brake lock-up to provide

the vehicle steer-ability. As a closed-loop control system, the developed VDC increases the safety

of the prototype hybrid electric vehicle and its performance is verified through the simulation in

Chapter 6.
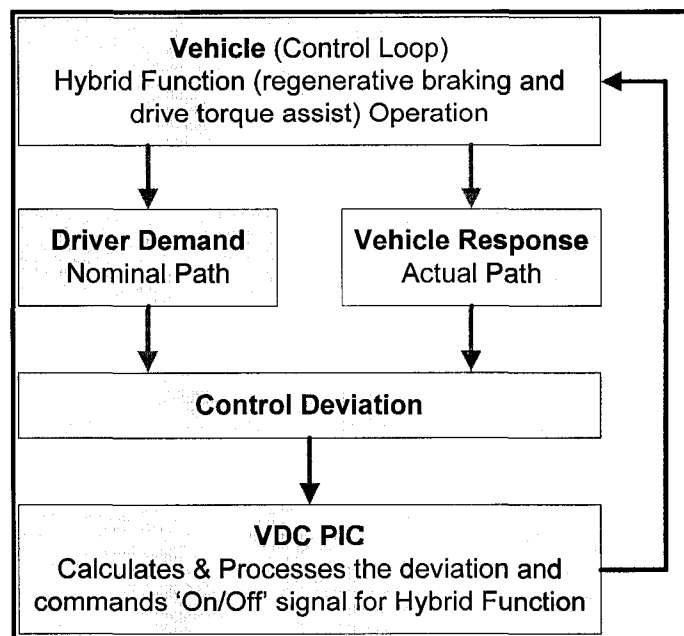
Figure 5.1 The developed VDC operation flowchart

Another design difference is that ESC processes the "nominal" and "actual" values of

both yaw rate and body slip angle to correct the yaw moment. VDC processes the "nominal" and

"actual" values of the lateral acceleration (yaw rate) and only calculates the actual body slip angle

to control the regenerative braking and drive torque assist function. The following table

summarizes the main difference between the conventional ESC and VDC.

---

[10] Recall that regenerative braking is delivered by the front two wheels through the common motor drive shaft; therefore, the individual braking control in the regenerative braking mode is impossible with the prototype system.

Table 5.1 Major differences between conventional ESC and developed VDC

	ESC	VDC
Control Method	$(r_{nominal} - r_{actual})$ & $(\beta_{nominal} - \beta_{actual})$	$(r_{nominal} - r_{actual})$ & β control
Control Execution & Effect	-Individual wheel braking or engine torque retardation for yaw moment control to regain vehicle stability -Keeps vehicle on driver intended path	- Wheel lock-up prevention in CS mode & wheelspin prevention in CD mode to avoid incipient vehicle instability - Keeps vehicle on driver intended path & increases regenerative braking and electric motor torque assisted acceleration performance

5.1 Development of Vehicle Dynamics Controller

Following the conventional ESC architecture, a controller is developed which calculates the nominal vehicle lateral acceleration and compares it to the actual vehicle lateral acceleration to determine driver's intent. However, when this control is used on slippery surfaces, a deviation occurs in lateral acceleration (higher response) and yaw rate (faster response) as the road coefficient of friction is lower than the normal. As a result, the vehicle lateral speed (v) increases rapidly and therefore body slip angle (β) increases ($\beta=v/u$) more than the normal situation. Figure 5.2 shows the different vehicle response to the same driver input of steer and vehicle speed.

51
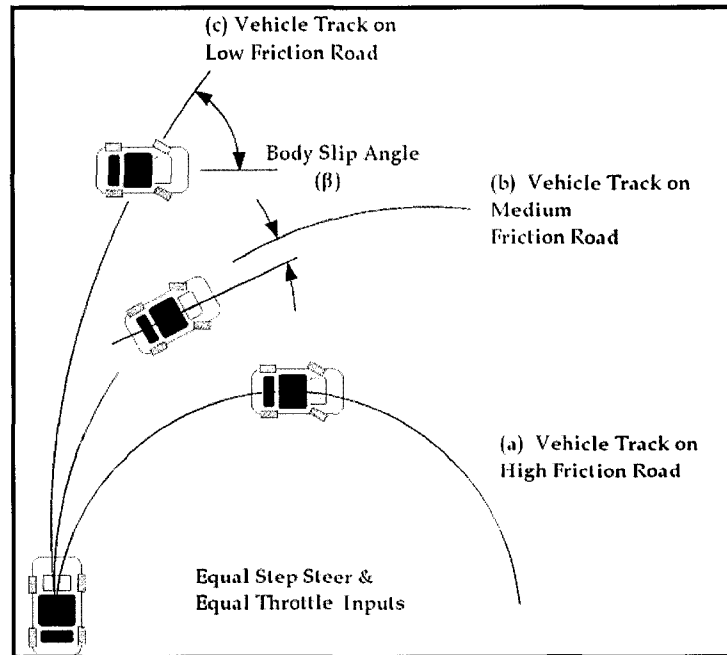
Figure 5.2 Vehicle response to the same driver input on
high & low μ-conditions

The nominal response is what the driver commands based on his/her experience on normal (high-μ) driving conditions. When the vehicle travels on a low-μ surface with the same input, it deviates from the driver's intended path and the yaw rate increases due to the lack of traction at tires and the body slip angle increases accordingly. Derived from this phenomenon, controlling the lateral acceleration and body slip angle response is an effective and robust method to control the vehicle motion. Calculating road friction conditions is unnecessary as estimating the nominal lateral acceleration and comparing it to the actual lateral acceleration to determine the path deviation is sufficient. This deviation is the direct result of the road μ-conditions.

5.2 Overall VDC Architecture

The following Figure 5.3 shows the overall architecture of the Vehicle Dynamics Controller (VDC) where various sensor and command signals are connected to sub-controller blocks to monitor the vehicle dynamics states and calculate the motor torque delivery signal for

52

hybrid system functions (CS & CD). The controller simulation environment contains *CarSim* and

Simulink, where the co-simulation is executed at the same simulation time-step.
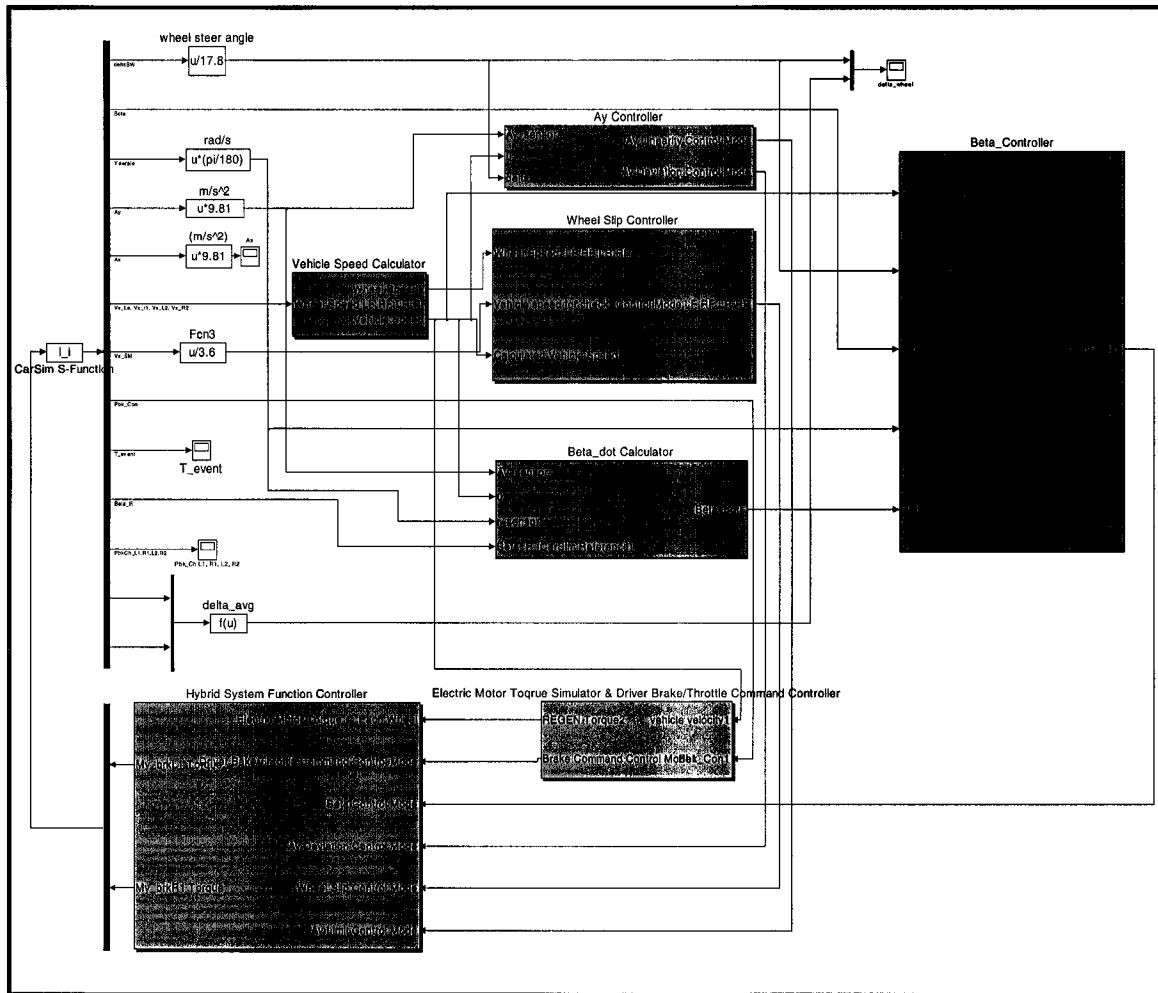
Figure 5.3 Overall VDC design architecture

The *CarSim* simulation block is represented by the 'S-function' block, namely "*CarSim* S-

Function". This block enables the *CarSim* and *Simulink* interfacing for exchanging data for

calculations. Predefined output values (export channel variables) from *CarSim* are relayed as

signals to each sub-controller blocks where calculations are performed. The export channel

variables are listed in the following table.

53

Table 5.2 CarSim 'S-function' Export Channel variable list

Export Channel Variables

1	δ_{SW}	7	R1 Wheel Speed	13	$\dot{\beta}$
2	β	8	L2 Wheel Speed	14	L1 Brk. Chmbr. Press.
3	r	9	R2 Wheel Speed	15	R1 Brk. Chmbr. Press.
4	a_y	10	Vehicle Speed	16	L2 Brk. Chmbr. Press.
5	a_x	11	Brake Cont'l Press.	17	R2 Brk. Chmbr. Press.
6	L1 Wheel Speed	12	Sim. Time	18 & 19	L1 & R1 Wheel Steer Angle

Similarly, the final command signals for brake torque or drive torque of the VDC are imported to the "CarSim S-Function" block to relay the motor torque output for CS or CD function to the CarSim model. The import channel variables are listed in the following table.

Table 5.3 CarSim 'S-function' block Import Channel variable list

Import Channel Variables

1	FL Brake Torque Output
2	FR Brake Torque Output

It is noted that although the import channel variable is named as brake torque output, it receives a positive torque (drive torque) in the case of CD function execution. As the import/export data exchange is done simultaneously, the VDC can process the signals from the CarSim simulation model in order to control the electric motor torque output and maintain the vehicle stability.

54

5.3   Vehicle Dynamics Controller Operation Process

There are seven subsystems in the VDC as listed in the following table.

<div align="center">

Table 5.4 VDC subsystems

VDC Subsystems

</div>

1	Vehicle Speed Calculator
2	Wheel Slip Controller
3	A_y Controller (Linearity Limit & $A_{y\_nominal}/A_{y\_actual}$ Ratio Threshold Limit)
4	$\dot{\beta}$ Calculator
5	β Controller
6	Electric Motor Torque Simulator
7	Hybrid System Function Controller

5.3.1 Subsystem1- Vehicle Speed Calculator

The vehicle speed calculator takes each rectilinear wheel speed through Input Port1. Through Output Port1, the four speeds are relayed for calculating the wheel slip in the next subsystem. Through Output Port2, the vehicle speed, which is obtained by Eq. 5.1, is relayed to the next subsystem.

$$\left(\frac{u_{L1} + u_{R1} + u_{L2} + u_{R2}}{4} \right) = u_{vehicle} \qquad \text{[Eq. 5.1]}$$

<div align="center">55</div>
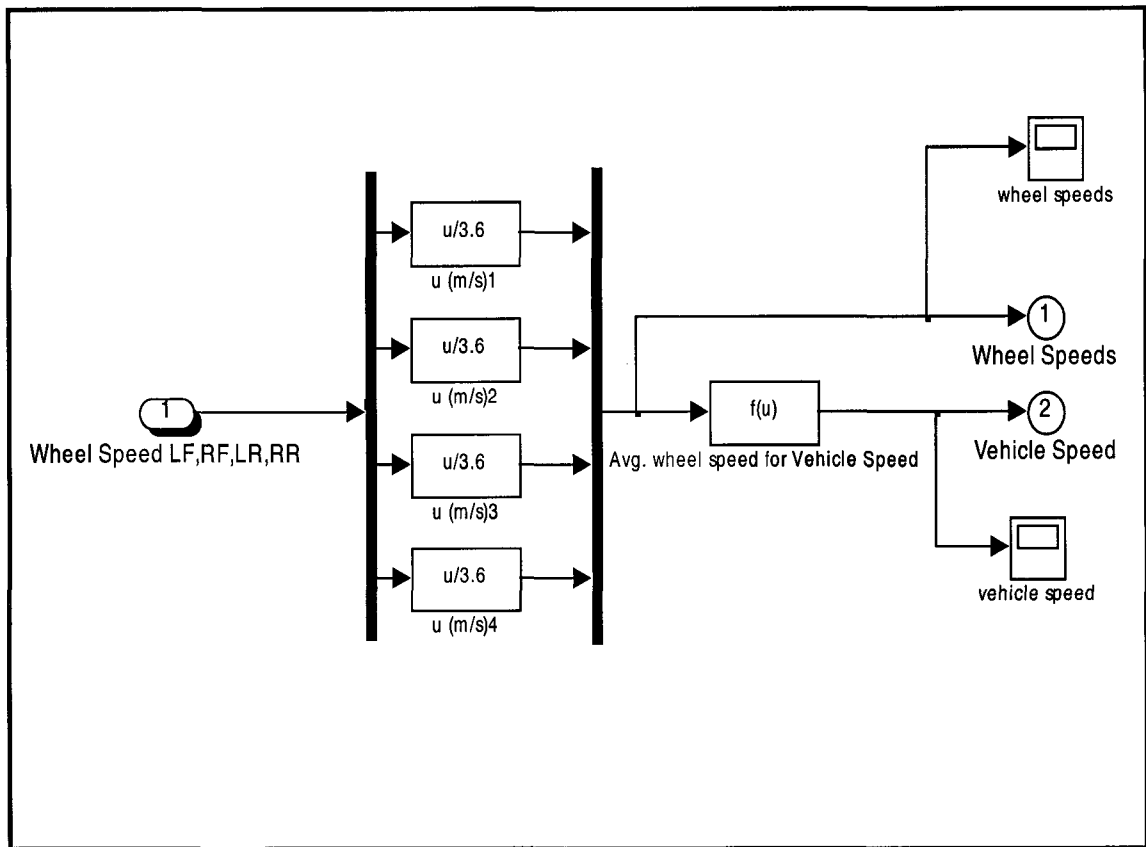
Figure 5.4 Vehicle speed calculator subsystem block

On the prototype *Pacifica*, the wheel rotation pulse signal will be processed via DAQ to calculate each wheel's rectilinear speed using Eq. 5.2.

$$u_{wheel} = \omega_{wheel} \times r_d$$

[Eq. 5.2]

5.3.2 Subsystem2- Wheel Slip Ratio Calculator

The wheel slip ratio calculator employs the similar logic as the ABS wheel slip controller. The underlying principle is controlling the slip on each wheel for maximum braking force generation. Recall that wheel slip is necessary to generate braking/traction force. From various literatures sources [7 & 8], it is found that wheel slip ratio of up to 0.18 is found to be effective for braking force generation. Therefore, the wheel slip ratio threshold value is set to 0.18 for suspending CS and CD function. The calculated vehicle speed (Input Port3) and wheel speeds

56

(Input Port1) from the previous subsystem are used as input variables. The calculated vehicle speed is used as the reference value for each wheel speed to calculate the wheel slip ratio.

$$\lambda = \frac{\left| u_{wheel\_L1} - u_{vehicle} \right|}{u_{vehicle}}$$

[Eq. 5.3]
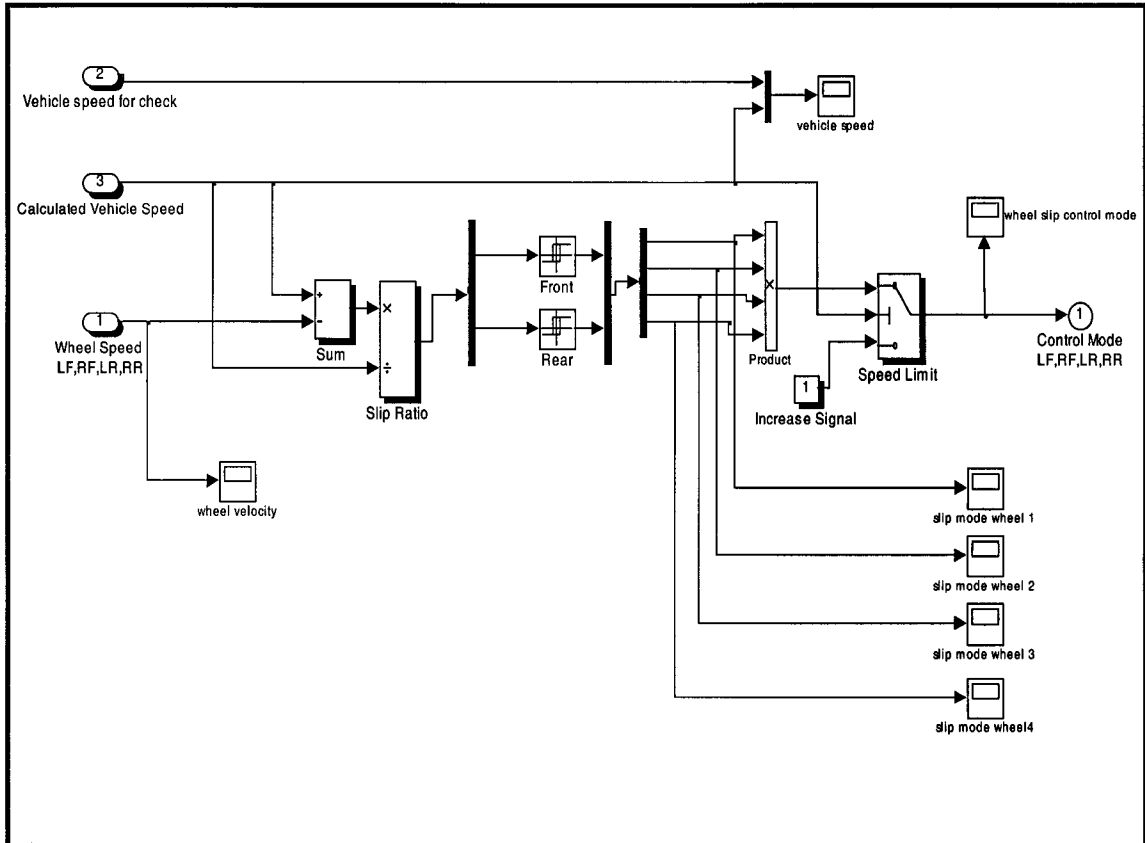
Figure 5.5 Wheel slip controller subsystem block

Both front and rear wheel slip threshold ratios are set to be 0.18 to trigger "OFF" signal for CS and CD functions. Each wheel produces its own 'ON/OFF' (1/0) signal for the hybrid system function and each signal is converged using a multiplication block. As a result, the converged signal delivered to the 'Output Port1' contains 'ON' (1) signal for the commanded hybrid function when each and every wheel slip ratio is less than 0.18. When the slip ratio exceeds 0.18, output of 'OFF' (0) is processed for that wheel control mode, identifying that the wheel is slipping excessively beyond the point where there is insufficient traction between the

57

tire and the road. This suspends the hybrid system functions as the vehicle would be under

unstable conditions and only ABS brakes are used to decelerate/control the vehicle in the case of

CS function. At speeds lower than 0.83 m/s, the slip control is bypassed so wheel lock-up or

wheelspin is allowed at very low speeds. This is analogous to standard ABS systems.

5.3.3 Subsystem3- Lateral Acceleration (A_y) Controller

This controller performs two independent threshold checks for lateral acceleration

information. Firstly, it checks the lateral acceleration is under a threshold value of 7.00 m/s² (0.71

g) as the prototype is capable of gripping to the road up to the value of a_y = 7.36 m/s² from the

preliminary simulations.
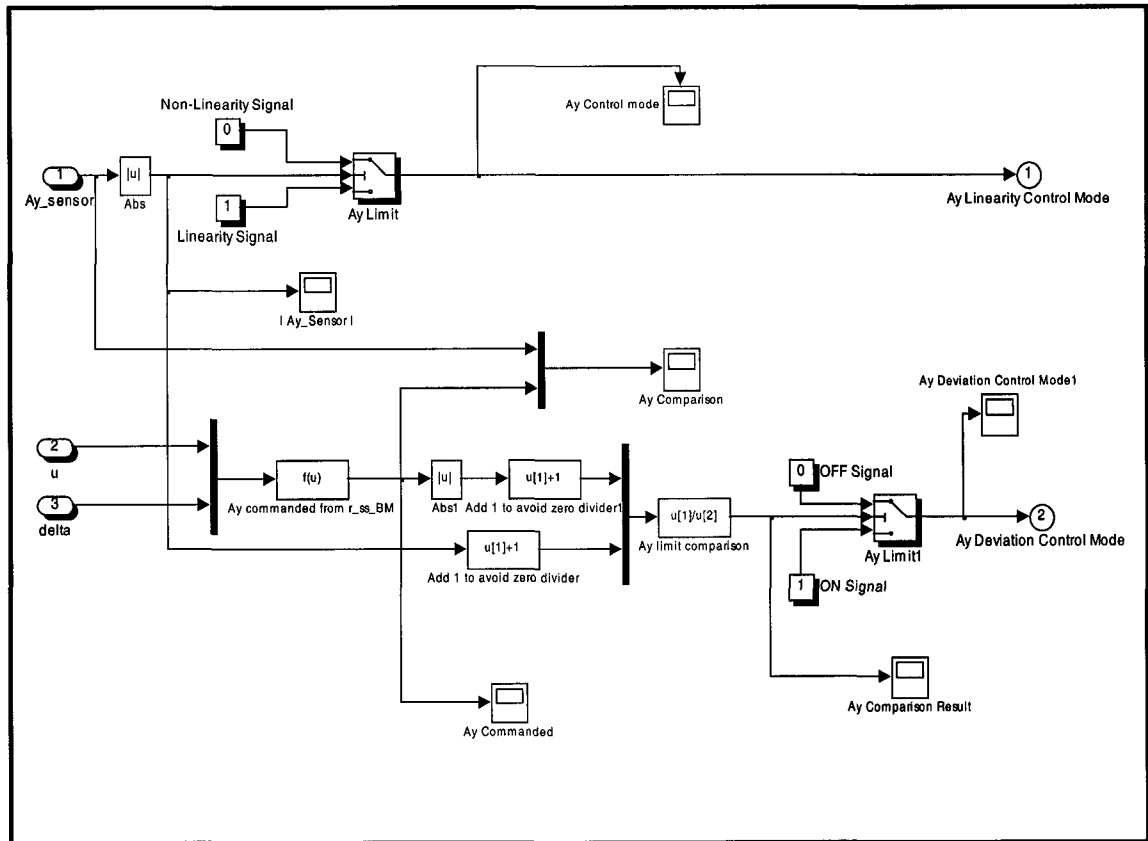
Figure 5.6 A_y controller subsystem block

Secondly, it calculates and compares the nominal lateral acceleration to the actual lateral

acceleration measured. The nominal lateral acceleration (Eq. 5.5), or steady-state lateral

58

acceleration, is essentially a rearranged transfer function of steady-state yaw rate (r_{ss}) from the following Eq. 5.4 and Eq. 2.16.

$$r_{ss} = \frac{a_{y\_measured}}{u} \qquad \text{[Eq. 5.4]}$$

$$a_{y\_no\,min\,al} = \left\{ u^2 \middle/ (a+b) - \left[\frac{m(ac_f - bc_r)}{(a+b)c_f c_r} \right] \right\} \delta_{wheel} \qquad \text{[Eq. 5.5]}$$

As discussed previously, the nominal lateral acceleration indicates what the driver is commanding for the vehicle response. Using Eq. 5.5, the nominal value is then compared to the actual lateral acceleration value (measured) to determine the delivery of hybrid function. The addition of 1 is implemented to avoid having an indeterminate value result due to the zero denominator.

$$a_y Ratio = \frac{\left| a_{y\_no\,min\,al} \right| + 1}{\left| a_{y\_measured} \right| + 1} \qquad \text{[Eq. 5.6]}$$

When $a_{y\_nominal}$ is greater than the a_{y_actual}, it essentially means that the driver is demanding more lateral force (via greater steering input and/or forward speed input) than what the vehicle is capable of responding due to the traction limit at the tire/road contact. At this instance, giving up the braking force (longitudinal traction force) allows gaining lateral traction force at the tire as discussed in Section 2.4.3. As a result, the vehicle responds to the driver's steering input better and thus follows the intended path better. This is the reason for suspending CS and CD function when a_y ratio threshold is reached. The threshold value for the ratio is set to 2 after a successive iteration in order to provide improved braking while maintaining a good steer-ability of the vehicle.

59

5.3.4 Subsystem4- $\dot{\beta}$ Calculator

The rate of body slip angle change, $\dot{\beta}$, is calculated to determine whether the vehicle is in a transient or non-transient (steady) state while in operation. In this controller design, it enables calculating the body slip angle without using a time derivative calculation as discussed in the section 5.3.5. Using the available sensor signals, namely a_y, u, and $r_{measured}$, it can be found as:

$$\dot{\beta} = \frac{a_y}{u} - r_{measured} \qquad \text{[Eq. 5.7]}$$
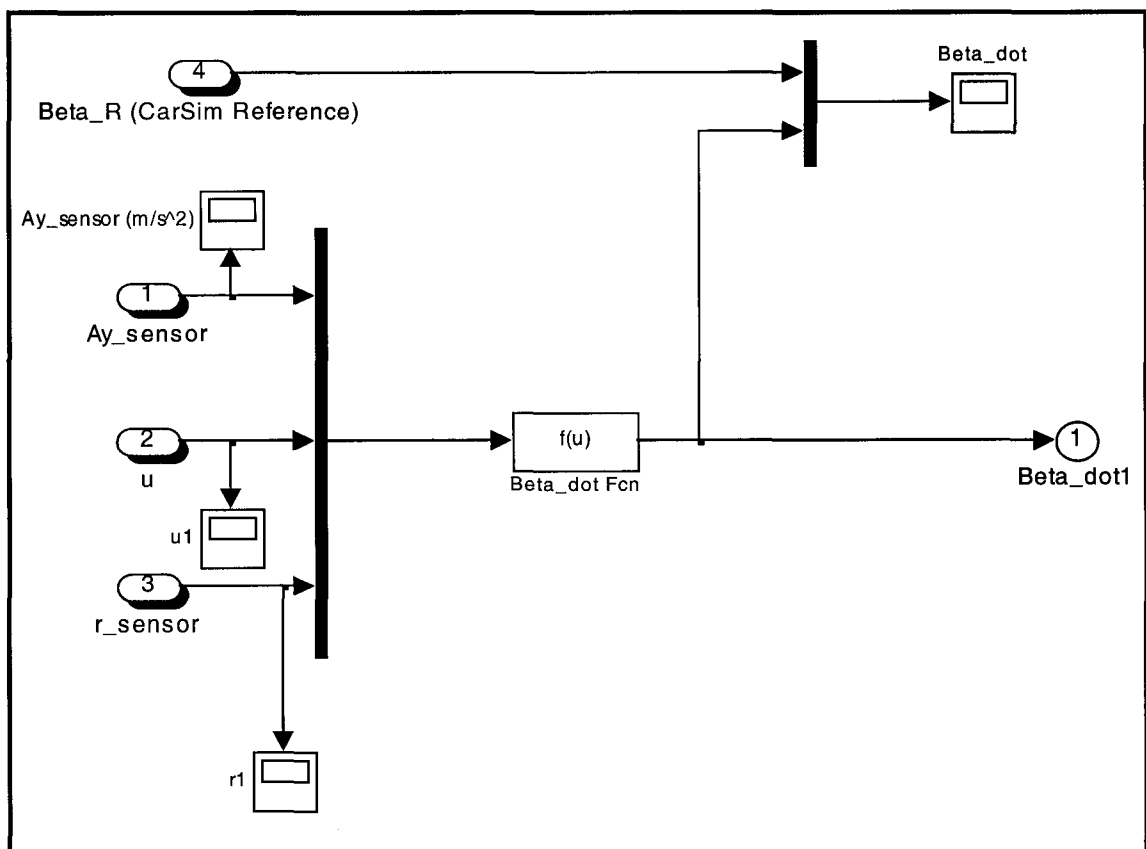
Figure 5.7 $\dot{\beta}$ calculator subsystem block

$\dot{\beta}$ information is relayed to the β controller subsystem to calculate body slip angle in both steady-state and transient state conditions.

60

5.3.5 Subsystem5- Body Slip Angle (β) Controller

The β controller has four inputs: u, δ_{wheel}, $r_{measured}$ and $\dot{\beta}$. It calculates the theoretical body slip angle for both steady-state and transient conditions with the rate of body slip angle change. The result produces a reasonable estimation to the actual body slip angle of the vehicle where the direct measurement by a sensor is impossible. The equation for the body slip angle is obtained by rearranging Eq. 2.16 and Eq. 5.7 into the following form.

$$\beta = \frac{\left[c_f \delta - (ac_f - bc_r)\frac{r_{measured}}{u} - \left(mu(\dot{\beta} + r_{measured})\right)\right]}{(c_f + c_r)} \qquad \text{[Eq. 5.8]}$$

Figure 5.8 β controller subsystem block

61
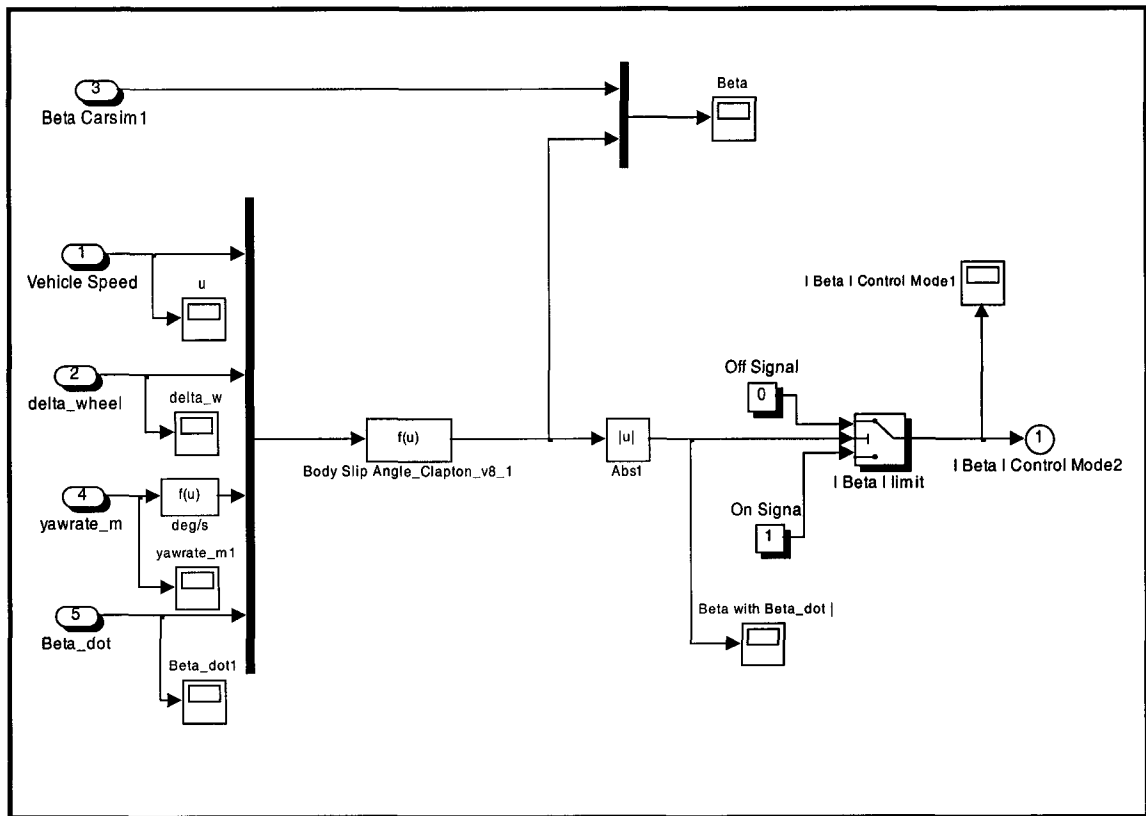
It is found that on high-friction surfaces, vehicle maneuverability is lost when β exceeds about 10° in magnitude[11], whereas on packed snow this value is 4°. [5] In addition, typical drivers are found to be inadequate in controlling vehicles with greater than 2° of body slip angle. [4] Therefore, the threshold limit of the β is set to the magnitude of 4°.

5.3.6 Subsystem6- Electric Motor Torque Simulator

Two different subsystem blocks are described here for CD and CS functions. Both subsystems calculate the available motor torque assuming 100% system efficiency i.e. the optimal S.O.C level to provide the 100% motor torque delivery.

The SIEMENS electric motor performance curve (Appendix A) is used to generate an 8th order polynomial function which closely represents the motor torque curve as a function of vehicle speed.

$$\tau_{ElectricMotor} = -3.2768e^{-8}x^8 + 5.5847e^{-6}x^7 - 3.7968e^{-5}x^6 + 0.012953x^5$$
$$- 0.22635x^4 + 1.8054x^3 - 5.2543x^2 + 1.6423x + 1014.3$$

[Eq. 5.9]

In the case of CS function command, a negative torque output is calculated. In the case of CD function command, a positive torque output is calculated.

The following Figure 5.9 shows the CS function (regenerative braking) block and it is designed to work with the prototype vehicle design speed of 0 km/h to 150 km/h. In this block, the brake control command from the driver input is processed to convert it to a brake 'ON/OFF' signal which is also relayed to the 'Hybrid System Function' controller. The CS function torque is simulated as an embedded system of the stock vehicle brake system. In simulation, when the driver presses the brake pedal, both the regenerative braking and ABS braking system is applied for braking.

---

[11] This was also confirmed by *CarSim* simulations of the prototype hybrid *Pacifica*.

62
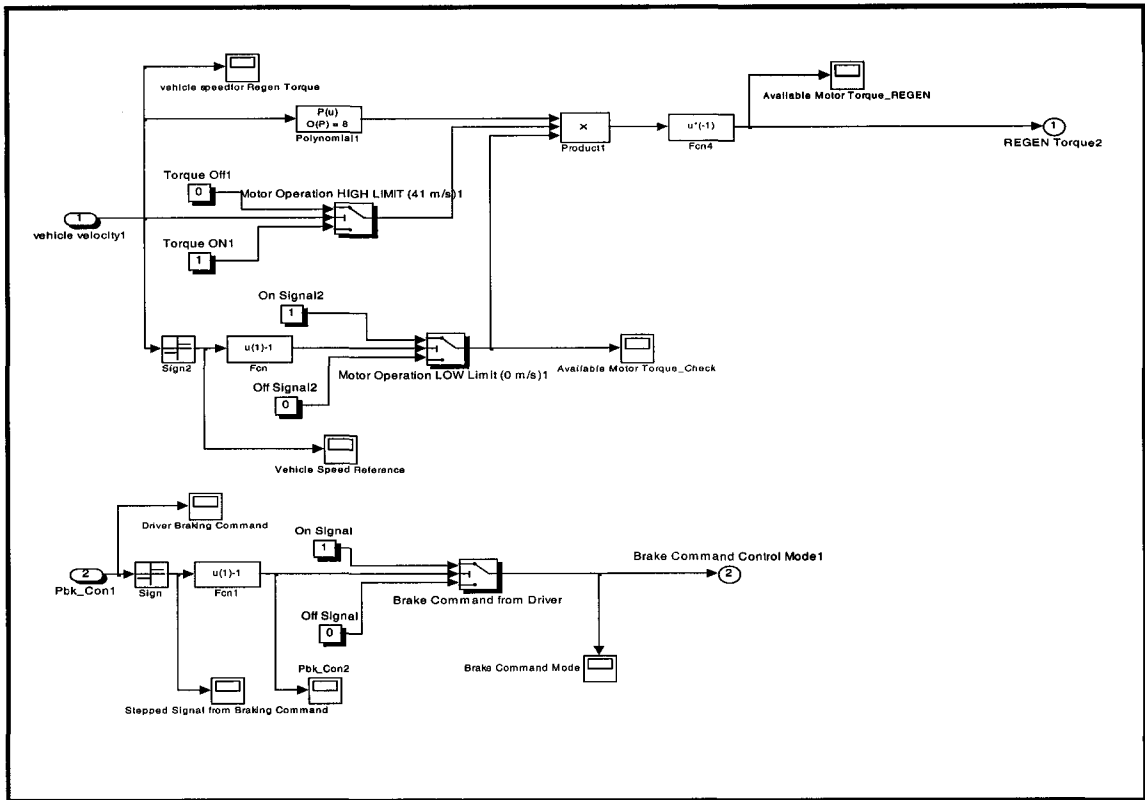
Figure 5.9 Electric motor torque simulator for regenerative braking (CS function) subsystem block

The available torque value is then delivered to the 'Hybrid System Function' controller to provide the braking torque at the front two wheels.

The following Figure 5.10 shows the CD function (drive torque assist) block and it is also designed to work with the prototype vehicle design speed of 0 km/h to 150 km/h. In this block, the throttle control command from the driver input is processed to convert it to a drive torque assist 'ON/OFF' signal which is then relayed to the hybrid system function controller. The CD function torque is simulated as an embedded system of the stock powertrain system. In simulation, when the driver presses the throttle pedal, both the drive torque assist of EM and ICE torque are applied for accelerating.

63
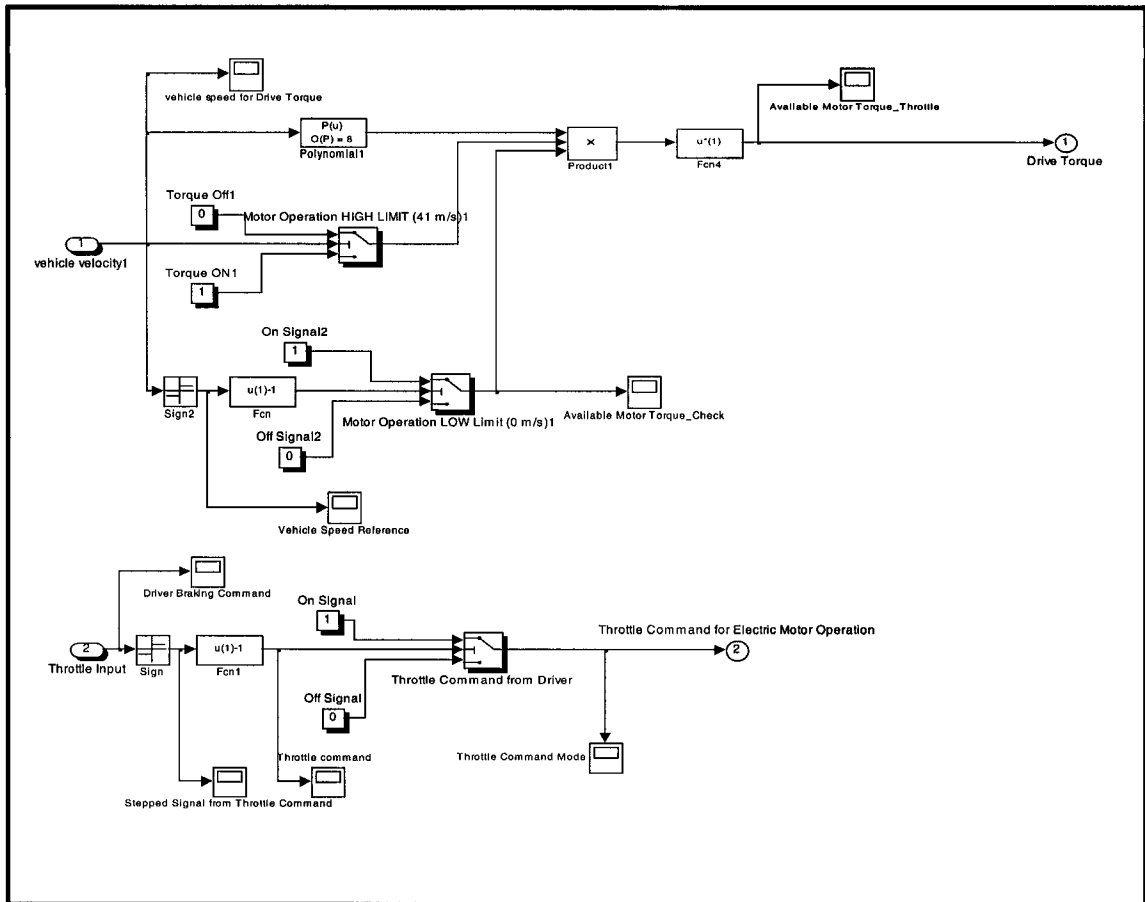
Figure 5.10 Electric motor torque simulator for drive torque assist (CD function) subsystem block

The available torque value is then delivered to the hybrid system function controller to provide the driving torque at the front two wheels.

5.3.7 Subsystem7- Hybrid System Function Controller

The Hybrid System Function controller, a Boolean logic controller, collects all the 'ON/OFF' actuating signal data from each of the subsystems to determine the final braking or drive torque delivered by the electric motor.

64
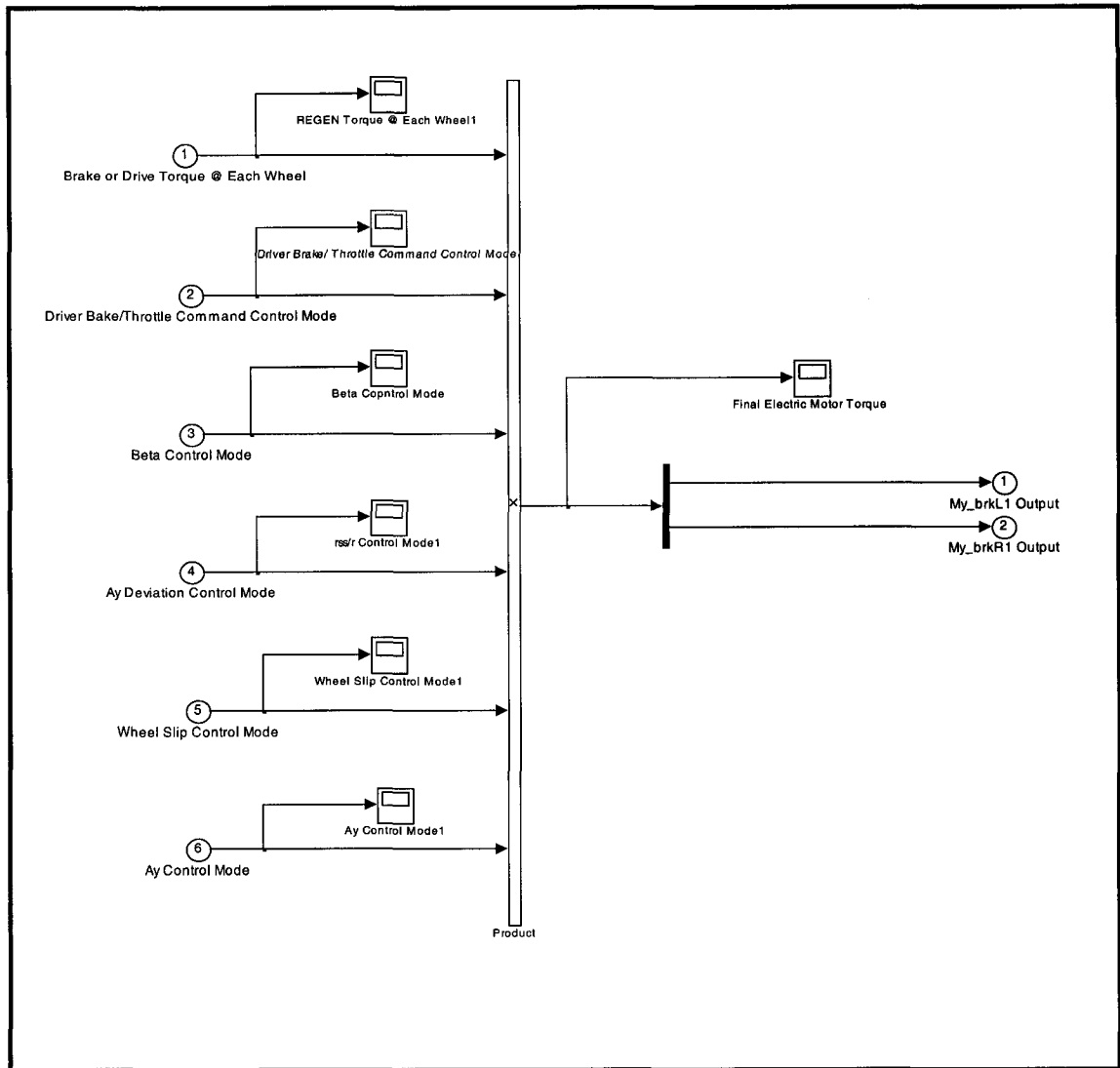
Figure 5.11 Hybrid system function controller subsystem block

The controlled torque is delivered to each of the front wheels as a braking or driving torque. Only the Input Port1 has the actual value of the transformed brake or drive torque and this value is multiplied by the 'ON/OFF' signal of each subsystem controller to control the final torque delivery. This in return controls the regenerative braking or drive torque assist function to work seamlessly with the simulation model ABS system or ICE in maintaining the prototype's vehicle stability in decelerating or accelerating operation.

65

5.4 VDC System Implementation using PIC18F458 μ-Controller

The above *Simulink* VDC design is implemented to a microprocessor using Microchip's PIC18F458. Details of the system architecture, data acquisition sensor implementation and Assembly language code details are included in Appendix D.

66

CHAPTER 6

VEHICLE DYNAMICS CO-SIMULATION

The goal of co-simulation was to investigate the realistic driving situations and evaluate the performance of the developed vehicle dynamics controller in maintaining the vehicle steer control and its lateral stability. First, the co-simulation interface validation is done using a set of steady-state and transient-state simulations. This is to verify how well the linear bicycle model matches the non-linear *CarSim* model in calculating vehicle dynamics states: nominal lateral acceleration ($a_{y\_nominal}$) and body slip angle (β).

For evaluating the VDC performance in CS function, three cases of transient-state simulations are performed to investigate the effect of VDC control on the regenerative braking. Then, the VDC system performance integration is validated with a vehicle configuration of an embedded regenerative braking with the stock ABS braking system.

For evaluating the VDC performance in CD function, two cases of transient state simulations are performed to investigate the effect of VDC control on the drive torque assist function. The VDC performance is validated for its ability to control the extra traction torque from the electric motor in acceleration mode (while the ICE traction torque is active).

67

6.1 Linear and Non-linear Model Response

The bicycle model is a linear system which uses a set of equations describing the vehicle motion (v & r) as discussed in Section 2.5. However, the *CarSim* simulation model uses a multi-DOF, non-linear mathematical model which represents the vehicle response in a more realistic manner. It is observed that, although effectively close for the VDC, the linear model response is inevitably different than the non-linear model, causing discrepancy in the vehicle state calculation. The source of discrepancy is from the non-linearity of the *CarSim* model primarily stemming from the tire model, suspension & steering kinematics and compliances.

6.2 Steady-State & Transient State Simulation

The steady-state condition analysis is performed to investigate the vehicle stability characteristics and more importantly to determine the stability threshold limits of the vehicle dynamics parameters under investigation.

The transient state simulation is performed to analyze how the vehicle responds to the dynamic steering and forward speed inputs[12]. Transient-state (dynamic) driving conditions represent the majority of driving situations. Therefore, it is vital to investigate the system response in transient conditions in order to control the vehicle stability in dynamic driving situations. The transient analysis is done to simulate real-world driving conditions that are common in causing vehicle instability. This approach allows investigation of realistic driving situations in order to evaluate the VDC performance. Also, this simulation demonstrates the limited yet very effective results of the linear bicycle model in calculating nominal lateral acceleration and body slip angle.

---

[12] Forward speed of vehicle is controlled by the throttle and brake input of the driver.

68

6.3   Simulation Model Configurations

For the development of the Vehicle Dynamics Controller (VDC), four cases of vehicle configuration were considered as follows.

Table 6.1 Vehicle configuration cases

Vehicle Design Configuration	
Case A	Hybrid *Pacifica* equipped with two front wheel hybrid system function only **without VDC** (ORANGE)
Case B	Hybrid *Pacifica* equipped with two front wheel hybrid system function only **with VDC** (WHITE)
Case C	Hybrid *Pacifica* equipped with two front wheel hybrid system function with stock powertrain and drivetrain functions **without VDC** (RED)
Case D	Hybrid *Pacifica* equipped with two front wheel hybrid system function with stock powertrain and drivetrain functions **with VDC** (BLACK)

Each vehicle configuration is tested for CS and CD functions of the hybrid system operation in developing Vehicle Dynamics Controller for the prototype hybrid *Pacifica*

69

6.4 Simulation Cases

Following Tables 6.2 and 6.3 summarize a select number of simulations performed in order to develop and validate the performance of the vehicle dynamics controller (VDC).

Table 6.2 Simulations performed for VDC evaluation and validation on CS function

6.5 Interface Development Validation	6.6 VDC Performance Validation on Regenerative Braking System		6.7 VDC Performance Validation on Hybrid Braking (REGEN+ABS) System	
	6.6.1 Without VDC Control (Orange)	6.6.2 With VDC Control (White)	6.7.1 Without VDC Control (Red)	6.7.2 With VDC Control (Black)
STEADY STATE I. SSC (μ=1.00) 30 KPH 60 KPH 90 KPH 120 KPH 150 KPH	I. SLB @ 100 KPH Mu=0.20 Mu=0.2L/0.6R Mu=0.85	I. SLB @ 100 KPH Mu=0.20 Mu=0.2L/0.6R Mu=0.85	I. SLB @ 100 KPH Mu=0.20 Mu=0.2L/0.6R Mu=0.85	I. SLB @ 100 KPH Mu=0.20 Mu=0.2L/0.6R Mu=0.85
TRANSIENT STATE II. DLX (μ=1.00) 30 KPH 60 KPH 90 KPH 120 KPH 150 KPH	II. DLX @ 90 KPH Mu=0.2/0.6 Mu=0.50 Mu=0.85 III. HWY EXIT RAMP @ 90 KPH Mu=0.6L/0.2L Mu=0.50 Mu=0.85	II. DLX @ 90 KPH Mu=0.2/0.6 Mu=0.50 Mu=0.85 III. HWY EXIT RAMP @ 90 KPH Mu=0.6L/0.2L Mu=0.50 Mu=0.85	II. DLX @ 90 KPH Mu=0.2/0.6 Mu=0.50 Mu=0.85 III. HWY EXIT RAMP @ 90 KPH Mu=0.6L/0.2L Mu=0.50 Mu=0.85	II. DLX @ 90 KPH Mu=0.2/0.6 Mu=0.50 Mu=0.85 III. HWY EXIT RAMP @ 90 KPH Mu=0.6L/0.2L Mu=0.50 Mu=0.85

Three stages of simulation are discussed in the following sections. The first stage is conducted to validate the *CarSim* vehicle model and *Simulink* Controller model interfacing and evaluate the responses of the nonlinear *CarSim* model and linear bicycle model in steady-state and transient-state conditions. This proves how the linear bicycle model is an effective estimator for the nonlinear *CarSim* model. The second stage is conducted to analyze the regenerative braking performance alone in conjunction with VDC. The third stage is conducted to see how embedded regenerative braking behaves with the existing ABS brake system at the vehicle system level in conjunction with VDC.

70

Table 6.3 Simulations performed for VDC evaluation and validation on CD function

6.8 VDC Performance Validation on Hybrid Powertrain (EM + ICE) System	
6.8.1 Without VDC Control (Red)	6.8.2 With VDC Control (Black)
I. SLA @ 60 KPH a) Mu=0.20 b) Mu=0.2L/0.6R c) Mu=0.85	I. SLA @ 60 KPH a) Mu=0.20 b) Mu=0.2L/0.6R c) Mu=0.85
II. DLX @ 60 KPH a) Mu=0.2/0.6 b) Mu=0.50 c) Mu=0.85	II. DLX @ 60 KPH a) Mu=0.2/0.6 b) Mu=0.50 c) Mu=0.85

Since the CS function has the same operational principle as the CD function, only the integrated hybrid powertrain system design is considered for the simulation discussions.

For the sake of space, only the most crucial system performance of each case is discussed in detail, which is in the split-μ condition. It is also noted that although the VDC system succeeds in maintaining the vehicle stability, the calculation results shown for the nominal lateral acceleration and body slip angle are the least accurate compared to the other simulation results. This is because the split friction condition (μ = 0.2L/0.6R) creates the greatest vehicle instability due to the traction limit disparity between the left and right tires of the vehicle. This disparity creates the largest yaw moment imbalance for the vehicle. Appendix E contains additional simulation results of a high road friction condition, where the linear bicycle model responses are very close to the non-linear *CarSim* results. This indicates that the bicycle model is a good estimator of the non-linear system response where the road coefficient of friction is high.

6.5 Simulation Interface Validation: Bicycle Model Evaluation with *CarSim* Model

The first purpose of this simulation is to verify that *CarSim* and *Matlab/Simulink* environments are interfaced seamlessly in order to conduct co-simulations. The second purpose

is to validate that the linear bicycle model is an effective and representative model as an estimator to the non-linear *CarSim* model. With validation, the developed method is verified to be valid for the VDC system development. The final and most important reason is to derive threshold limit values for the control variables of VDC via steady-state and transient-state simulations.

6.5.1 Steady State Simulation

According to van Zanten et al., it is useful to start the validation of the vehicle within the linear range of the model where the linear response of a vehicle is conventionally seen at less than $a_y = 0.4$ g (3.92 m/s^2) with $\mu = 1.0$. [4] Therefore, simulations are performed at $\mu=1.0$ surface starting from a low vehicle speed to the maximum vehicle speed of the prototype (150 km/h). The vehicle speed was maintained at a preset value in each case. Then it was increased incrementally to see the effects of non-linear behaviour of the model where a_y is greater than 0.4 g level.

Two cases of simulation at 90 KPH and 120 KPH are presented. The 90 KPH simulation is shown since the lateral acceleration is at the limit of linear response region. The 120 KPH simulation is shown since the lateral acceleration actually coincides with the actual test result[13] of 7.36 m/s^2. Simulations performed under 90 KPH resulted in good response behaviour and 150 KPH simulation showed unstable vehicle response.

---

[13] Motor Trend magazine conducted a 60 m radius skid pad test to find out the average lateral acceleration limit of 0.75 g for 2004 Chrysler *Pacifica*. [26]

72

6.5.1.1 Constant Radius Track Cornering (R= 150 m) @ 90 KPH, μ=1.00
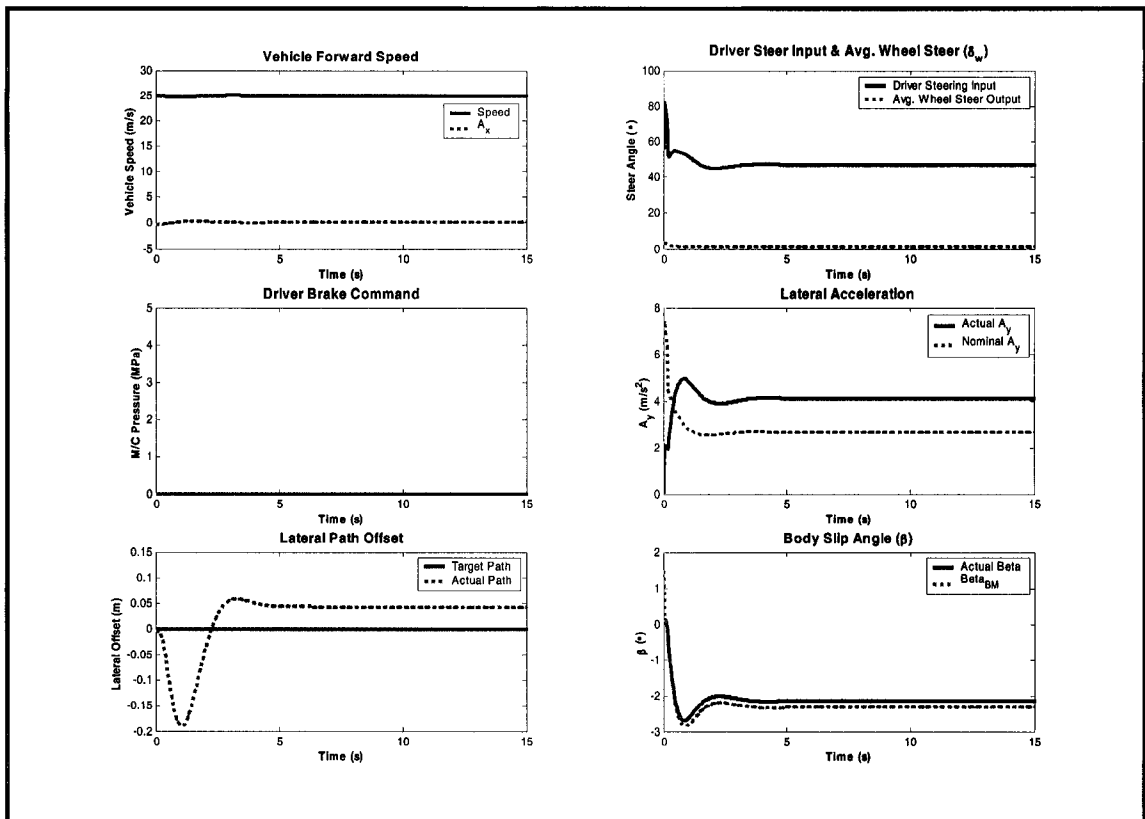
Figure 6.1 Steady State cornering of hybrid Pacifica @ 90 KPH; μ=1.00

The actual lateral acceleration is at 4.10 m/s², which is at 0.42 g level. The $a_{y\_nominal}$ response is at 2.67 m/s². The reason for such disparity in the nominal lateral acceleration is because it is found using the steady state yawrate transfer function of the bicycle model. The fairly large (worst among all SSC simulations) error of 34.87 % is derived from the non-linearity of *CarSim* model in its suspension and steering kinematics and compliances. The disparity between the bicycle model's curve-fit linear tire data vs. the non-linear empirical data of the *CarSim* model is another major source of error. This can be validated since at a higher lateral acceleration level (shown in the next simulation), the a_{y_actual} and $a_{y\_nominal}$ are very close to each other.

Both body slip angle responses are very close (β_{actual} = -2.13° vs. β_{BM} = -2.31°). This can be explained as β_{BM} is found with "measured" data (a_y & r) of actual vehicle state in its transfer

73

function; therefore, its result is very close to the actual value. The lateral offset is at 0.05m which is negligible for the vehicle path deviation. The following table summarizes the peak value comparison of lateral acceleration and body slip angle values of the simulation.

Table 6.4 Summary of lateral acceleration and body slip angle results

	a_{y_CarSim} (m/s²)	$a_{y\_nominal}$ (m/s²)	β_{CarSim} (°)	β_{BM} (°)
Results	4.10	2.67	-2.13	-2.31
Error Margin (%)	34.88		8.45	

74

6.5.1.2   Constant Radius Track Cornering (R= 150 m) @ 120 KPH, μ=1.00
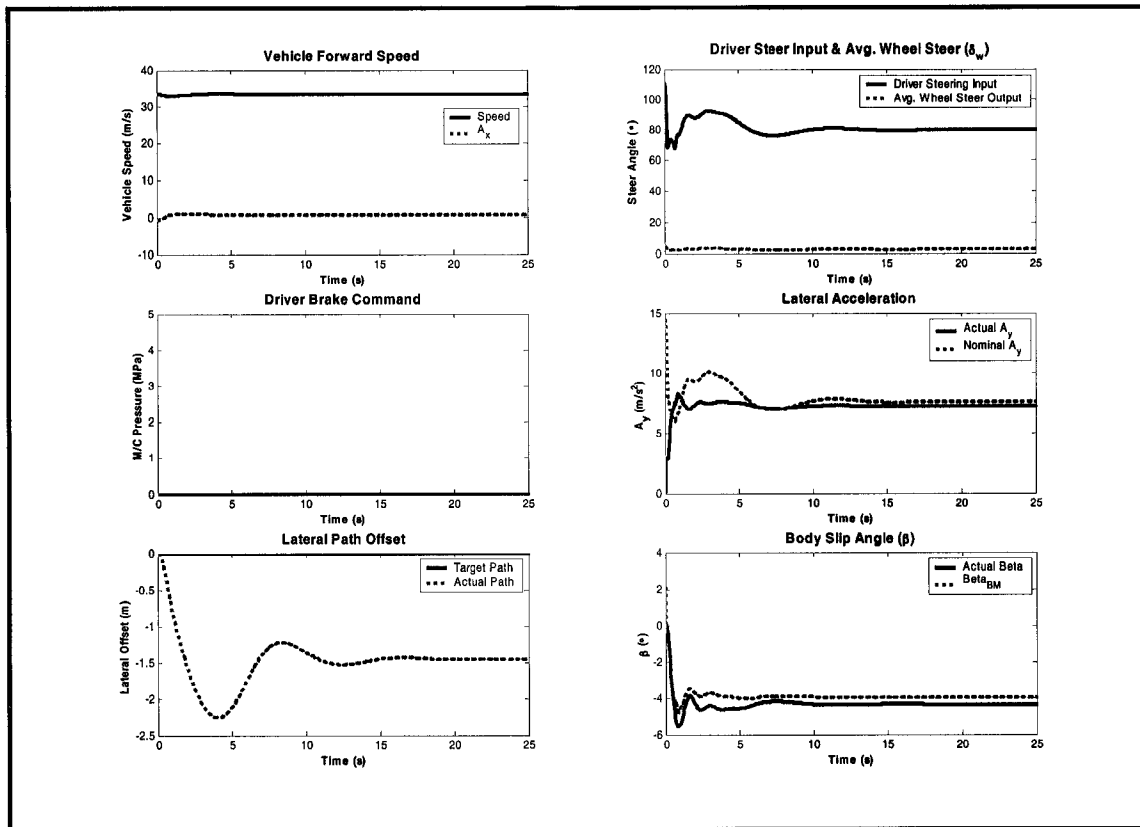
Figure 6.2 Steady State cornering of hybrid Pacifica @ 120 KPH; μ=1.00

The above figure shows the vehicle response very close to the production *Pacifica*'s actual lateral acceleration limit of 7.36 m/s². This close result can be a good indicator that the simulation model created with various assumptions is in fact a very good representative model of the actual *Pacifica*. At 120 KPH, the vehicle takes more time to reach its steady state. The following table summarizes the peak value comparison of lateral acceleration and body slip angle values of the simulation.

Table 6.5 Summary of lateral acceleration and body slip angle results

	a_{y_CarSim} (m/s2)	$a_{y\_nominal}$ (m/s²)	β_{CarSim} (°)	β_{BM} (°)
Results	7.23	7.61	-4.33	-3.96
Error Margin (%)	5.26		8.55	

75

The same reasoning applied in the previous 90 KPH run can be applied to explain the margin of error between the non-linear and linear models.

6.5.2 Transient State Simulation
6.5.2.1 Double Lane Change @ 90 KPH, μ=1.00
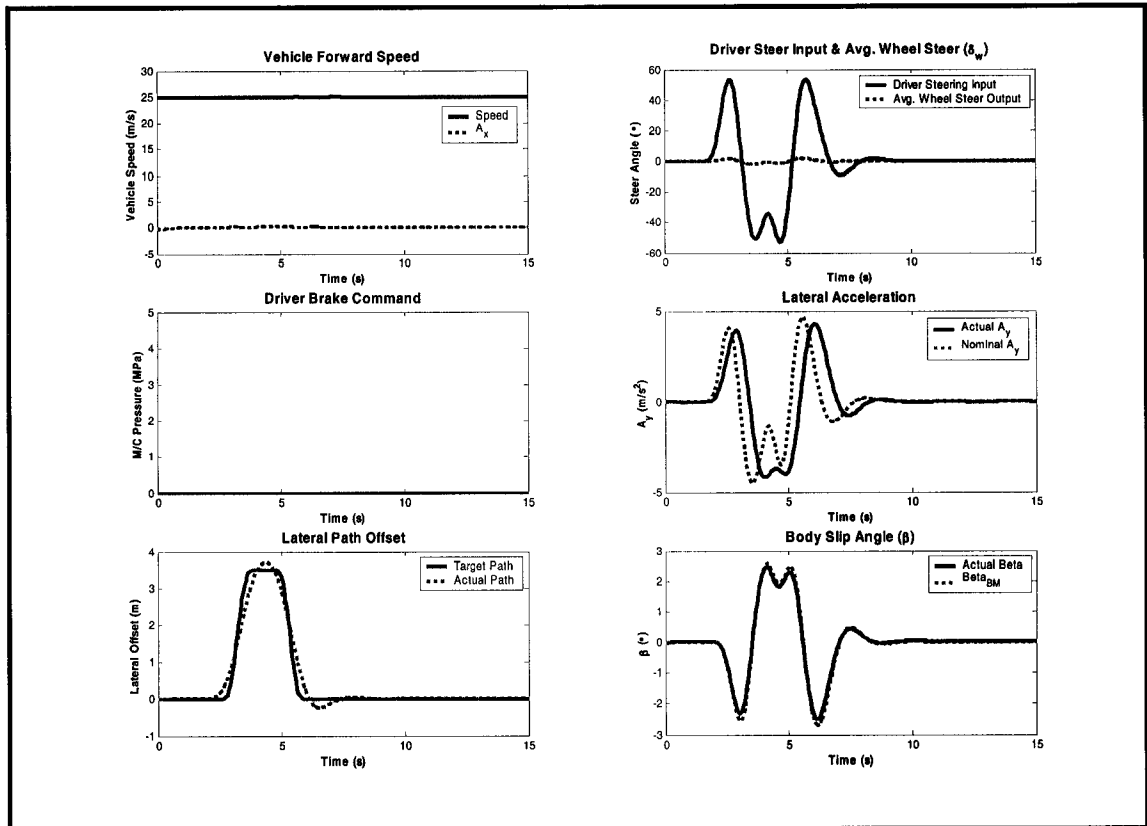
Figure 6.3 Double Lane Change manoeuvre of hybrid Pacifica @ 90 KPH; μ=1.00

In the double lane change manoeuvre, similar to the steady-state simulation, the lateral acceleration calculation is not as accurate as body slip angle calculation. The phase-lag in the response of a_{y_actual} compared to $a_{y\_nominal}$ is due to the inertial effects of the actual vehicle response. Recall that the $a_{y\_nominal}$ transfer function assumes the steady-state condition and thus, it does not use vehicle yaw moment of inertia (I_{zz}) around the z-axis. The result is that $a_{y\_nominal}$ calculates the results direct to the driver's steering input without the lag. The response of β_{BM} is very close to the real value because it takes account of the inertial effect as it is calculated with $\dot{\beta}$ information which uses the measured lateral acceleration and yaw rate data from sensors. The

76

measured values involve the yaw moment of inertia effect as it is an actual measurement of the

vehicle motion in time. The following table summarizes the peak value comparison of lateral

acceleration and body slip angle values of the simulation.

Table 6.6 Summary of lateral acceleration and body slip angle results

	a_{y_CarSim} (m/s²)	$a_{y\_nominal}$ (m/s²)	β_{CarSim} (°)	β_{BM} (°)
Results	6.53 & -8.64	8.01 & -9.10	-4.71 & 7.09	-4.79 & 6.13
Error Margin (%)	18.48 & 5.05		1.67 & 13.54	

6.5.2.2 Double Lane Change @ 150 KPH, μ=1.00
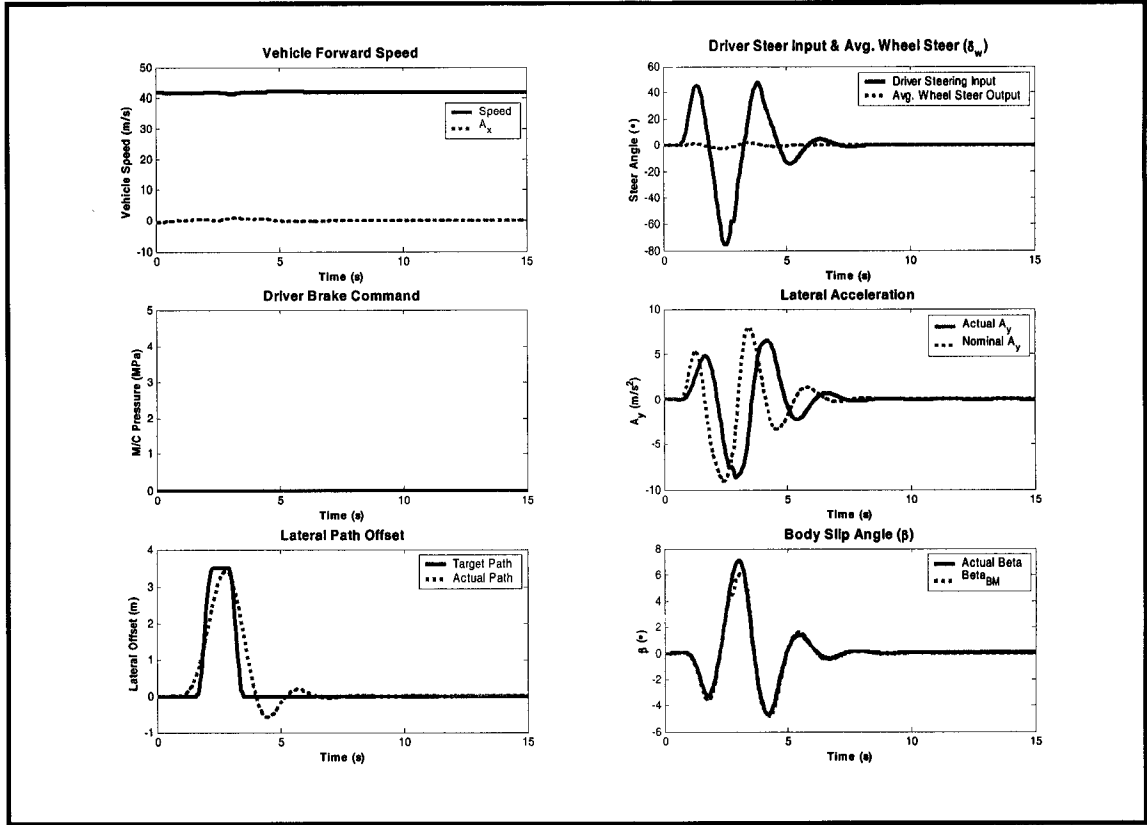
Figure 6.4 Double Lane Change manoeuvre of hybrid Pacifica @ 150 KPH; μ=1.00

The similar analysis done in the previous 90 KPH run can be used for the error margin in the lateral acceleration comparison. The following table summarizes the peak value comparison of lateral acceleration and body slip angle values of the simulation.

Table 6.7 Summary of lateral acceleration and body slip angle results

	a_{y_CarSim} (m/s²)	$a_{y\_nominal}$ (m/s²)	β_{CarSim} (°)	β_{BM} (°)
Results	6.53 & -8.64	8.01 & -9.104	-4.71 & 7.09	-4.79 & 6.13
Error Margin (%)	22.66 & 5.37		1.70 & 13.54	

As the vehicle speed is much higher, the error on the nominal lateral acceleration is greater with longer delay time. This in turn causes greater steering input by the driver to

78

navigate the vehicle through the target path. Based on the observation, the following values are decided for the VDC implementation.

Table 6.8 Threshold limit values implemented in VDC

	a_{y_CarSim} (m/s^2)	$a_{y\_nominal}$ / a_{y_CarSim}	β_{CarSim} (°)
Limit Values	7	2	4

The same threshold limit values are used for the VDC system of all simulation cases to verify that the developed VDC is a robust controller for all types of driving conditions.

79

6.5.3 Straight-Line Braking Simulation

In order to evaluate the straight-line braking performance with effects of VDC, a vehicle with VDC and another without VDC are simulated for the same simulation conditions. For the simulation environment, the only variable is the road coefficient of friction. In the case of split 0.20L/0.60R μ-condition, the left side of the vehicle is in contact with 0.20 μ surface (Ice) and the right side of the vehicle is in contact with 0.60 μ surface (snowy). The simulation condition can be seen in the following animated figure.
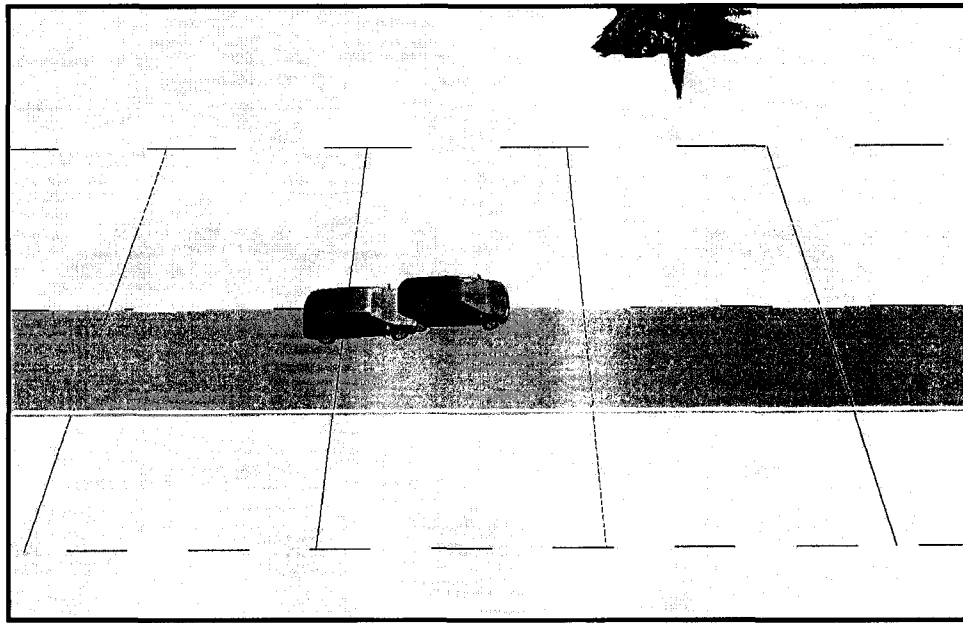
Figure 6.5 Straight Line Braking performance on snowy highway (μ=0.20L/0.60R)

The friction split is defined with respect to the road centre-line, in global coordinates, in which the vehicle is initially centered. For example, if the vehicle moves to the left by more than its half-track width, then vehicle is on the complete 0.20 μ surface. If it moves to the right by the same amount, then the vehicle is on the complete 0.60 μ surface. The *CarSim* "Driver Path Follower Mode" is used for steering wheel angle input control. Hence, the vehicle receives a constant wheel steer angle correction in order to keep the vehicle in its targeted path which coincides with the road centre-line. This driver path follower essentially represents the driver's attempt to follow the target path.

The vehicle target path is predefined in *CarSim*. In this case, it is set to be a straight line course for the duration of the simulation run. The initial vehicle speed is kept at 100 km/h, and the throttle input is maintained to keep the vehicle speed at 100 km/h until the braking command is activated. For a regenerative braking command, a step input of full-scale regenerative braking (generates $a_x \approx$ -2.7 m/s² on μ = 0.85 surface) is applied at 1 s. Since the regenerative braking is designed to be activated via the master cylinder chamber pressure input, a brake pressure of 1 Pa is used as the input. This adds a braking torque of 3.5×10^{-4} N•m, which is negligible[14]. In the case of embedded regenerative and ABS braking command, a 7 MPa of hydraulic braking command along with full regenerative braking (generates $a_x \approx$ -7.5 m/s² on μ = 0.85 surface) are applied at 1 s. Detailed analyses for both cases are done in Sections 6.6.1 and 6.7.1 respectively.

---

[14] In *CarSim*, the generic big SUV braking torque is defined as 350 N•m per 1 MPa of brake delivery pressure.

6.5.4 Double Lane Change Braking Simulation

This simulation set is an industry standard for ESC/ABS performance evaluation. The simulation course uses two 4 m wide lanes marked with cones that represent a path that the vehicle should negotiate. Road friction is set as $\mu = 0.20L/0.60R$, the vehicle is on a split-μ surface initially, and travels on $\mu = 0.20$ road once it enters the left lane.
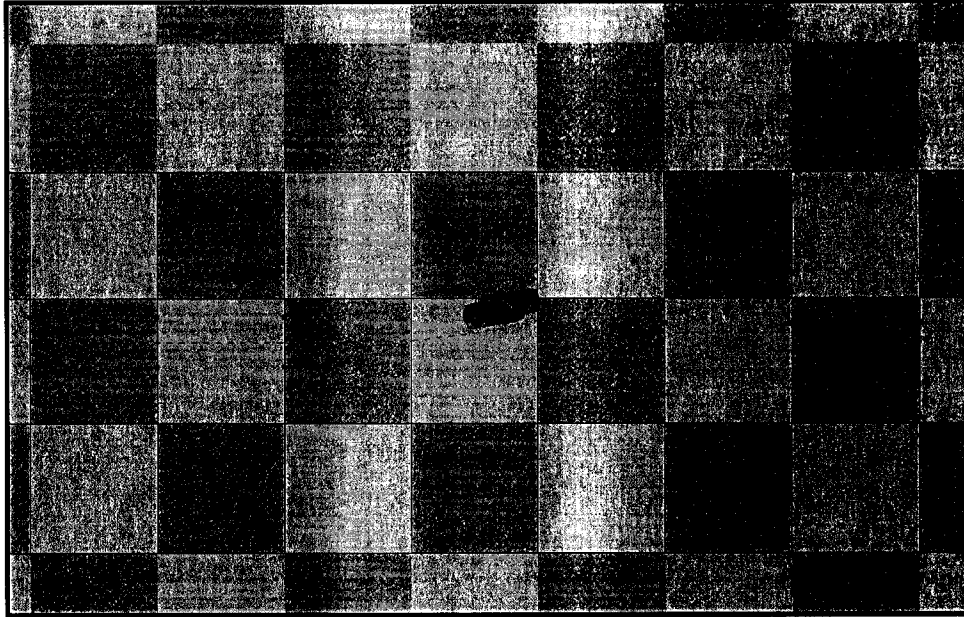
Figure 6.6 Double Lane Change Braking performance on snowy highway (μ=0.20L/0.60R)

Driver steering input is set to follow the predefined target path (DLX) with 1 s driver preview time. Throttle is applied in order to keep the preset speed of 90 km/h and when braking is activated, the throttle is set to release. For the design configuration of regenerative braking-only scenario, the full regenerative torque is commanded at 0.78 s of each simulation. This is 2 s prior to the time when the vehicle would enter the second lane, with the speed of 90 km/h (2 s of driver preview of road). This braking generates 2.5 m/s² of deceleration at the on-set of braking and continues to provide up to 2.7 m/s² of deceleration.

Although the braking force does not match the "panic" braking condition, it is the maximum regenerative braking force available and the timing simulates the panic braking

82

response. In the case of the integrated braking system, 3 MPa of hydraulic braking along with the full regenerative braking is applied to simulate a realistic "panic" braking scenario. This combined braking generates approximately 5.0 m/s^2 of deceleration at the on-set of braking and continues to provide up to approximately 6.1 m/s^2 of deceleration. Detailed analyses for both cases are done in Sections 6.6.2 and 6.7.2 respectively.

6.5.5 Highway Exit-Ramp (Decreasing Radius) Braking

This simulation case simulates a vehicle exiting from the highway onto an exit ramp with a decreasing radius. A "gentle" brake input is applied gradually and consistently throughout the bend as a normal driver would do. Initial vehicle speed is set to be 90 km/h in "coasting" mode and the brakes are applied at the 1 s of the simulation which is 2.5 s before the time the vehicle would reach the start of the bend without any braking input. The road surface condition is set to μ =0.60L/0.2R for this right-turn bend with the same convention used in SLB and DLX simulations. The following figure represents a sample simulation condition.
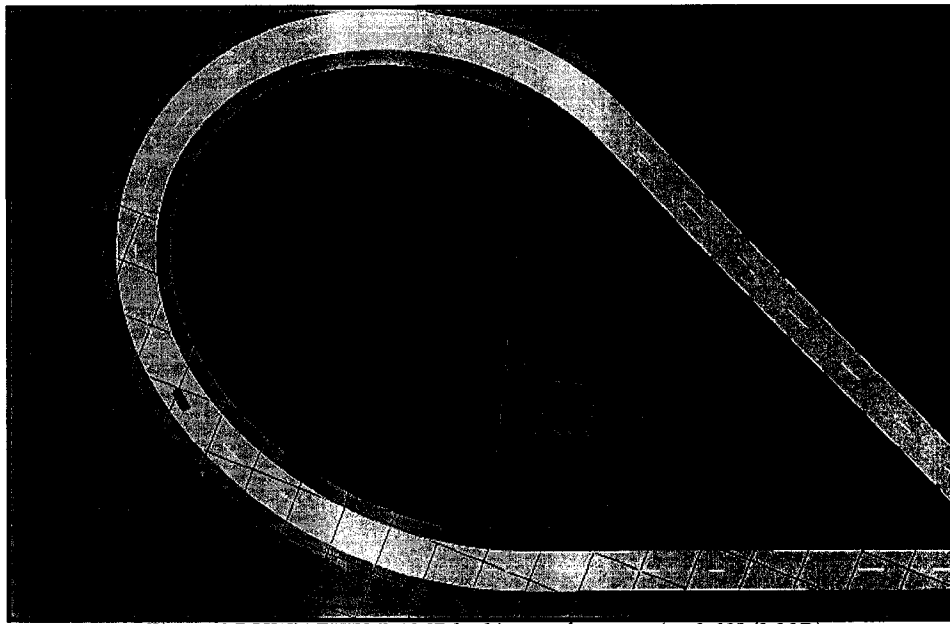
Figure 6.7 HWY EXIT-RAMP braking performance (μ=0.60L/0.20R)

The steering control is set to be a path follower. In the case of regenerative braking (VDC Validation Stage), the full step input of regenerative braking torque (generates $a_x \approx$ -2.7 m/s² on μ = 0.85 surface) is commanded at 1 s. This different input is performed since for regenerative braking, the interest is investigating the VDC system performance evaluation for the maximum braking regenerative braking output. For the integrated braking system validation, the magnitude of braking applied is a 'ramp' input of 1 MPa (generates $a_x \approx$ -3.9 m/s² on μ = 0.85 surface) over duration of 3 s, which is a realistic braking practice for normal driving.

6.5.6 Straight-Line Acceleration Simulation

This simulation setting is essentially the same as the straight line braking simulation. Only differences are:

- The initial vehicle speed is set at 60 km/h.

- A normalized throttle input of 0.2 is given at the beginning of the simulation to accelerate the vehicle. This actuates both the ICE and EM to provide traction torque to the vehicle.

6.5.7 Double Lane Change Acceleration Simulation

This simulation setting is essentially the same as the double lane change acceleration simulation. Only differences are:

- The initial vehicle speed is set at 60 km/h.

- A normalized throttle input of 0.2 is given at 6 s of the simulation time to accelerate the vehicle. The command actuates both the ICE and EM to provide traction torque to the vehicle. This is when the vehicle is in the second (left) lane and accelerating moderately to return to the first (right) lane.

6.6 VDC Performance Validation on Regenerative Braking System

This set of simulations is done to investigate the component level performance of regenerative braking on the prototype and the control performance of the Vehicle Dynamics Controller. The braking simulation is done using regenerative braking function of front two wheels only, i.e. the stock ABS braking system is not used. Three main criteria are considered for the VDC performance evaluation:

- Steer Effort by Driver (Steering Wheel Angle Input)

- Lateral Path Deviation (Steer-ability of vehicle)

- Braking Time (Subjective to the situation)

These three criteria ultimately determine the safety and efficiency of braking performance as the least steer effort with controlled vehicle motion and minimum braking distance represent the ideal braking performance.

86

6.6.1 Straight Line Braking Simulation @ 100 KPH, μ=0.20L/0.60R

6.6.1.1 SLB without VDC Control
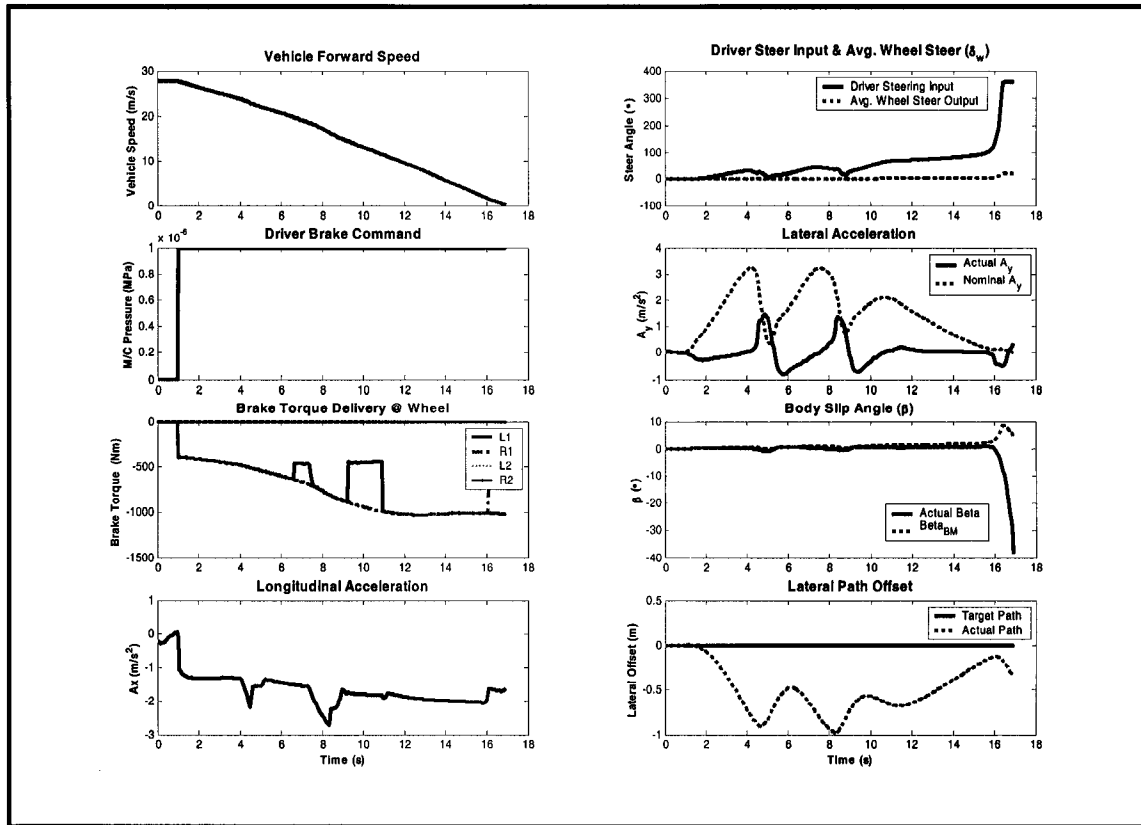
Figure 6.8 SLB performance of hybrid Pacifica without VDC @ 100 KPH; μ=0.2L/0.6R

Without VDC, regenerative braking is provided regardless of the vehicle instability. The dips in the front-left (L1) wheel brake torque are due to the low friction coefficient (μ= 0.20) of the road. This is explained as the tire is only capable of generating braking force up to the limit of its available traction. As expected, the $a_{y\_nominal}$ is higher than the a_{y_actual} because the road friction condition is low at 0.20L/0.60 so the vehicle cannot respond to yaw (turn) as fast as the driver intends it. Consequently, the vehicle leaves its target path as much as 1 m to the right. The deviation to the right is caused due to the vehicle yaw moment, M_z, imbalance in clockwise direction caused by the higher braking force of the front-right tire. The driver corrects the steering wheel as much as 350° [CCW]. The braking time takes about 17 s.

87

6.6.1.2 SLB with VDC Control
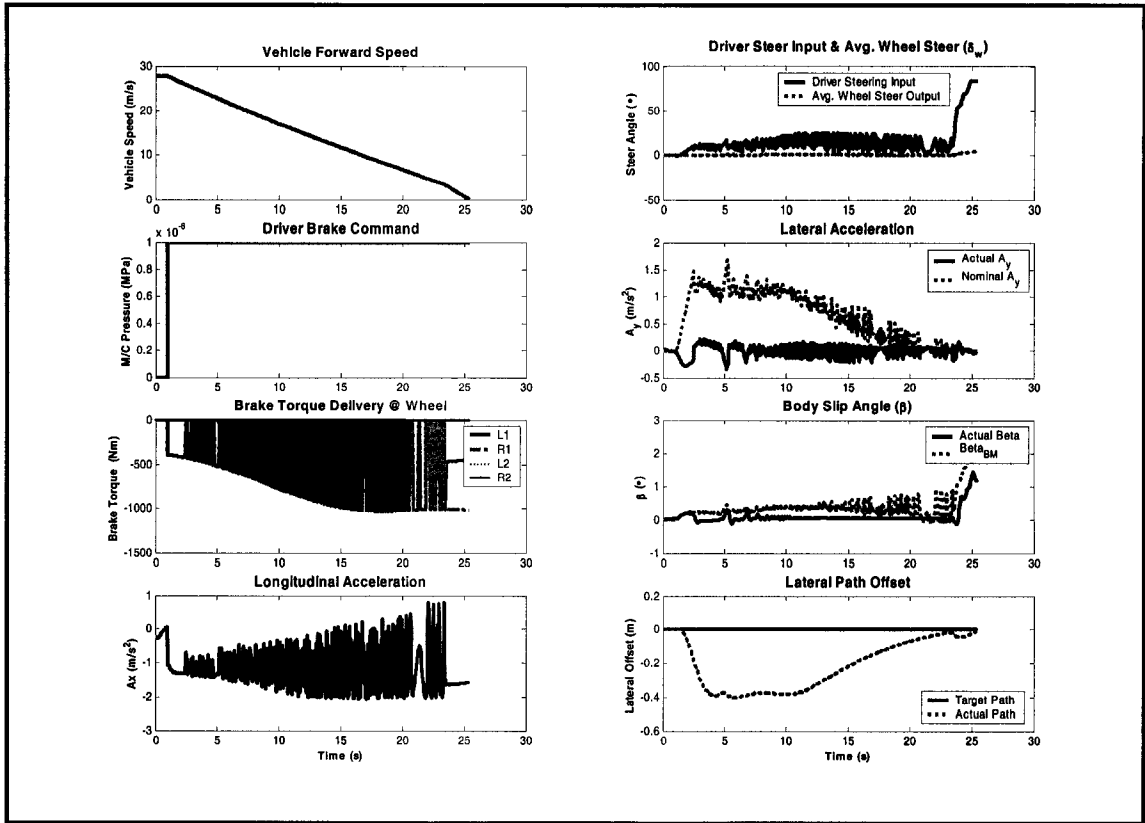
Figure 6.9 SLB Performance of hybrid Pacifica with VDC @ 100 KPH; μ=0.2L/0.6R

With VDC, regenerative braking is controlled as seen in the above figure (Brake Torque plot) due to wheel slip and the discrepancy in $a_{y\_nominal}$ and a_{y_CarSim}. The vehicle leaves its target path up to 0.4 m to the right, which is within the limit to keep the vehicle in its designated lane. Since the controlled braking force enables gaining the lateral force at tire, the driver gives a less steering input to navigate the vehicle. Therefore, the $a_{y\_nominal}$ commanded is closer to the a_{y_CarSim}. However, the braking time is extended by 8 s to bring the vehicle to a full stop.

Table 6.9 VDC performance comparison in SLB

	Steer Input Magnitude (°)	Max. Lateral Deviation Magnitude (m)	Braking Time (s)	Vehicle Path Control Maintained?
No VDC	350	1.0	17	Yes
VDC	80	0.4	25	Yes

88

6.6.2 Double Lane Change Braking Simulation @ 90 KPH; μ=0.20L/0.60R

6.6.2.1 DLX Braking without VDC Control
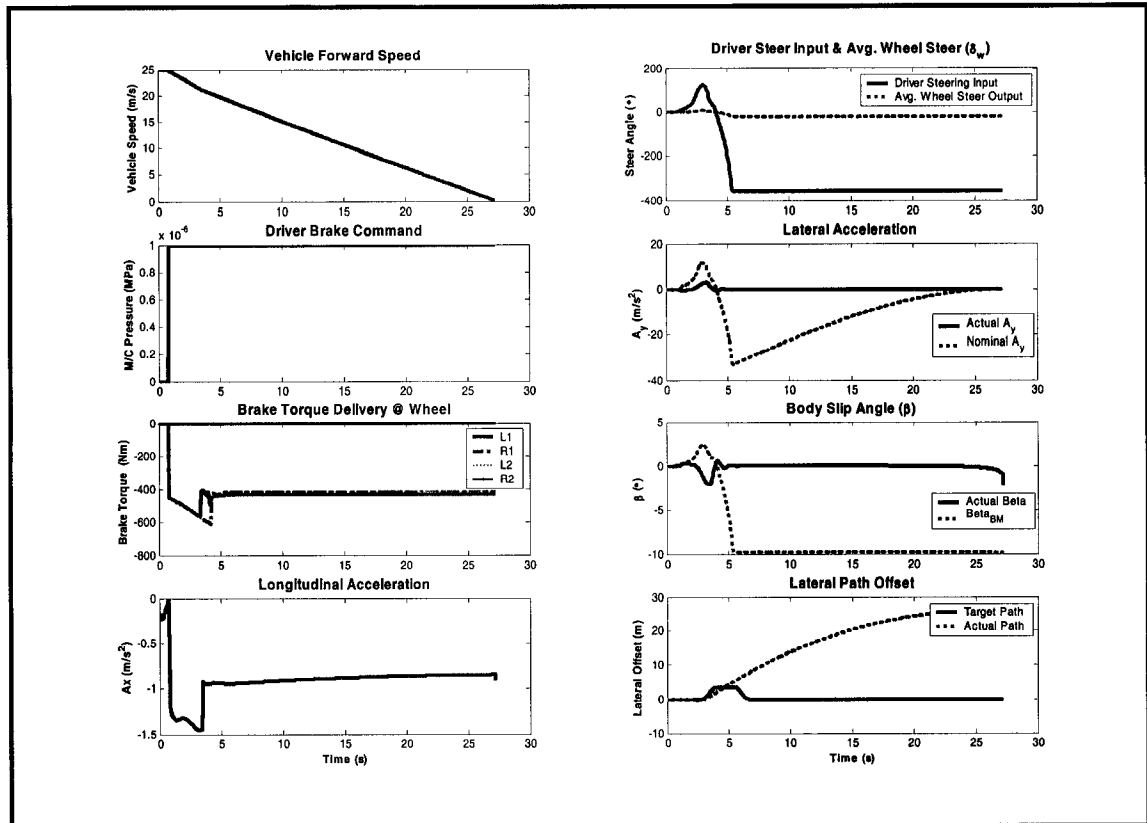
Figure 6.10 DLX braking performance of hybrid Pacifica without VDC @ 90 KPH; μ=0.2L/0.6R

Due to the lack of VDC control, a constant brake torque of about 400 N•m (traction limited) is delivered. This is due to the fact that the vehicle loses its steer-ability and remains in μ=0.20 region for the remainder of the run as it is skidding down the icy surface. The driver commands a fixed steer input of 370° [CW]

89

6.6.2.2 DLX Braking with VDC Control
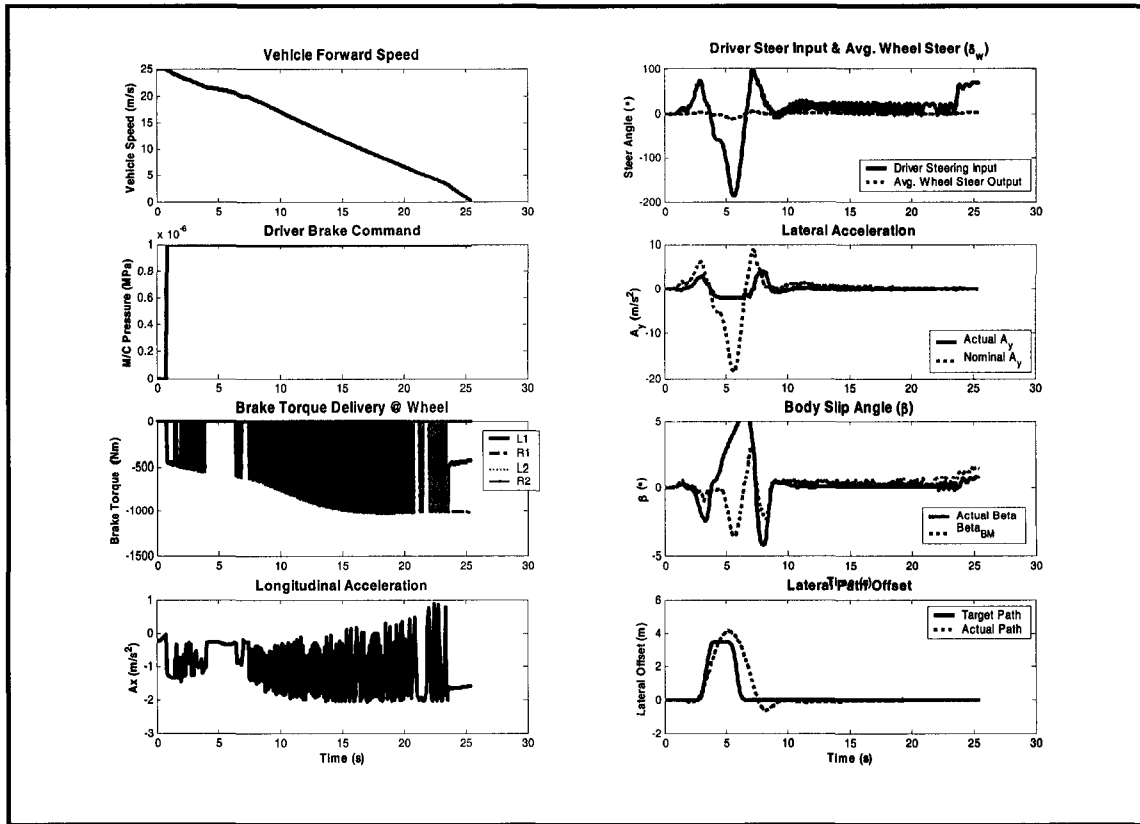
Figure 6.11 DLX braking performance of hybrid Pacifica with VDC @ 90 KPH; μ=0.2L/0.6R

A controlled regenerative brake torque up to its maximum capacity (1015 N•m) is delivered to each wheel, which effectively maintains the vehicle control for steer-ability. The prolonged dip in brake torque matches the valley of $a_{y\_nominal}$ plot, where it exceeds the limit. The path deviation is acceptable and the vehicle completes the DLX manoeuvre. The driver commands steering input in the range of 100° [CCW] to 190° [CW].

Table 6.10 VDC performance comparison in DLX braking

	Steer Input Magnitude (°)	Max. Lateral Deviation Magnitude (m)	Braking Time (s)	Vehicle Path Control Maintained?
No VDC	Lost @ 380	27	17	No
VDC	-100 to 190	2	25	Yes

90

6.6.3 Highway Exit Ramp Braking @ 90 KPH; µ = 0.6L/02R

6.6.3.1 HWY Exit Ramp Braking without VDC Control
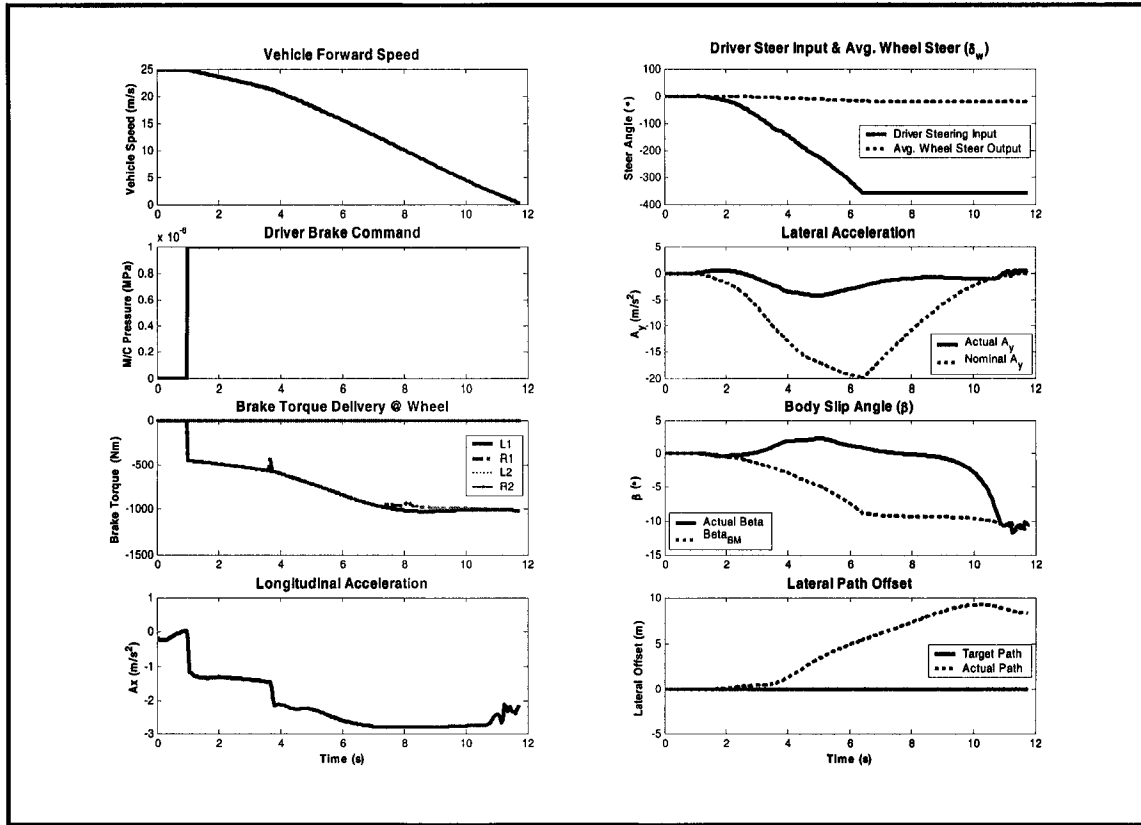
Figure 6.12 HWY EXIT-RAMP braking performance of hybrid Pacifica without VDC @ 90 KPH; µ=0.60L/0.20R

Due to the lack of VDC control, the full regenerative brake torque is delivered. As seen in the locked steering input and both of the lateral acceleration and body slip angle plots, the vehicle is skidding away to the left of the highway ramp. On the snowy 0.60 µ surface, the vehicle deviates from it path as much as 9.2 m. The vehicle loses steer-ability and the driver commands a fixed steer input of 360° [CW]

91

6.6.3.2 HWY Exit Ramp Braking with VDC Control
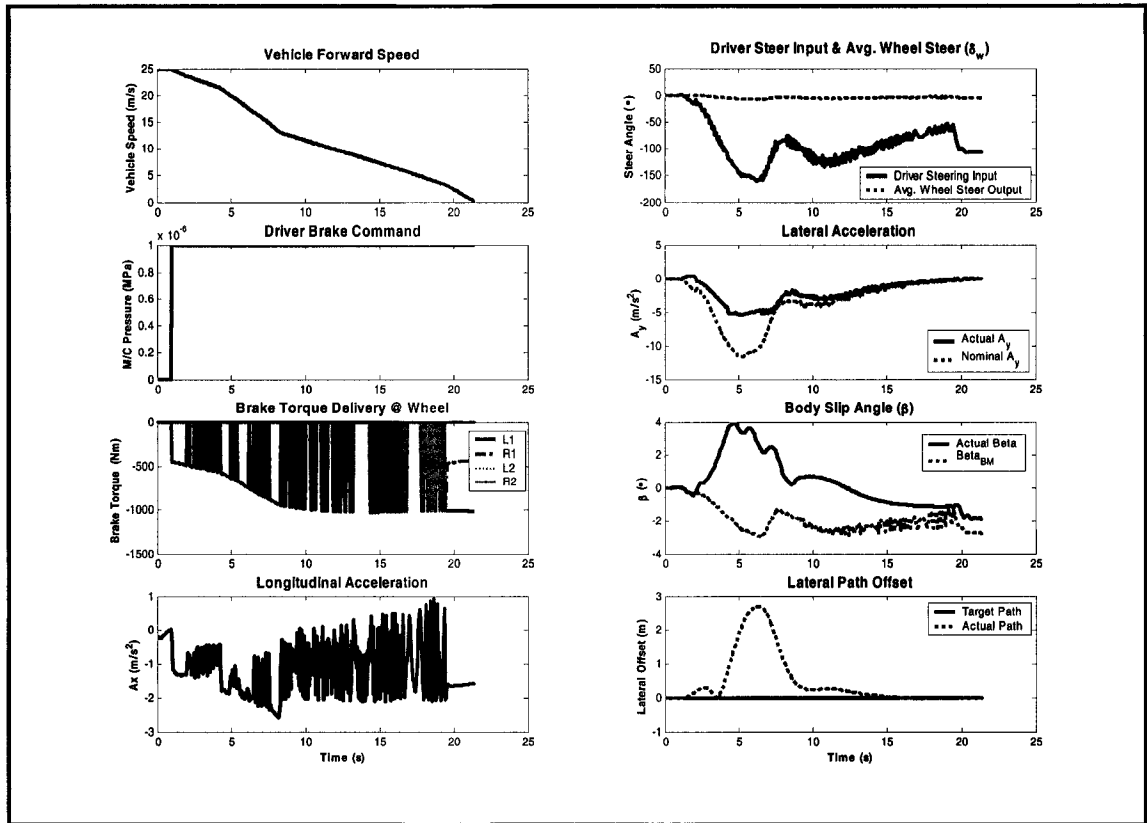
Figure 6.13 HWY EXIT-RAMP braking performance of hybrid Pacifica with VDC @ 90 KPH; μ=0.6L/0.2R

With VDC, a controlled regenerative brake torque is delivered. The driver is able to steer

the vehicle throughout the bend with as much as 2.7 m path deviation.

Table 6.11 VDC performance comparison in HWY EXIT RAMP braking

	Steer Input Magnitude (°)	Max. Lat. Deviation Magnitude (m)	Braking Time (s)	Vehicle Path Maintained?
No VDC	Lost @ 360	9.2	21	No
VDC	-150 to 50	2.7	12	Yes

6.7 VDC Performance Validation on Integrated Braking System (Regenerative Braking & ABS)

This set of simulation investigates how regenerative braking system performs when integrated with the simulated stock *Pacifica* ABS system. Furthermore, the performance of VDC which controls regenerative braking along with the stock ABS system is evaluated for vehicle system level validation.

As with Section 6.6, the same three criteria are considered for the VDC performance evaluation:

- Steer Effort by Driver (Steering Wheel Angle Input)

- Lateral Path Deviation (Steer-ability of vehicle)

- Braking Time (Subjective to the situation)

93

6.7.1 Straight Line Braking @ 100 KPH, μ = 0.20L/0.6R

6.7.1.1 SLB without VDC Control
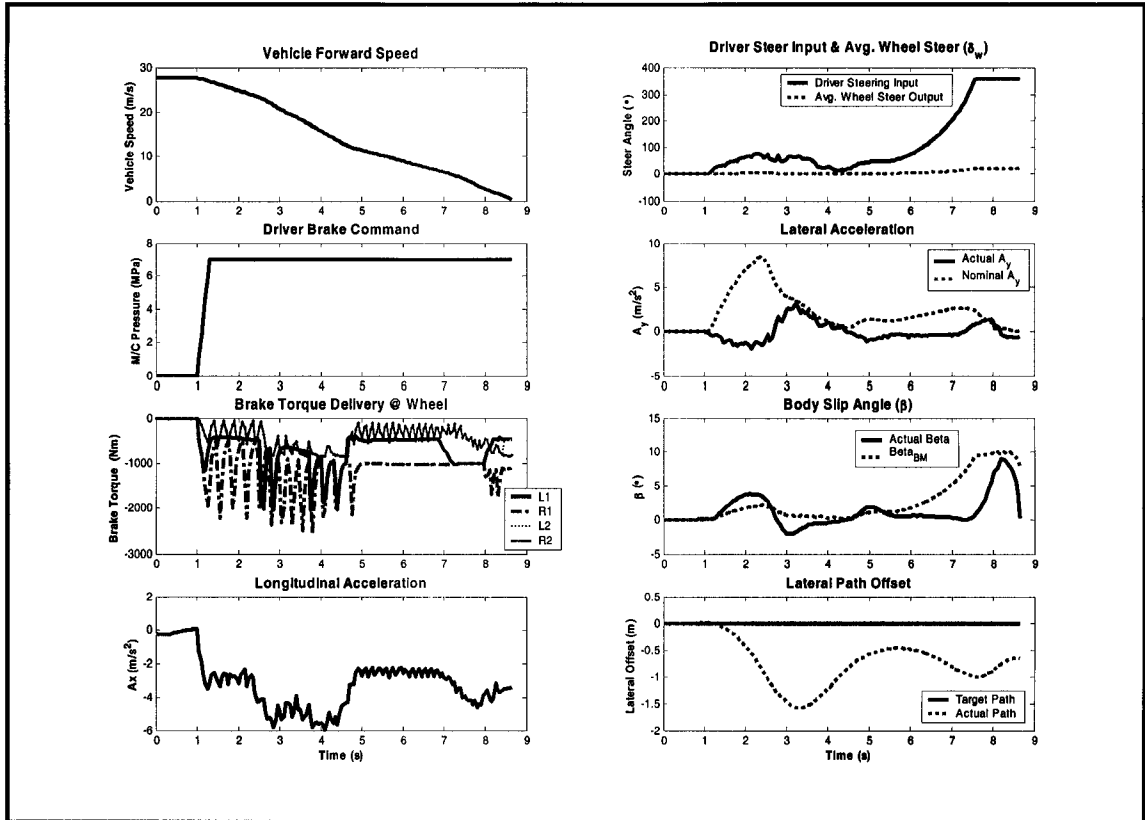
Figure 6.14 SLB performance of hybrid Pacifica without VDC @ 100 KPH; μ=0.2L/0.6R

Without VDC, regenerative braking is provided regardless of the vehicle instability. ABS braking, on the other hand, is active to control the hydraulic braking torque output. This can be verified on the 'Brake Torque' plot of Figure 6.14 as the L1 brake output is at a constant -500 N•m and R1 is at a constant -1015 N•m from 5 s to 8 s. With the lost steer-ability, as with Section 6.6.1.1, the vehicle skids on the icy surface to the left with the lateral deviation of up to 1.5 m. The deviation to the right is caused due to the front brake force imbalance that induces the clockwise vehicle yaw moment, M_z. The driver corrects the steering wheel as much as 360° [CCW]. The braking time takes about 8.7 s.

94

6.7.1.2 SLB with VDC Control
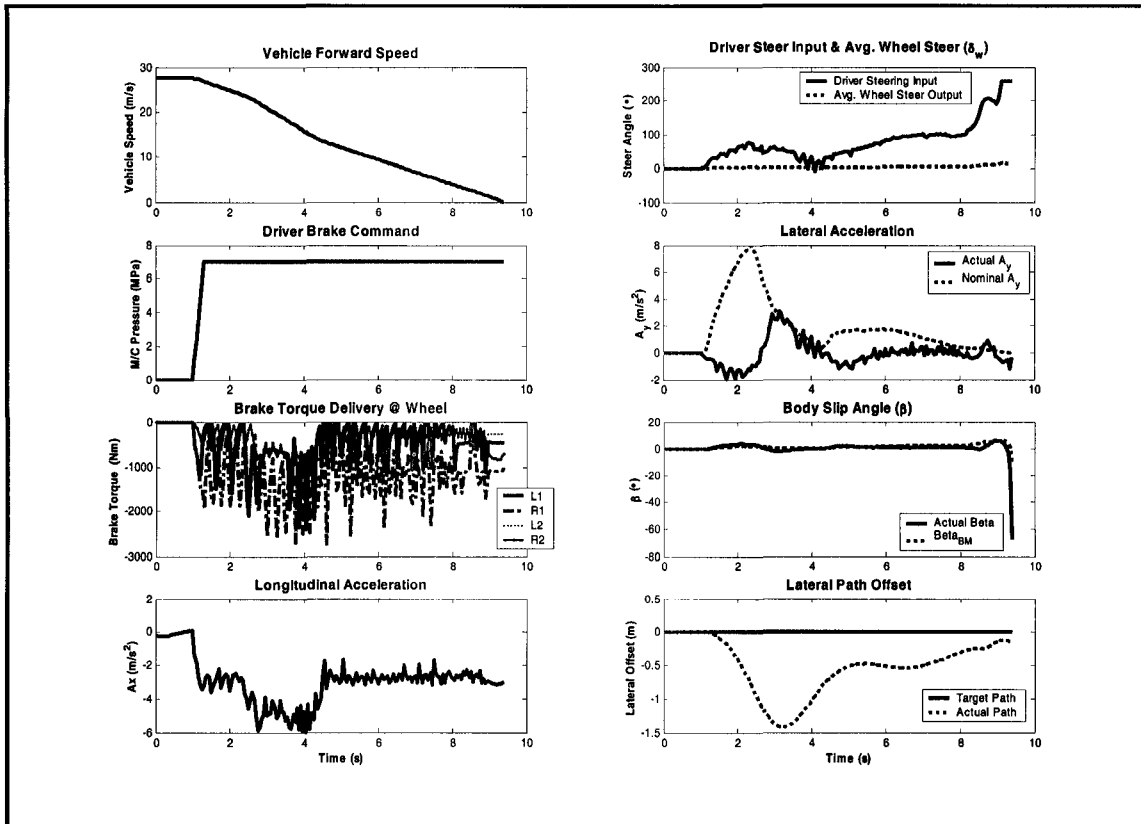
Figure 6.15 SLB performance of hybrid Pacifica with VDC @ 100 KPH; μ=0.2L/0.6R

As can be observed in 'Brake Torque' plot of Fig. 6.15, both regenerative and ABS braking are controlled by the wheel slip and lateral acceleration limits. Compared to Section 6.7.1.1, the lateral path deviation is similar but the steering input is considerably less for VDC controlled braking. The braking time takes about 9.3 s.

Table 6.12 VDC performance comparison in SLB braking

	Steer Input Magnitude (°)	Max. Lat. Deviation Magnitude (m)	Braking Time (s)	Vehicle Path Maintained?
No VDC	Eventually Lost @ 360	1.6	8.7	Yes
VDC	0 to 260	1.4	9.3	Yes

95

6.7.2 Braking during a Double Lane Change @ 90 KPH, µ = 0.20L/0.60R

6.7.2.1 DLX Braking without VDC Control
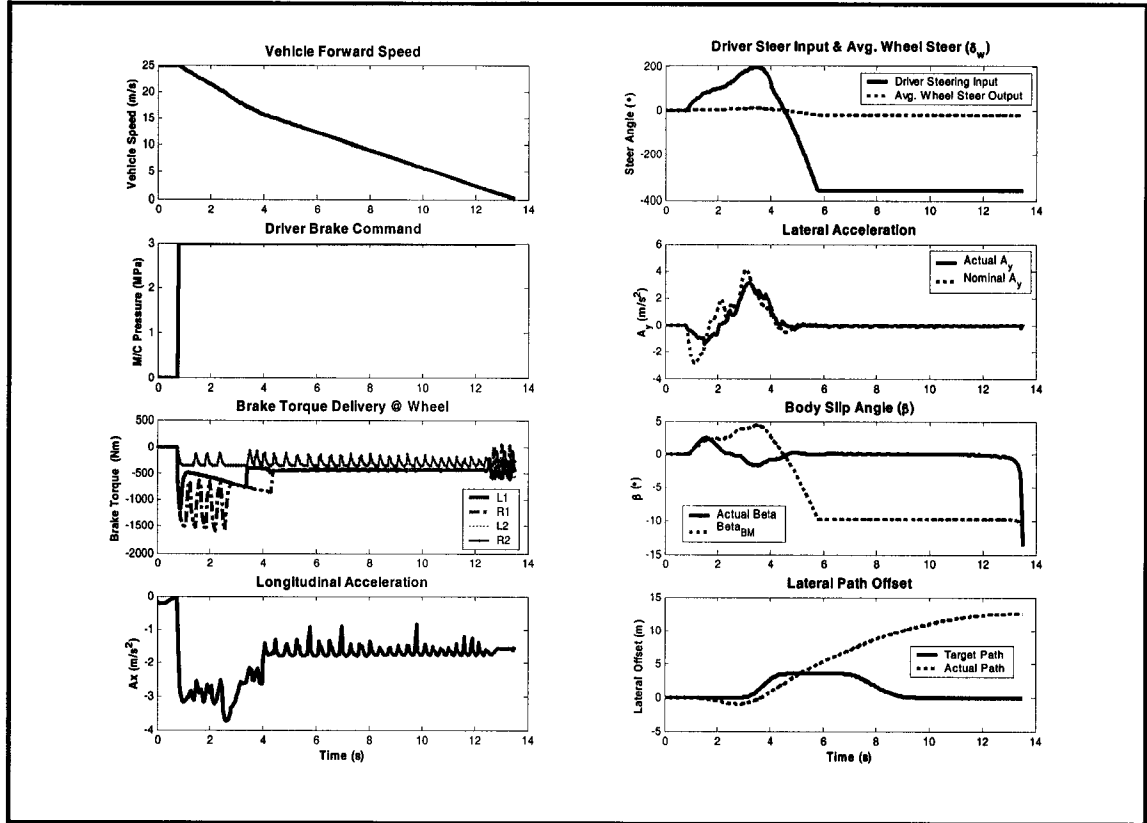
Figure 6.16 DLX braking performance of hybrid Pacifica without VDC @ 90 KPH; µ=0.2L/0.6R

Even though ABS braking is controlled, the regenerative braking still outputs a constant traction limited brake torque which leads to the loss of steer-ability and path deviation. As shown in the above subplots, the nominal lateral acceleration matches the actual lateral acceleration fairly well due to controlled braking by the ABS controller up to about 4.3 s. The vehicle still skids away to the left, however, due to the fact that it is now on the icy surface with locked front two wheels. The driver cranks the steering wheel to 370° clockwise direction in an attempt to bring the vehicle back to the target path. The total deceleration time is 13.5 s.

96

6.7.2.2 DLX Braking with VDC Control
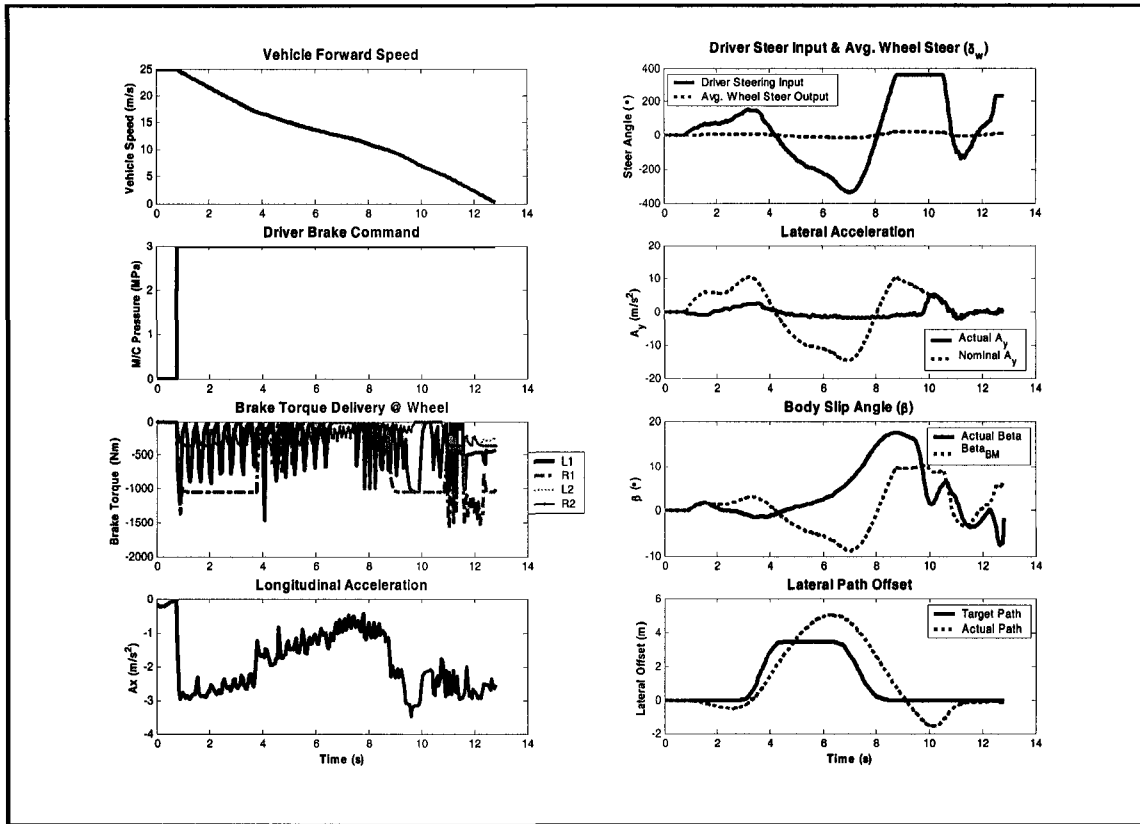
Figure 6.17 DLX braking performance of hybrid Pacifica with VDC @ 90 KPH; μ=0.2L/0.6R

With the large lateral acceleration and body slip angle discrepancies, regenerative braking is mostly inactive for the duration of the run. With front two wheels providing a controlled regenerative torque, the ABS controller distributes the optimal braking torque at each wheel of the vehicle to maintain its steer-ability. With a constant steering correction, ranging from 350° [CW] and 380° [CCW], the driver is able to bring the vehicle to its target path although the path deviation is as large as 3 m.

Table 6.13 VDC performance comparison in DLX Braking

	Steer Input Magnitude (°)	Max. Lat. Deviation Magnitude (m)	Braking Time (s)	Vehicle Path Maintained?
No VDC	Lost @ 360	13	13.5	No
VDC	-350 to 380	3	12.8	Yes

6.7.8 Highway Exit Ramp Braking @ 90 KPH; μ = 0.6L/02R

6.7.8.1 HWY Exit Ramp Braking without VDC Control
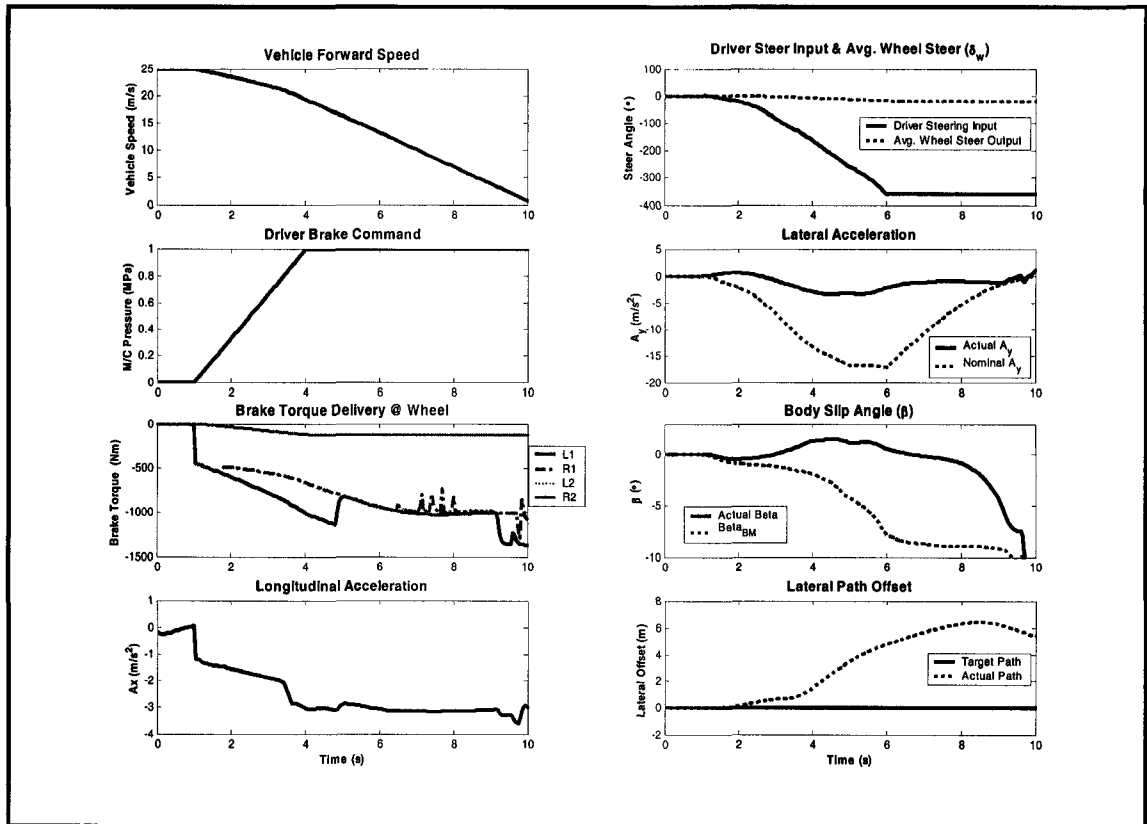
Figure 6.18 HWY EXIT RAMP braking performance of hybrid Pacifica without VDC @ 90 KPH; μ=0.6L/0.2R

The vehicle is going through a right-hand turn of the exit ramp so the vehicle drifts to the left on the snow dusted μ = 0.60 road surface. The presence of L2 and R2 brake torques of 140 N•m indicates that ABS braking is active for the entire run of the simulation. Regenerative braking provides all the front wheel brake torque dictated by the traction limit. This limit occurrence is also communicated to the ABS controller as wheel slip signal. Hence, no additional front braking torque is delivered by the hydraulic system. The vehicle steer control is not possible and the steering input is ineffectively locked at -350°. As a result, the vehicle skids on the snow dusted side of the road (left) and leaves the intended path by 5.8 m. Braking time is just over 10 s.

98

6.7.8.2 HWY Exit Ramp Braking with VDC Control
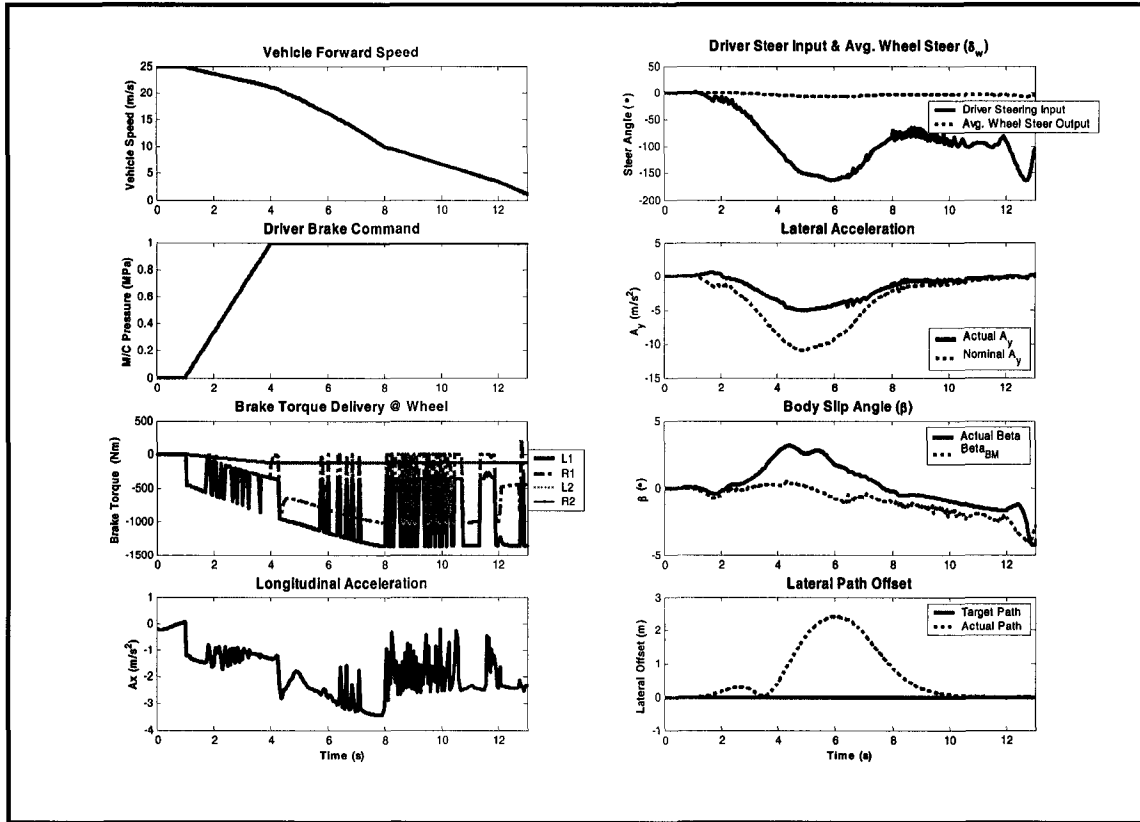
Figure 6.19 HWY EXIT RAMP braking performance of hybrid Pacifica with VDC @ 90 KPH; μ=0.6L/0.2R

Both VDC and ABS braking controllers effectively generate optimal braking (longitudinal) forces while preserving lateral forces of each tire. Thus, the vehicle maintains its control and returns to the intended path although the vehicle stops about 3.5 s later than its counterpart.

Table 6.14 VDC performance comparison in HWY EXIT RAMP braking

	Steer Input Magnitude (°)	Max. Lat. Deviation Magnitude (m)	Braking Time (s)	Vehicle Path Maintained?
No VDC	Lost @ -350	5.8	10.2	No
VDC	0 to -160	2.3	13.5	Yes

99

6.8 VDC Performance Validation on Integrated Powertrain System (ICE & Electric Motor)

This set of simulation investigates how the electric motor traction (drive) torque affects the vehicle stability when coupled with the stock ICE torque output in vehicle acceleration. The performance of VDC that controls drive torque assist function with the stock ICE is evaluated for vehicle system level validation.

As with the CS function evaluation in Sections 6.6 and 6.7, the similar performance criteria are considered for the VDC system evaluation:

- Steer Effort by Driver (Steering Wheel Angle Input)

- Lateral Path Deviation (Steer-ability of vehicle)

- Final Speed at the end of simulation

6.8.1 Straight Line Acceleration @ 60 KPH, μ = 0.20L/0.6R

6.8.1.1 SLA without VDC Control
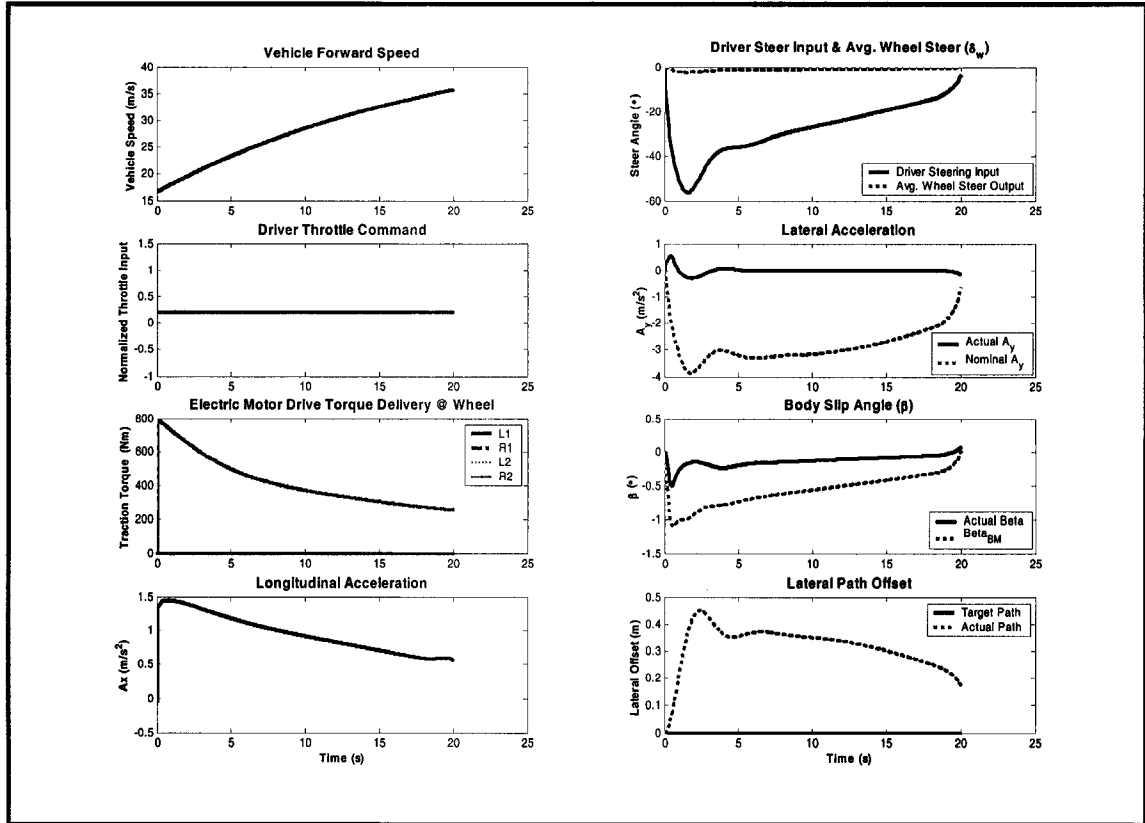
Figure 6.20 SLA performance of hybrid Pacifica without VDC @ 60 KPH; μ=0.2L/0.6R

Without VDC, the electric motor traction torque is provided continuously. The vehicle continues to accelerate with a decreasing electric motor torque output. As before, the excessive traction torque reduces the lateral tire forces and therefore the vehicle deviates from its target path by as much as 0.45 m.

101

6.8.1.2 SLA with VDC Control
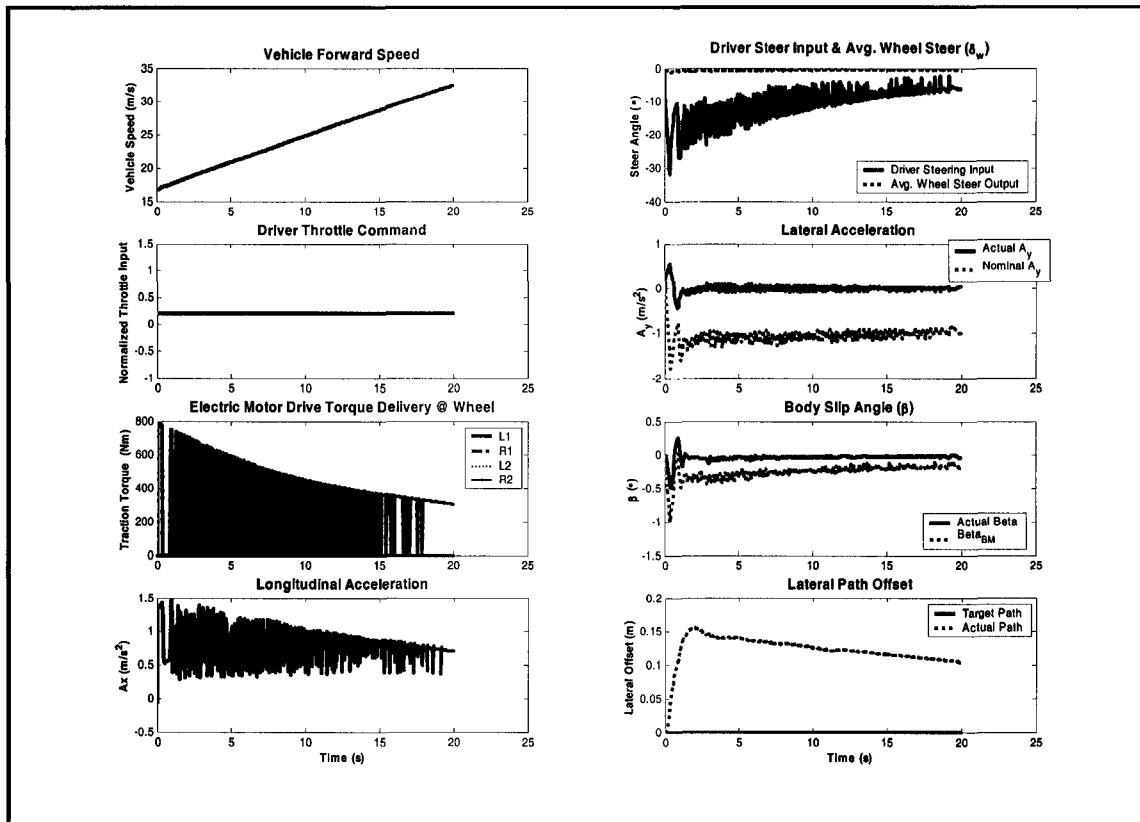
Figure 6.21 SLA performance of hybrid Pacifica with VDC @ 60 KPH; μ=0.2L/0.6R

VDC detects the slippery condition of the road surface from its wheel slip and a_{y_ratio} controllers and provides regulated electric motor traction torque to the vehicle. The result is the less lateral path deviation of 0.15 m and a smaller steering wheel angle input by the driver.

Table 6.15 VDC performance comparison in SLA@ 60 KPH; μ=0.2L/0.6R

	Steer Input Magnitude (°)	Max. Lat. Deviation Magnitude (m)	Final Vehicle Speed (m/s)	Vehicle Path Maintained?
No VDC	Up to 58	0.45	35	Yes
VDC	Up to 32	0.15	33	Yes

102

6.8.2 Accelerating during a Double Lane Change @ 60 KPH, μ = 0.2L/0.6R

6.8.2.1 DLX Acceleration without VDC Control
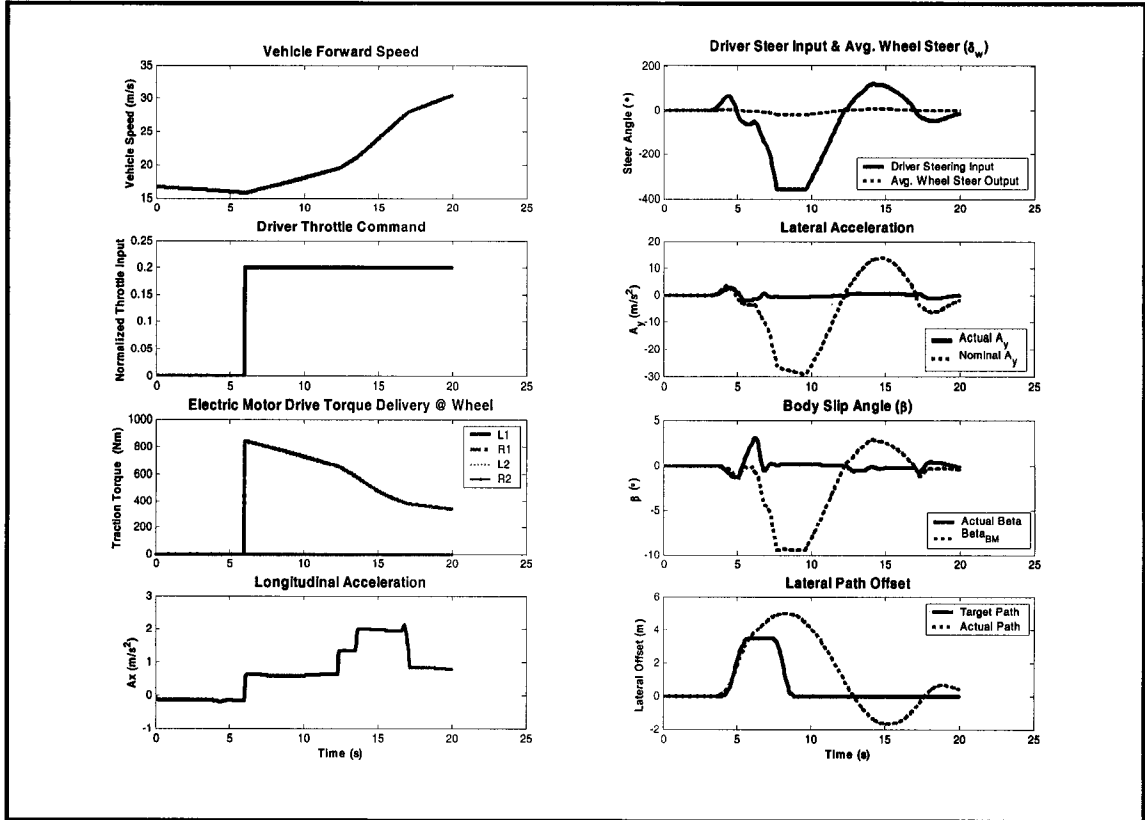
Figure 6.22 DLX acceleration performance of hybrid Pacifica without VDC @ 60 KPH; μ=0.2L/0.6R

As soon as the throttle command is given on the icy road surface at 6 s, both the nominal lateral acceleration and body slip angle start to deviate from the actual values. Barely any lateral acceleration is present since there are very little lateral tire forces available for the vehicle. As a result, there is a considerable deviation in the actual vehicle path and the vehicle leaves its designated lane.

103

6.8.2.2 DLX Acceleration with VDC Control
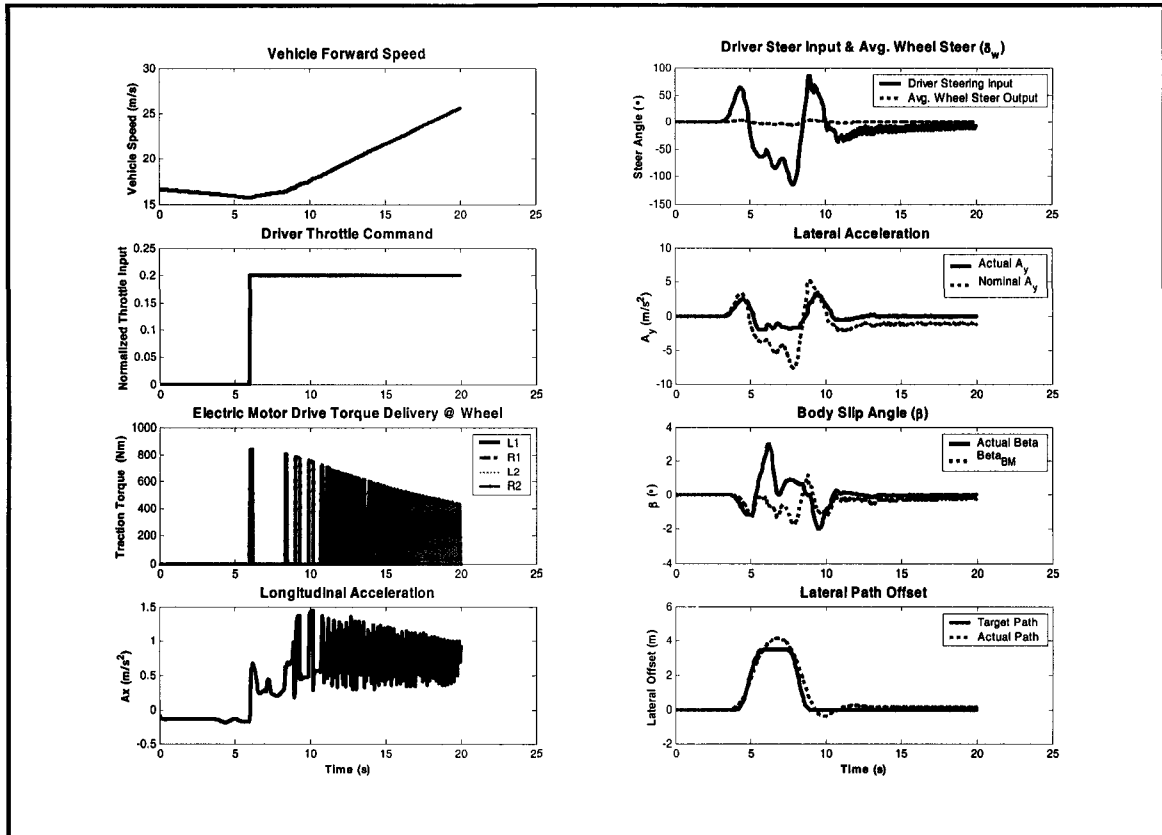
Figure 6.23 DLX acceleration performance of hybrid Pacifica with VDC @ 90 KPH; μ=0.2L/0.6R

Although the stock ICE continues to provide its traction torque when the throttle input is commanded, the electric motor torque output is controlled as shown in the Figure 6.23. As a result, the vehicle is controlled to respond better to the driver's input (the lateral acceleration values are close to each other). Therefore, the driver provides a much less steering wheel angle amount and the lateral path deviation is minimized allowing the vehicle to complete its manoeuvre successfully.

Table 6.16 VDC performance comparison in DLX acceleration

	Steer Input Magnitude (°)	Max. Lat. Deviation Magnitude (m)	Final Vehicle Speed (m/s)	Vehicle Path Maintained?
No VDC	-380 to 110	5	30	No
VDC	-100 to 80	0.5	26	Yes

104

6.9 Discussion of Results

The results have found that VDC effectively controls regenerative braking and drive torque assist function to reduce the driver steering input for safety. As well, it preserves the lateral traction forces of front two wheels, hence maintaining the vehicle lateral stability. This further allows the vehicle to follow its target path much better than the vehicle without VDC control.

While the acceleration performance is suffered with the intervention of VDC control, the driver steer effort is reduced and the vehicle follows the driver's intended path safely. This results in the safe high way driving. It is also noted that the deceleration performance is reduced in general, resulting in a longer braking time/distance. However, this is a subjective safety criterion. An unstable vehicle leaving its designated lane to stop sooner and a stable vehicle maintaining steer-ability to stop later have a different safety outcome depending on the situation. For example, if the vehicle is about to collide with a moose on the ice covered Trans-Canada highway in Manitoba, the shorter braking distance is preferred. If the vehicle is traveling on Highway 101 in the rainy coast (cliff) of British Columbia, the steer-ability around the bend is preferred. Appendix E shows further simulation results with a good VDC estimation performance due to a high friction road surface condition.

CHAPTER 7

CONCLUSIONS & RECOMMENDATIONS

The unique post-transaxle electric motor implementation of the hybrid system presented a design challenge that could affect vehicle stability for the prototype vehicle. This prompted investigating the effects of the hybrid drivetrain on the vehicle dynamics through simulation. A representative, non-linear, and multi-degree-of-freedom prototype vehicle model was created in *CarSim* vehicle dynamics simulation software and various realistic simulation cases were investigated for the vehicle response with the effects of controlled and uncontrolled regenerative braking and motor torque acceleration. Based on the results, a vehicle dynamics controller using motion sensors and a linear estimator (bicycle model) was developed to monitor and maintain stability of the prototype vehicle. The co-simulation method was conducted in the *CarSim/Simulink* environment to verify the controller performance. The validated Vehicle Dynamics Controller was then implemented using a micro-controller which is designed and programmed to work with the actual motion sensors which will be integrated with the data acquisition system of the prototype hybrid *Pacifica*.

Brake-by-wire and throttle-by-wire systems are discussed in order to demonstrate that the braking or throttle actuation command modeled in the co-simulation is an achievable and realistic approach; therefore, validating the developed VDC is designed for actual implementation on the prototype vehicle.

106

The Vehicle Dynamics Controller developed in this study is found to be an effective safety system which:

- aids the driver in steering effort (both in magnitude and correction frequency) to reduce the chance of causing vehicle instability induced by the excessive steer input.

- allows the optimal traction at driven wheels and therefore sustaining steer-ability of the vehicle

- prevents vehicle instability from occurring by controlling brake/drive torque output of the electric motor in situations where the vehicle instability is incipient.

As with the ABS system, one drawback of the VDC system is the extended braking distance on slippery road conditions in exchange for steer-ability. However, the drawback negates itself because in "wheel lock-up" situations, the system reverts to the stock ABS system which is proved to be an effective and robust safety feature in modern braking technology.

The linear bicycle model used in Vehicle Dynamics Controller is found to be effective for the robust controller performance. Furthermore, the simple steady-state calculation of state variables, namely $a_{y\_nominal}$ and $\dot{\beta}$, without using time-integration, which would be required for the non-linear observer design, allows faster calculation time for the chosen micro-controller.

It is also found that the linear bicycle model is limited in accurately calculating the controlled state variables. To remedy the problem, a non-linear observer can be implemented to increase the accuracy of the result. The non-linear observer with its closed-loop feedback control will produce better estimation results to the non-linear vehicle response. However, for slippery road conditions, the results will still be inaccurate as the road coefficient of friction calculation cannot be performed easily nor accurately. One possible way to address the issue is using infrared sensors to determine the road surface condition but it still does not yield reliable result

to determine an accurate road surface condition. For example, a puddle of water is hard to distinguish from ice and vice versa for the infrared sensor. Such a system is very costly to implement for production vehicles.

The bicycle model can also be replaced with a two-track model which adds roll, pitch, bounce, and forward speed as a variable. The estimation result will be improved with a better accuracy due to a realistic weight transfer based on motion on four wheels. As well, inclusion of Pacejka non-linear tire model in the controller model design will generate more realistic tire forces. Combining the two will yield more accurate lateral and longitudinal tire forces that will calculate more realistic state variable values closer to the actual vehicle response. However, this is an idealized controller design which requires an extensive computing power.

Actual track/road testing remains to be done for the VDC performance validation on controlling the actual hybrid system function. It is expected that an iterative testing procedure will be required to verify and tune the developed VDC as the bicycle model parameters used are simulated estimates of the prototype vehicle. The same applies for the validation of the *CarSim* simulation results as the simulation model was developed using estimated values.

REFERENCES

1. Kiers, M.T. "Automotive Regenerative Braking Utilizing Electrochemical Capacitor Energy Storage." Diss. (M.A.Sc. Thesis) University of Waterloo, Canada, 2004.

2. van Zanten, A.T., Erhardt, R., Pfaff, G. "VDC, The Vehicle Dynamics Control system of BOSCH [SAE Paper Number: 950759]." Electronic Braking, traction, and Stability Controls. Warrendale, Pennsylvania: SAE International, 1999.

3. Wakefield, E.H. History of the Electric Automobile- Hybrid Electric Vehicles. Warrendale, Pennsylvania: SAE International, 1998.

4. van Zanten, A.T., Erhardt, Lutz, A., Neuwald, W., Bartels, H. "Simulation for the Development of the BOSCH-VDC [SAE Paper Number: 960486]." Electronic Braking, traction, and Stability Controls. Warrendale, Pennsylvania: SAE International, 1999.

5. Tseng, E.H., Ashrafi, B., Madau, D., Brown, T.A., Recker, D. "The Development of Vehicle Stability Control at Ford." IEEE/ASME Transactions on Mechatronics. Vol. 4, No. 3, Sept. 1999.

6. Panagiotidis, M., Delagrammatikas, G., Assanis, D. "Development and Use of a Regenerative Braking Model for a Parallel Hybrid Vehicle [SAE Paper Number: 2000-01-0995]." Warrendale, Pennsylvania: SAE International, 2000.

7. Khatun, P., Bingham, C.M., Schofield, N., Mellor, P.H. "An Experimental Laboratory Bench Setup to Study Electric Vehicle Antilock Braking/Traction Systems and their Control [IEEE Paper Number: 0-7803-7467-3/02]." Institute of Electrical and Electronics Engineers. 2002.

8. Mi, C., Lin, H., Zhang, Y. "Iterative Learning Control of Antilock Braking of Electric and Hybrid Vehicles." IEEE Transactions on Vehicular Technology, Vol., 54, No. 2. Mar. 2005.

9. Hori, Y. "Future Vehicle driven by Electricity and Control- Research on Four Wheel Motored "UOT Electric March II"-." IEEE Publications, 2002.

10. Soga, M., Shimada, M., Sakamoto, J.I., Otomo, A. "Development of vehicle dynamics management system for hybrid vehicles: ECB system for improved environmental and vehicle dynamic performance." Japanese Society of Automotive Engineers Review 23 (2002): pg. 459-464

11. Limpert, R. Brake Design and Safety, 2nd Ed. Warrendale, Pennsylvania: SAE International, 1999.

12. Husain, I. Electric and Hybrid Vehicles- Design Fundamentals. USA: CRC Press, 2003.

13. Westbrook, M.H. The Electric and Hybrid Electric Car. Warrendale, Pennsylvania: SAE International, 2001.

14. Pacejka, H. Tyre and Vehicle Dynamics. Oxford: Butterworth Heinemann, 2002.

15. Karnopp, D. Vehicle Stability. New York: Marcel Dekker Inc., 2004.

16. Milliken, W.F., Milliken, D.L. Based on previously unpublished technical notes by Olley, M. Chassis Design Principles and Analysis. Warrendale, Pennsylvania: SAE International, 2002.

17. Dixon, J.C. Tires, Suspension and Handling 2nd Ed. Warrendale, Pennsylvania: SAE International, 1996.

18. Robert BOSCH GmbH. The vehicle dynamic control system, ESP Presentation, CD-ROM. 2001.

19. Robert BOSCH GmbH. Automotive Handbook, 4th Ed. Stuttggart, Germany: Robert BOSCH GmbH, 1996.

20. Robert BOSCH GmbH. Driving-safety systems, 2nd Ed. Warrendale, Pennsylvania: Society of Automotive Engineers International, 1999.

21. Walker Jr., J. "Introduction to Brake Control Systems (SAE Seminar)." SAE Professional Development Program. Detroit, Michigan, Feb. 2005.

22. Continental-TEVES Corporation. Brake-by-Wire Technologies. 15 Aug. 2004 <http://www.conti_online.com/generator/www/us/en/continentalteves/continentalteves /themes/products/brake_by_wire/overview_en.html>.

23. Heydinger, G.J., Bixel, R.A., Garrott, W.R., Pyne, M., Howe, J.G., Guenther, D.A. "Measured Vehicle Parameters-NHTSA's Data Through November 1998 [SAE Paper Number: 1999-01-1336]." Warrendale, Pennsylvania: SAE International, 1999.

24. Biernacki, M. DAIMLERCHRYSLER Corp., Chrysler Technical Center- Advanced Powertrain Group. Auburn Hills, Michigan. 2005.

25. John, J. DAIMLERCHRYSLER Corp., Chrysler Technical Center- Powertrain Group. Auburn Hills, Michigan. 2005.

26. Motor Trend. Road Test: 2005 Ford Freestyle vs 2004 Chrysler Pacifica. 17 Jul. 2005 <http://www.motortrend.com/roadtests/suv/112_0501_free_paci/index4.html>.

27. 2004 SAE World Congress, Detroit, Michigan, 2004.

28. Arndt, M., Ding, E.L., Massel, T. "Identification of Cornering Stiffness During Lane Change Maneuvers." 2004 IEEE International Conference on Control Applications. Taipei, Taiwan. 2-4 Sept., 2004

29. Brogan, W.L. Modern Control Theory, 3rd Ed. New Jersey: Prentice-Hall, Inc., 1991.

30. Brown, J.W., Sherbert, D.R. Introductory Linear Algebra with Applications. Boston, Massachusetts: Prindle, Weber &Schmidt, 1984.

31. Chen, C. Linear System Theory and Design, 3rd Ed. New York: Oxford University Press, 1999.

32. DAIMLERCHRYSLER Corporation. CS Platform Technical Manual. Auburn Hills, Michigan. 2005.

33. Erb, D. "Design of Hybrid Electric Vehicles (SAE Seminar)." SAE Professional Development Program. Troy, Michigan, Jul. 2004.

34. Franklin, G.F., Powell, J.D., Emami-Naeini, A. Feedback Control of Dynamic Systems, 3rd Ed. USA: Addison Wesley Publishing Company Inc., 1994.

35. Gillespie, T.D. Fundamentals of Vehicle Dynamics. Warrendale, Pennsylvania: SAE International, 1992.

36. Hac, A., Simpson, M. "Estimation of Vehicle Side Slip Angle and Yaw Rate [SAE Paper Number: 2000-01-0696]." Warrendale, Pennsylvania: SAE International, 2000.

37. Hodkinson, R., Fenton, J. Lightweight Electric/Hybrid Vehicle Design. Warrendale, Pennsylvania: SAE International, 2001.

38. Johansson, R., Rantzer, A. eds. Nonlinear and Hybrid Systems in Automotive Control. Sweden: Springer, 2003.

39. Jurgen, R.K. ed. Electronic Braking, Traction, and Stability Controls. Warrendale, Pennsylvania: SAE International, 1999.

40. Kiencke, U., Nielsen, L. Automotive Control Systems, 2nd Ed. Germany: Springer, 2005.

41. Maiorana, J.G. "Active Suspension Simulation Through Software Interfacing." Diss. (M.A.Sc. Thesis) University of Windsor, Canada, 2004.

112

42. Meriam, J.L., Kraige, L.G. Engineering Mechanics- Dynamics, 4th Ed., USA: John Wiley & Sons, 1998.

43. Minaker, B.P. "Active Geometry Suspension for Road Vehicles." Diss. (Ph.D. Thesis) Queen's University, Canada, 2001.

44. Minaker, B.P. "Development of a Computer Model to Study the Effects of Design Parameters on Vehicle Handling." Diss. (M.A.Sc. Thesis) Queen's University, Canada, 1995.

45. Rice, B.J., Strange, J.D. Ordinary Differential Equations with Applications, 3rd Ed. California: Brooks/Cole Publishing Company, 1993.

46. Stewart, J. Calculus- Early Transcendentals, 3rd Ed. California: Brooks/Cole Publishing Company, 1995.

47. Test drive. Honda 2005 Hybrid Civic. February, 2004.

48. Test drive. Toyota 2005 Prius. February, 2004.

49. Wong, J.Y. Theory of Ground Vehicles, 3rd Ed. Canada: John Wiley & Sons, Inc., 2001.

50. Zehnder II, J.W., Kanetkar, S.S., Osterday, C.A. "Variable Rate Pedal Feel Emulator Designs for a Brake-By-Wire System [1999-01-0481]." SAE International, Warrendale, Pennsylvania, 1999.

APPENDIX

A

SIEMENS ELECTRIC MOTOR PERFORMANCE DATA

114
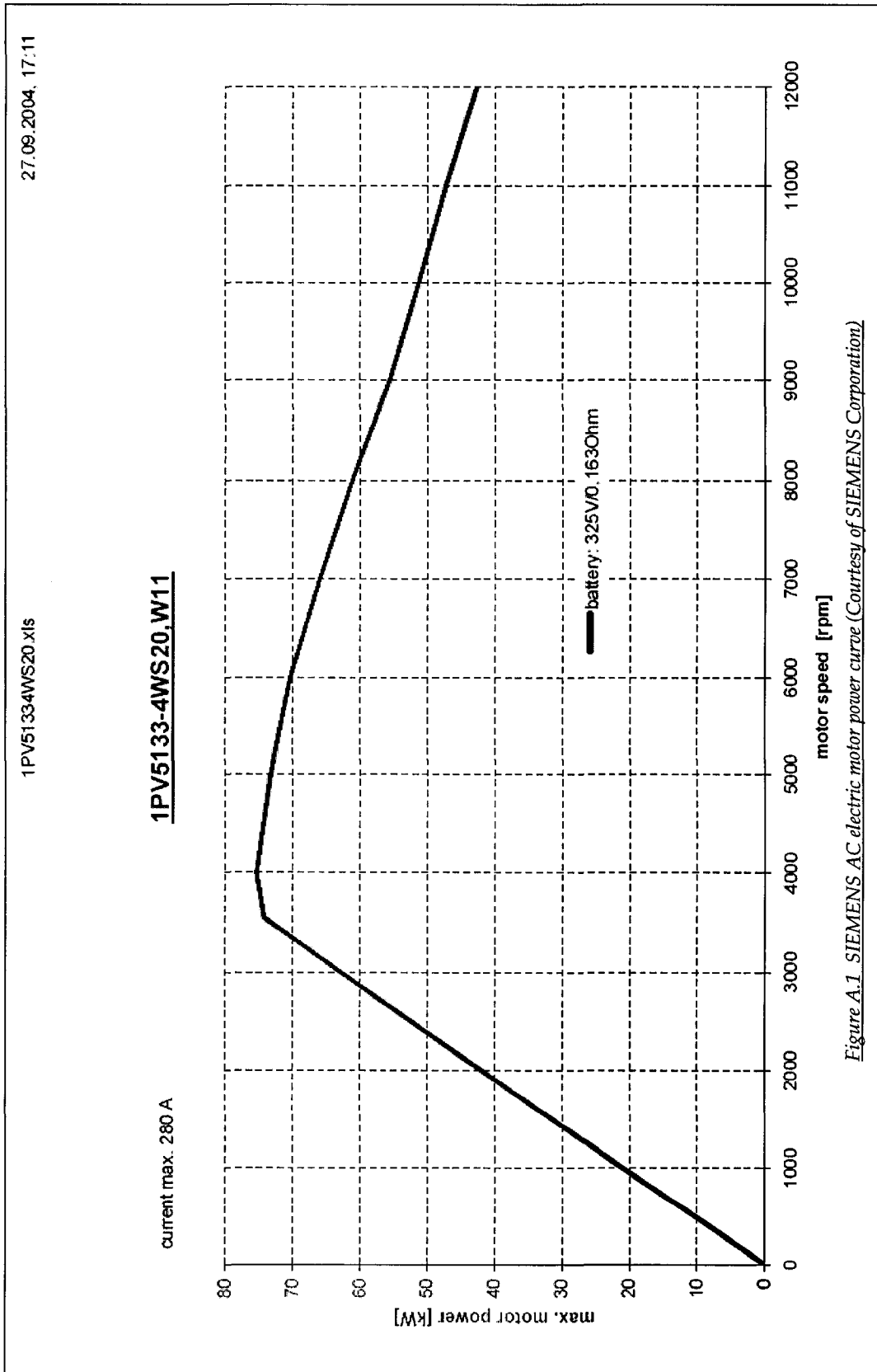
Figure A.1 SIEMENS AC electric motor power curve (Courtesy of SIEMENS Corporation)
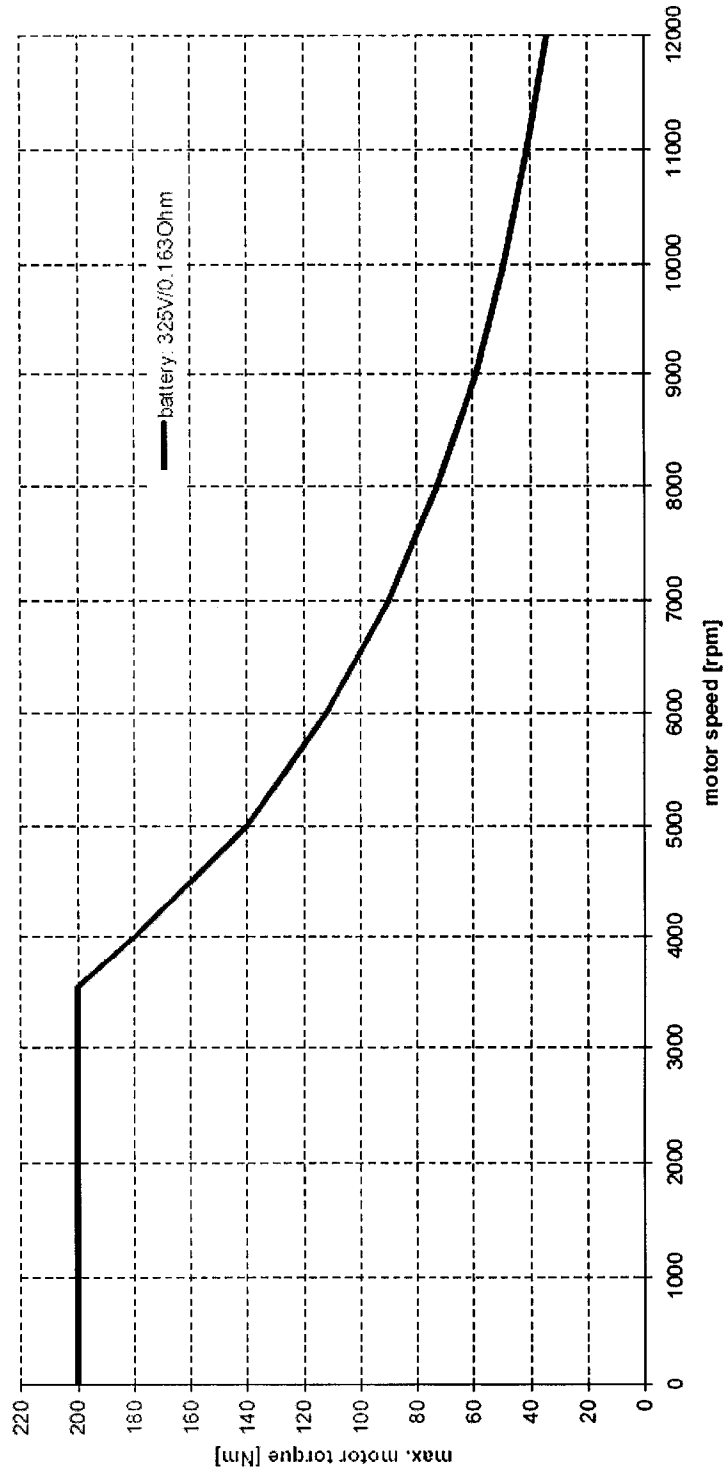
Figure A.2 SIEMENS AC electric motor curve (Courtesy of SIEMENS Corporation)

116

APPENDIX

B

BRAKE-BY-WIRE OPERATION LOGIC

Two Stage Braking System Functional Block Diagram

Driver Input:
Brake Pedal Angle
(T^*_{brake})

Hydraulic Brake System:
Actuated when pedal travel is in Stage II region

M/C Pressure

Pacifica DAQ

PIC 18F458- Regenerative Braking Controller:
1) Calculate T_{Regen} from pedal angle
2) Process T_{Regen} command
(Hydraulic is independent of this system, additional braking of hydraulics will only be actuated by driver's foot when regen braking cannot provide sufficient deceleration)

Hybrid Master Controller:
1) Process all DAQ data

T^*_{regen}

Hydraulic braking torque delivered independent of the Hybrid System

Motor Controller

Braking at Wheel

Legend
T^*_{brake}- Braking Torque Command by Driver
T^*_{regen}- Regenerative Braking Torque Command by Controller

Figure B.1 "Dual-Stage" brake-by-wire system functional diagram

118

Brake-By-Wire Control Logic Flowchart

Ed Oh, 12/14/04, Rev.2.0
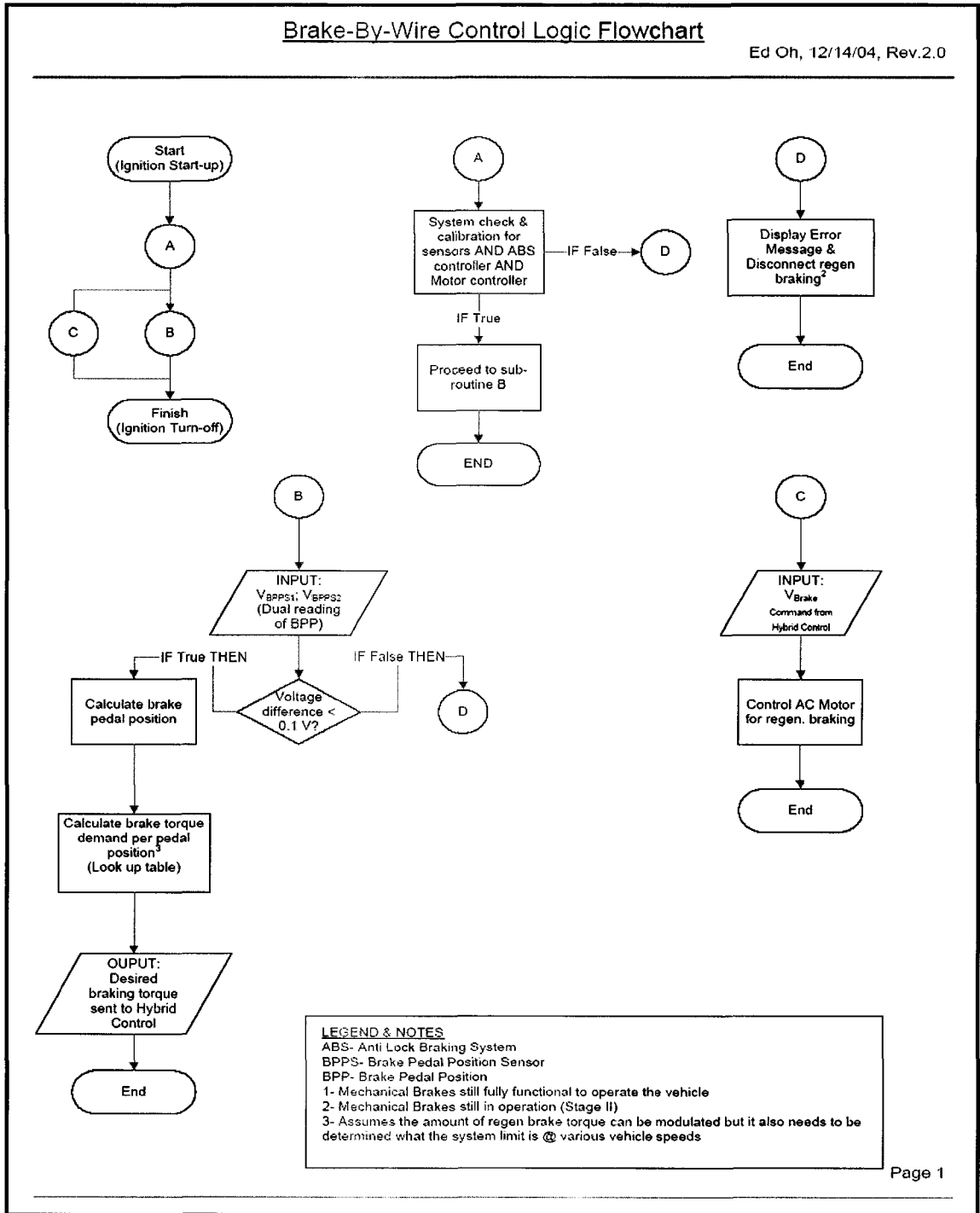
Figure B.2 "Dual-Stage" brake-by-wire control logic flow chart

119

APPENDIX

C

PROTOTYPE HYBRID *PACIFICA* MODELING DATA

Figure C.1 Prototype hybrid Pacifica mass & dimensional properties used in CarSim simulation model

Formula SAE
Univ. of Windsor
Ontario, Canada
8-919-696

C:\Program Files\Mitchell\Geometry\Pacifica\050727-pacifica front macpherson strut-good with camber.GEM

Ride
0.000

Camber
-0.976

Roll
0.000

Camber
-0.976

Steer*
-0.000

Steer
0.000

Steer*
0.000

NetStr*
-0.000

Spring
0.000

Spring
-0.000

Scrub
-0.000

Scrub
0.000

NetScrub
-0.000

Twist
0.000

SVSA	Ins.Cen.	ARBratio		Roll Cen	ARBratio	Ins.Cen.	SVSA
1817.350	1464.549	-0.000		-0.000	0.000	1464.549	1817.350
202.254	264.910			154.158		264.910	202.254

Figure C.2 Racing by the Numbers software used for Pacifica suspension kinematics analysis

122

APPENDIX

D

VEHICLE DYNAMICS CONTROLLER IMPLEMENTATION USING PIC18F458 MICRO-CONTROLLER

123

D.1 Physical Architecture

The *Simulink* VDC design obtained in Chapter 5 is implemented to a microprocessor

using Microchip's PIC18F458. The VDC transfer functions and the design architecture developed

in this study are programmed in 'Assembly' language and it is implemented[15] on the VDC PIC

microcontroller which is an integral part of the hybrid system controller on the prototype vehicle.

The following figure describes the physical architecture of the VDC PIC controller. It shows the

interaction among the motion sensors, VDC PIC, and hybrid system controller PIC.
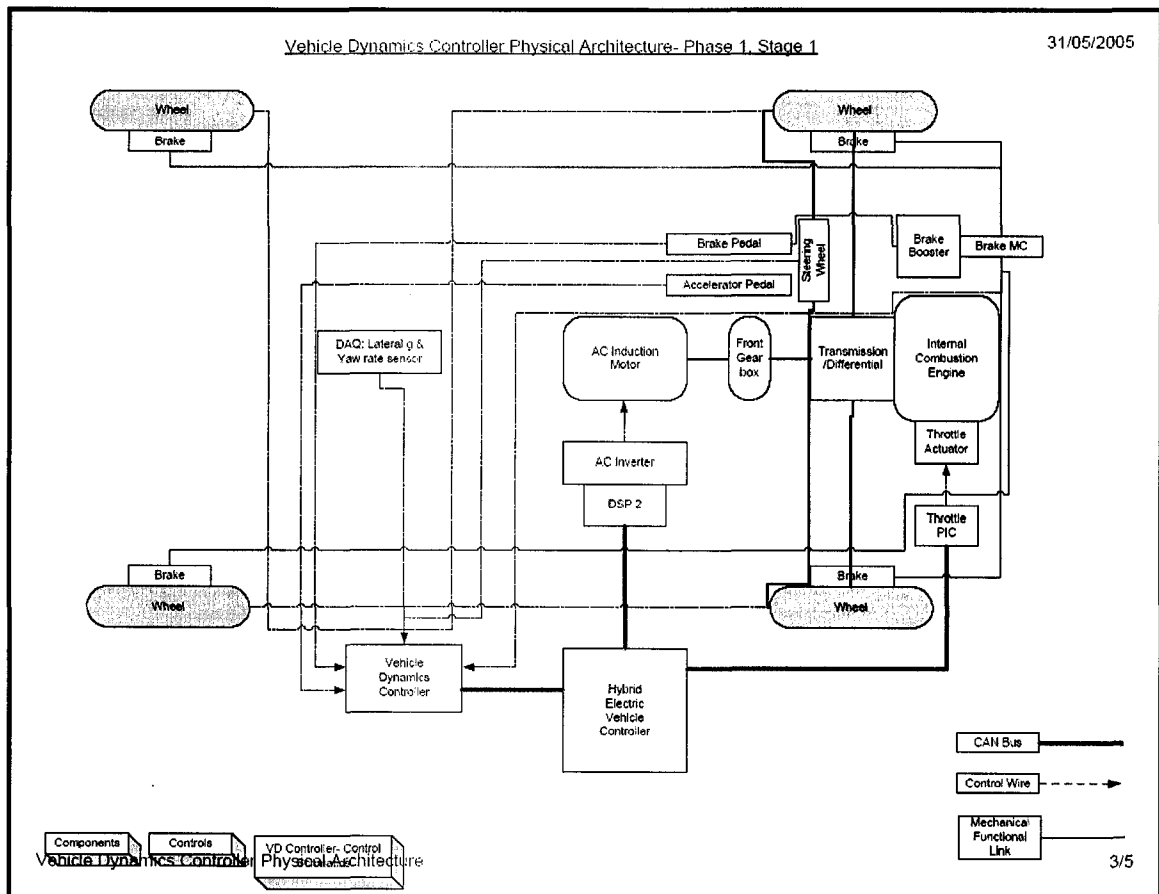
Figure D.1 Physical architecture of VDC PIC on hybrid Pacifica

---

[15] Dr. M. Marei and M. Wei at the University of Waterloo have co-developed the hybrid system controller and VDC
PIC *Assembly* programming and implementation are executed by the researchers.

124

D.2 System Architecture
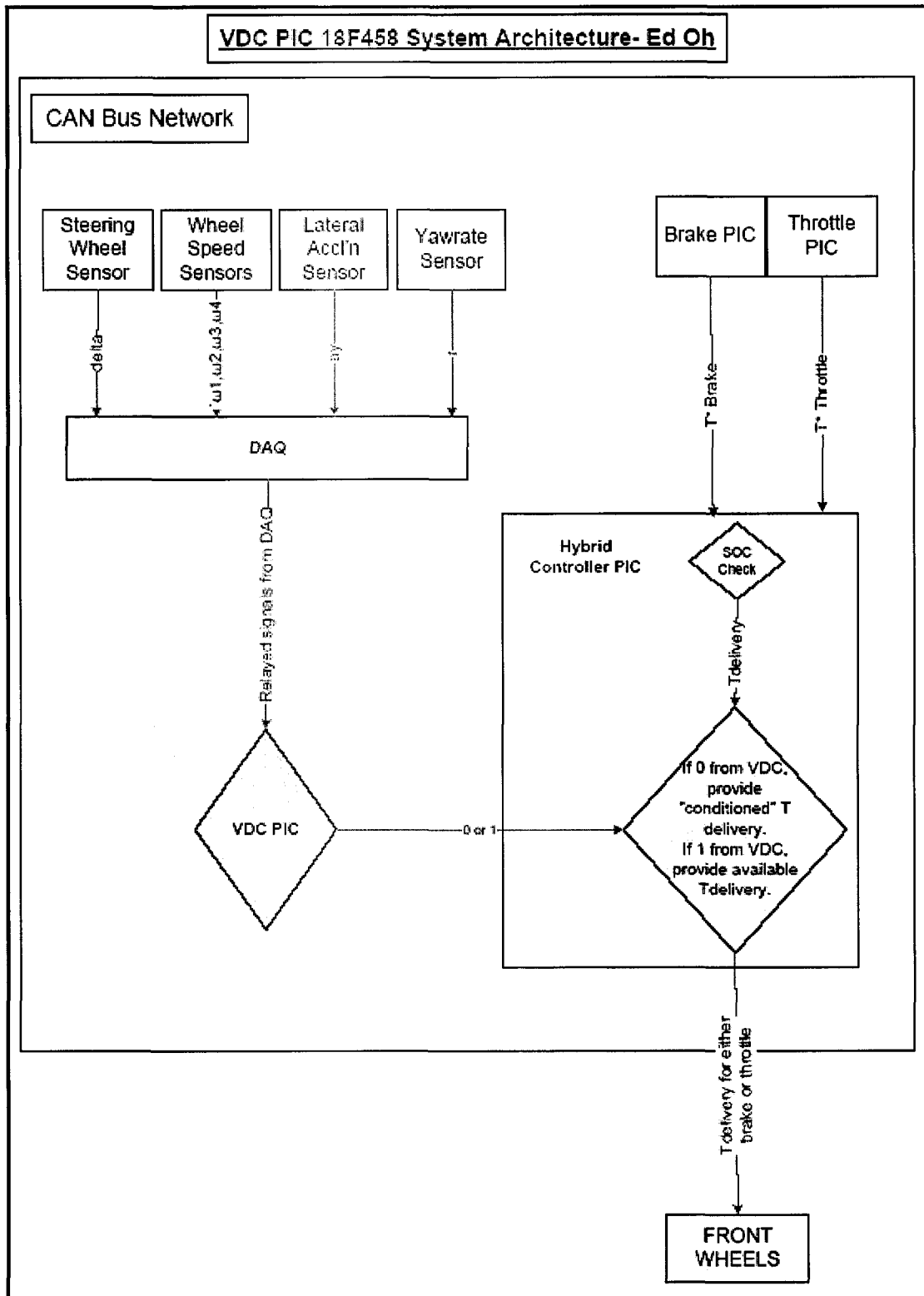
Figure D.2 VDC system architecture

125

Figure D.2 shows the system architecture of the VDC PIC and its interaction with motion sensor signals and the hybrid system controller PIC. Driver's speed input, either brake or throttle, is processed directly by the hybrid system controller and the request is processed based on the SOC level of the ultracapcitor pack. At the same time, the VDC PIC calculates the vehicle dynamics state of the vehicle as described in the section 5.2. Its output signal is given as 0 or 1 digital signal in which 0 translates to 'suspend' and 1 to 'deliver' to the torque delivery command of the hybrid system controller PIC. As a result, this controls either the regenerative braking or drive assist torque from the electric motor in order to maintain the vehicle stability in driving.

126

D.3 Motion Sensors

For VDC operation, the following motion sensors are used. These sensors are planned to be implemented with the vehicle data acquisition system.

Table D.1 List of motion sensors used for VDC function

Item	Sensor Description	Quantity	Analog/Digital
1	Steering Wheel Angle Sensor	1	A
2	Lateral Acceleration Sensor	1	A
3	Yaw Rate Sensor	1	A
4	Wheel Speed Sensor	4	D

Using the sensor technical specification, attached at the end of this appendix, each of the sensor signal input voltage is designed to be converted as values listed in Table D.2. The converted signal data are then used as input values in the VDC PIC calculation.

Table D.2 Input sensor signal conversion data

Input Signal	Variable Name	Sensor Range [V]	Units	Range
Wheel speed 1	u1	0 to 5	m/s	0 to $\omega_{max}/0.353$
Wheel speed 2	u2	0 to 5	m/s	0 to $\omega_{max}/0.353$
Wheel speed 3	u3	0 to 5	m/s	0 to $\omega_{max}/0.353$
Wheel speed 4	u4	0 to 5	m/s	0 to $\omega_{max}/0.353$
Steering Angle	steer	0 to 1.87	°	-32.16 to +32.16
Lateral Acceleration	Aym	0.65 to 4.35	m/s²	-17.658 to 17.658
Measured Yaw Rate	yawm	0.65 to 4.35	°/s	-100 to 100
ABS Signal	ABS	0, 5	unitless	0,1

D.3.1 Wheel Speed Sensor Technical Specification

The technical specification of the wheel speed sensor used in *Mark 25 ABS System* on *Pacifica* was obtained from CONTINENTAL TEVES Corporation. However, due to the confidentiality agreement, the specification data is not published.

127

D.3.2 Steering Wheel Angle Sensor Technical Specification

Miniature
MP series

Description

AMETEK Rayelco™ Miniature Position Transducer has been designed to provide maximum user flexibility. This unit can be mounted in confined areas and by simply loosening a single bolt, direct the cable in any direction by turning the transducer body 360 degrees and the mounting swivel 180 degrees. Slotted cable entry allows the cable to be out of alignment by as much as ±10 degrees in one axis.

Features

- ≥ Standard Accuracy ±0.1% FS*
- ≥ Ranges to 20 inches
- ≥ 'A' Circuit Output Equals Input
- ≥ Extra Long-Life Replaceable Cable
- ≥ Precision Hybrid or Wirewound Potentiometer
- ≥ All Anodized Aluminum and Stainless Steel Construction

*±0.25% FS, 0-2", 0-5" and 0-10"
High Accuracy ±0.15% FS Option Available

Applications

- • Automotive Testing
- • Robotics Control
- • Aircraft Stress Testing
- • Injection Mold Equipment Control
- • Aircraft Door Sensing
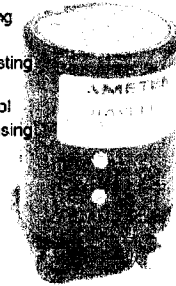
Basic Specifications

Performance

Ranges:	0-2" through 0-20"
Linearity (BFSL):	±0.1% FS
	±0.25% FS, 0-2", 0-5" and 0-10"
Resolution:	Infinite (Hybrid Potentiometer)

Individual Calibration Sheet Provided

Electrical

Excitation:	AC or DC up to 25 volts

Input Impedance:	'A' Circuit	500 ohms
Output Impedance:	'A' Circuit	0-500 ohms

Environmental

Temperature:	0-200°F
Humidity:	95% RH @ 75°F
Shock:	50g for 10 ms
Vibration:	20g 20Hz-2 kHz

Physical

Construction:	Anodized Aluminum and Stainless Steel
Electrical Cable Type:	8', 3 conductor shielded, teflon jacketed

Replaceable long-life cable

Specification Table

Model	mV/V/inch "A" cir	Tension oz
MP-2	500	24
MP-5	200	24
MP-10	100	24
MP-15	66	24
MP-20	50	24

Ordering Information

MP - 20 A

Model | Range | Circuit
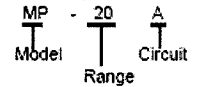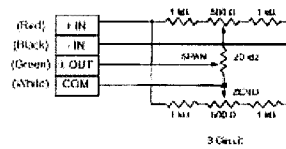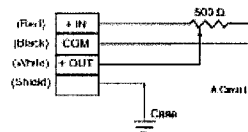
Circuit Diagram

4-20 mA & "B" Circuit External Conditioner Enclosure
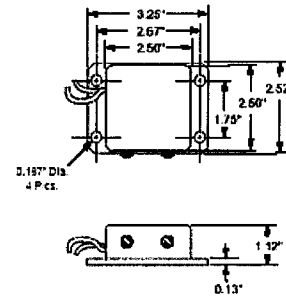
Model Diagram
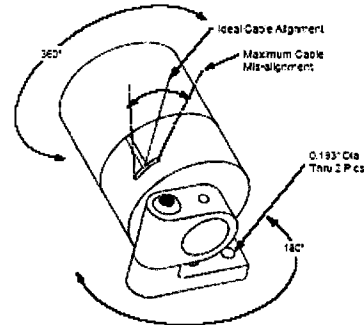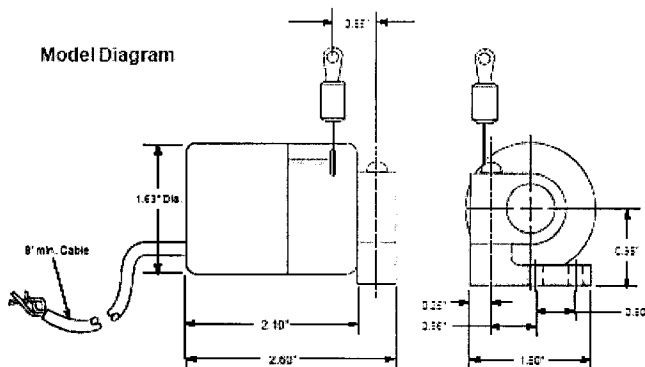
Specifications subject to change without notice

Durham Instruments, 1400 Bayly St. Unit 23, Pickering, Ontario, L1W 3R2

888-DISENSOR, www.disensors.com, sales@disensors.com

128

D.3.3 Yawrate & Lateral Acceleration Sensor Technical Specification

K1 Original Equipment Information   ⊕   **BOSCH**
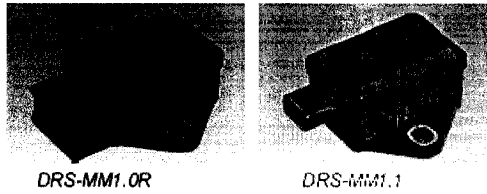
DRS-MM1.0R   DRS-MM1.1

Figure 3   Yaw rate sensors DRS-MM1.0R (analog) and DRS-MM1.1 (digital interface).

The DRS-MM family is a rugged and compact sensor offering viability. Its 12 V battery compatibility and additional safety functions make it the preferred choice for automotive endurance applications. Further application fields for the yaw rate sensor DRS-MM1 are available e.g. in navigation systems.

3 Features and Applications

The currently available versions of the DRS MM1 are shown in figure 3. It can be supplied either with an analog (DRS-MM1.0R) or digital (DRS-MM1.1) interface. For both sensors the output signals comprise simultaneously the yaw rate and the linear acceleration normal to the driving direction. The yaw rate output signal is superimposed by an internally generated reference voltage of 2,5V. Check- and safety-functions of the complete sensor unit are realized by an externally triggered, alternating signal. For each sensor at the end of line, the offset is trimmed in temperature and the sensitivity is controlled over the specified temperature range.

The DRS-MM1.0R provides an output voltage between 0,5 and 4,5V (see figure 4). An extra connector pin provides the reference voltage.

For the DRS-MM1.1, the yaw rate signal is calculated internally and transmitted simultaneously with the acceleration signal using a CAN protocol.
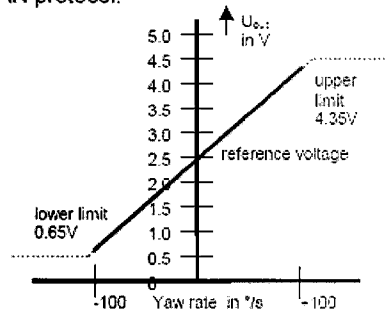
Figure 4   Typical characteristic curve of the yaw rate sensors DRS MM1.0R.

4 Specifications DRS-MM1

Yaw rate sensor (typical values)	
Measuring range	± 100 °/s
Resolution	±0.2 °/s
Scale factor	18 mV/°/s
Scale factor error	≤5 %
Offset error	≤2 °/s
Non-linearity, maximal deviation	≤1 % FSO
Ready time	≤1.0 s
Electrical noise (@ 100 Hz bandwidth)	≤5 mV_rms

| Linear acceleration sensor (typical values)	
Measuring range	± 1.8 g
Scale factor	1000 mV/g
Scale factor error	≤5 %
Offset error	≤0.06 g
Ready time	≤1.0 s
Electrical noise (@ 100 Hz bandwidth)	≤5 mV_rms
Non-linearity, maximal deviation	≤3 % FSO

General data	
Dynamic response	≥30 Hz
Operating temperature range	-40...+85 °C
Supply voltage range	8.2...16 V (12 V nominal)
Current consumption at 12V	70 mA analog, 140 mA CAN

Further Information	Technical Sales Product Team Sensors
	Tel. +(49)-711/811 –34303
	Fax +(49)-711/811 –24873
Version 1.06, 9.11.1999	E-mail K1.sensors@bosch.com

D.4 VDC PIC 18F458 Controller

The PIC18F458 microcontroller is designed to work with the controller area network (CAN) bus electronic network of many automotive applications. Since the SIEMENS motor controller uses the CAN bus network, it was necessary to use such controller. PIC18F458 has the operating frequency of DC- 40MHz with 32K Bytes of internal program memory. It also features 40 pin connections to handle signal communications. For VDC, 8 pins are used for motion and ABS sensor signals and 1 pin is used for communicating with the hybrid system controller PIC.

The VDC PIC controller performs three main operations. The first stage of operation is to process the motion sensor data (Table D.2) from the vehicle data acquisition system. In the second stage, the VDC PIC performs the calculations listed in the following Table D.3. The equations listed are the same equations used in the *Simulink* model.

Table D.3 VDC PIC calculations for vehicle dynamics states

Calculations	Variable Name	Equation	Units
Linear Speed	ua	ua= 0.25 × (u1+u2+u3+u4)	m/s
Slip Ratio 1	slip1	If ua = 0, slip1=0 Else, slip1= |u1-ua|/ua	unitless
Slip Ratio 2	slip2	If ua = 0, slip2=0 Else, slip2= |u2-ua|/ua	unitless
Slip Ratio 3	slip3	If ua = 0, slip3=0 Else, slip3= |u3-ua|/ua	unitless
Slip Ratio 4	slip4	If ua = 0, slip4=0 Else, slip4= |u4-ua|/ua	unitless
Steady State Yaw Rate	yawss	If ua = 0, yawss=0 Else, yawss= (Aym/ua) × (180/π)	°/s
Beta_dot	betadot	betadot= yawss – yawm	°/s
Beta	beta	If ua=0, beta=0 Else, beta= (Cf*steer-[(a*Cf-b*Cr)*r/u]-m*u*(Beta_dot-r)/(Cf+Cr)	°
Ay_commanded (Ay_nominal)	Ayc	= {u²/[(a+b)-(m(aCf-bCr)/(a+b)CfCr)]}steer	m/s²
Ay_commanded/ Ay_measured	AyRatio	=(|Ay_commanded|+1)/(|Aym|+1)	unitless

In the last stage of the VDC PIC operation, the final safety check is performed in deciding the delivery of electric motor torque to the driven wheels. The digital 0 (suspend) or 1 (deliver) signal is the output of the following 'safety check' calculations.

Table D.4 VDC PIC safety check calculations for electric motor torque delivery decision for the hybrid system controller

Safety Checks	Variable Name	Units	Condition for Safe	Condition for Unsafe
Slip Ratio 1 Threshold Check	slip1	unitless	≤ 0.18	> 0.18
Slip Ratio 2 Threshold Check	slip2	unitless	≤ 0.18	> 0.18
Slip Ratio 3 Threshold Check	slip3	unitless	≤ 0.18	> 0.18
Slip Ratio 4 Threshold Check	slip4	unitless	≤ 0.18	> 0.18
Lateral Acceleration Threshold Check	Ay	m/s^2	≤ 7.00	> 7.00
Lateral Acceleration_commanded/Lateral Acceleration_measured	Ay Ratio	unitless	≤ 2	> 2
Beta Steady State	beta	°	≤ 4	> 4
ABS Trigger Signal	ABS signal	unitless	OFF	ON

The final commanding signal of VDC PIC is relayed to the hybrid system controller PIC for the final delivery of driver's torque request.

131

D.4.1 VDC PIC Assembly Code

```
;*******************************************************************************
;     Filename: Vehicle Dynamics                                              *
;     Date: August 2, 2005                                                    *
;     File Version: v5                                                        *
;         Oct 13,2005 - implement input from A/D module                       *
;         Dec 12,2005 - scale analog input by 4 (10 bits down to 8bits)       *
;         Jan 15,2006 - new functions and inputs                              
;                                                                             *
;         Jan 20,2006 - new functions again                                   
;                                                                             *
;                                                                             *
;     Author: Maria Wei, Mostafa Marei                                        *
;     Company: University of Waterloo                                         *
;*******************************************************************************
;     Files required:        P18F458.INC, MATH18.INC                          
*
;                            FP24.A18, VD.A18, Compare.A18, Safety.A18        
*
;*******************************************************************************

        title "PIC18F458 Vehicle Dynamics"
        LIST P=18F458        ;directive to define processor
        #include <P18F458.INC>    ;processor specific variable definitions
        #include <MATH18.INC>     ;AN00575 floating point math routines

;*******************************************************************************
;Configuration bits

        __CONFIG _CONFIG1H, _OSCS_OFF_1H & _HSPLL_OSC_1H
        __CONFIG _CONFIG2L, _BOR_OFF_2L & _PWRT_OFF_2L
        __CONFIG _CONFIG2H, _WDT_OFF_2H
        __CONFIG _CONFIG4L, _STVR_OFF_4L
        __CONFIG _CONFIG5L, _CP0_OFF_5L & _CP1_OFF_5L & _CP2_OFF_5L & _CP3_OFF_5L
        __CONFIG _CONFIG5H, _CPB_OFF_5H & _CPD_OFF_5H
        __CONFIG _CONFIG6L, _WRT0_OFF_6L & _WRT1_OFF_6L & _WRT2_OFF_6L &
_WRT3_OFF_6L
        __CONFIG _CONFIG6H, _WRTB_OFF_6H & _WRTC_OFF_6H & _WRTD_OFF_6H
        __CONFIG _CONFIG7L, _EBTR0_OFF_7L & _EBTR1_OFF_7L & _EBTR2_OFF_7L &
_EBTR3_OFF_7L
        __CONFIG _CONFIG7H, _EBTRB_OFF_7H

;*******************************************************************************
;Variable definitions

; CBLOCK 0x000 is for math routines
                CBLOCK 0x100
                COUT                    ;
                STATUS_SAVE, W_SAVE     ; variables for context saving
                u1EXP, u10, u11                 ; input u
                u2EXP, u20, u21                 ; input u
                u3EXP, u30, u31                 ; input u
                u4EXP, u40, u41                 ; input u
                steerEXP, steer0, steer1; input steer
                AymEXP, Aym0, Aym1      ; input lateral acceleration
                yawmEXP, yawm0, yawm1   ; input yaw rate
                uaEXP, ua0, ua1                 ; calculated reference speed
                slip1EXP, slip10, slip11; calculated slip 1
                slip2EXP, slip20, slip21; calculated slip 2
                slip3EXP, slip30, slip31; calculated slip 3
                slip4EXP, slip40, slip41; calculated slip 4
                yawssEXP, yawss0, yawss1; calculated yaw rate
```

132

```
              AycEXP, Ayc0, Ayc1        ; calculated lateral acceleration
              AyrEXP, Ayr0, Ayr1        ; lateral acceleration ratio
              betaEXP, beta0, beta1     ; calculated beta
              blahEXP, blah0, blah1     ; variables used for temporary storage
              mehEXP, meh0, meh1        ; variables used for temporary storage
              ENDC

#define ADGOBit ADCON0, 2
#define CARRYBit STATUS, 0
#define TM2IFBit PIR1, 1
#define ABS PORTB, 0
;#define TM2IO PORTD, 0              ; Testing to check period of interrupt
subroutine
#define StarBit PORTD, 7

testlitH equ 0x01                   ; for testing purposes when call GetInTest
testlitL equ 0xB1


;*******************************************************************************
;EEPROM data
;*******************************************************************************
;Reset vector
              ORG     0x0000

              goto    Main          ;go to start of main code

;*******************************************************************************
;High priority interrupt vector
;*******************************************************************************
;Low priority interrupt vector and routine
;*******************************************************************************
;High priority interrupt routine

              ORG 0x0008


;         *** high priority interrupt code goes here ***

; Push upon entering interrupt
        movwf W_SAVE          ; save w
        swapf STATUS, F       ; swap STATUS
        swapf STATUS, W
        movwf STATUS_SAVE     ; save STATUS

;       bsf TM2IO             ; Testing to check period of interrupt
subroutine

        call GetIn            ; Get Inputs
;       call GetInTest        ; Get Inputs Testing
        call VDFun            ; Call Transfer Functions
        call SafetyFun        ; Call Safety Checks

;       bcf TM2IO             ; Testing to check period of interrupt
subroutine

; Pop upon exiting interrupt
        swapf STATUS_SAVE, F  ; restore STATUS
        swapf STATUS_SAVE, w
        movwf STATUS
        swapf W_SAVE, F       ; restore W
        swapf W_SAVE, W

        bcf TM2IFBit          ; clear T2 Int Flag
```

133

```
        retfie

;*******************************************************************************
;Start of main program

Main:

        clrf INTCON ; disable interrupts
        clrf PIR1 ; clear flags

; ================================
; A/D Initialization
        movlw b'10000000'    ; Right justify, C/R = 8/0
        movwf ADCON1;

; ================================
; I/O Initialization
        clrf PORTA            ; Clear PORTA
        clrf LATA
        movlw 0xFF            ; Set PORTA to be input
        movwf TRISA           ; PORTA(0): u1 input (analog)
                                    ; PORTA(1): u2 input (analog)
                                    ; PORTA(2): u3 input (analog)
                                    ; PORTA(3): u4 input (analog)
                                    ; PORTA(4): steer input (analog)
                                    ; PORTA(5): lateral acceleration input
(analog)
                                    ; PORTA(6): yaw rate input (analog)

        clrf PORTB            ; Clear PORTB
        clrf LATB
        movlw 0xFF            ; Set PORTB to be input
        movwf TRISB           ; PORTB(0): ABS input (digital)

        clrf PORTD            ; Clear PORTD
        clrf LATD
        movlw 0x00            ; Set PORTD to be output
        movwf TRISD           ; PORTD(0): timer2 interrupt output
                                    ; PORTD(7): Safety output


; ================================
; T2 initialization for period generations
        movlw 0x50    ; 1/PR2=foc(10MHz)/4/80=31.25kHz
        movwf PR2     ; Period of Timer 2
        movlw 0x07    ; postscaler = 1, Enable T2, prescale = 16
        movwf T2CON ; T2 freq. fsw=31.25kHz/(postscale * prescale) = 1.953125 kHz

; ================================
; Interrupts
        movlw 0x02    ; T2
        movwf PIE1    ; enable T2 interrupt
        clrf PIE2     ; disable all other interrupts
        clrf PIE3     ; disable all other interrupts
        movlw 0x02    ; T2 is High Priority Interrupt
        movwf IPR1
        movlw 0xC0    ; enable global and peripheral interrupts
        movwf INTCON;

self
        goto self

        #include <FP24.A18> ; floating point math routines
```

134

```
        #include <Compare.A18>; floating point comparison
        #include <Inputs.A18>; obtain analog inputs with offset
        #include <VD.A18>    ; transfer function calculations
        #include <Safety.A18>; safety calculation

; ================================
; End of program
END
```

135

APPENDIX

E

ADDITIONAL CO-SIMULATION RESULTS

The following simulation results are obtained from the same simulation cases performed in Chapter 6. The difference is the friction coefficient of road surface where $\mu = 0.85$. The results illustrate that the linear bicycle model produces very good estimation values for the nominal lateral acceleration and body slip angle of the non-linear *CarSim* prototype *Pacifica* model.

137

E.1 VDC Performance Validation on Regenerative Braking System

Double Lane Change Braking Simulation @ 90 KPH; μ=0.85
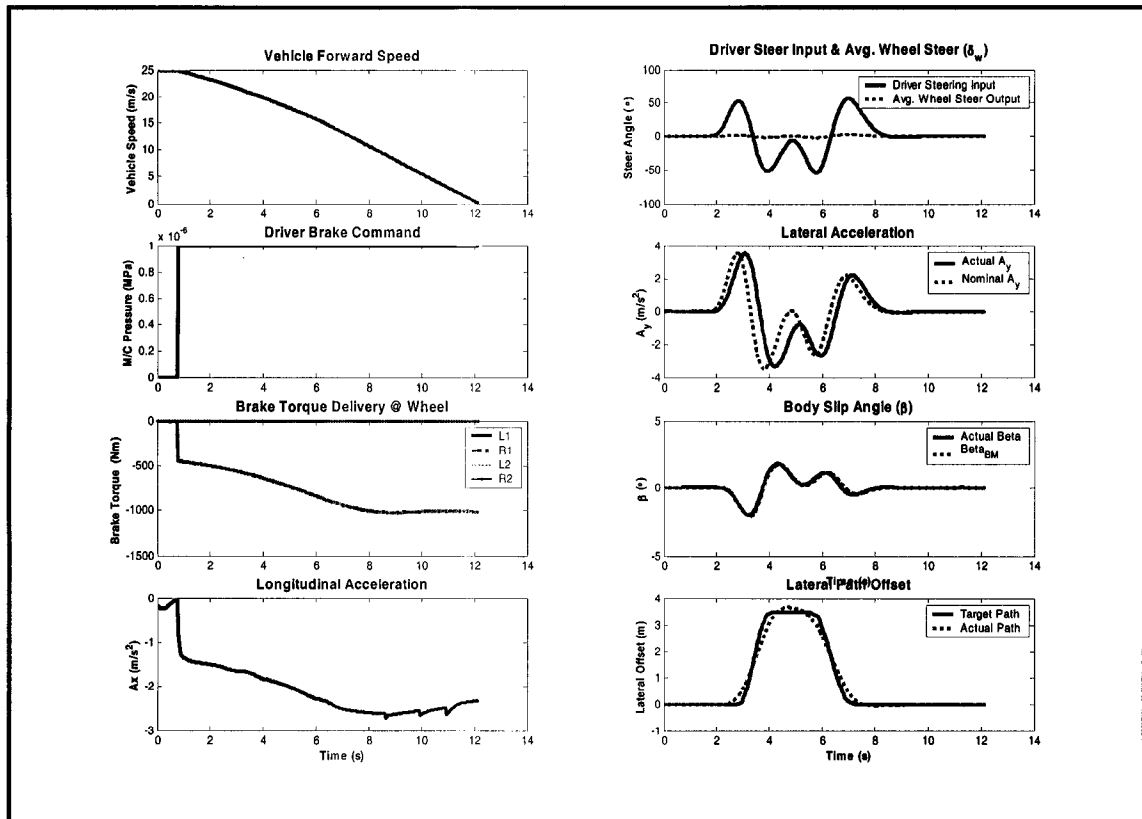
DLX Braking without VDC Control

Figure E.1 DLX REGEN braking without VDC Control @ 90 KPH; μ=0.85

Since the road surface friction is high, the tires are able to generate both braking and lateral forces to decelerate the vehicle while maintaining its lateral stability. Nominal lateral acceleration only deviates by little and the body slip angle response is very close to the non-linear response of the hybrid *Pacifica* simulation model.
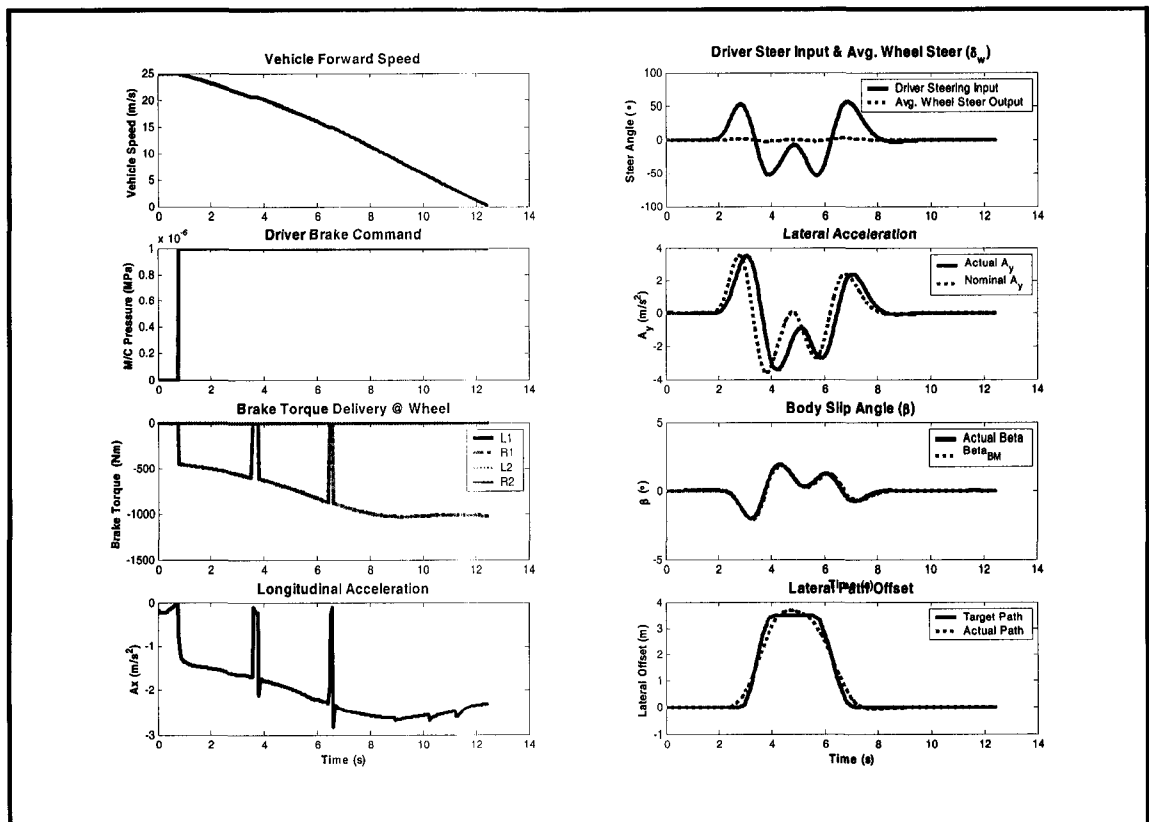
DLX Braking with VDC Control

Figure E.2 DLX REGEN braking with VDC Control @ 90 KPH; μ =0.85

As with the first case, the estimation performance of the linear bicycle model is very good to the non-linear response. Due the discrepancy between the nominal and actual value of the lateral acceleration, regenerative braking torque is controlled by VDC as shown in Figure E.2. Both vehicles brake at almost the same time and the lateral path deviation is negligible for both cases.

E.2 VDC Performance Validation on Integrated Braking System (Regenerative Braking & ABS)

Double Lane Change Braking Simulation @ 90 KPH; μ=0.85
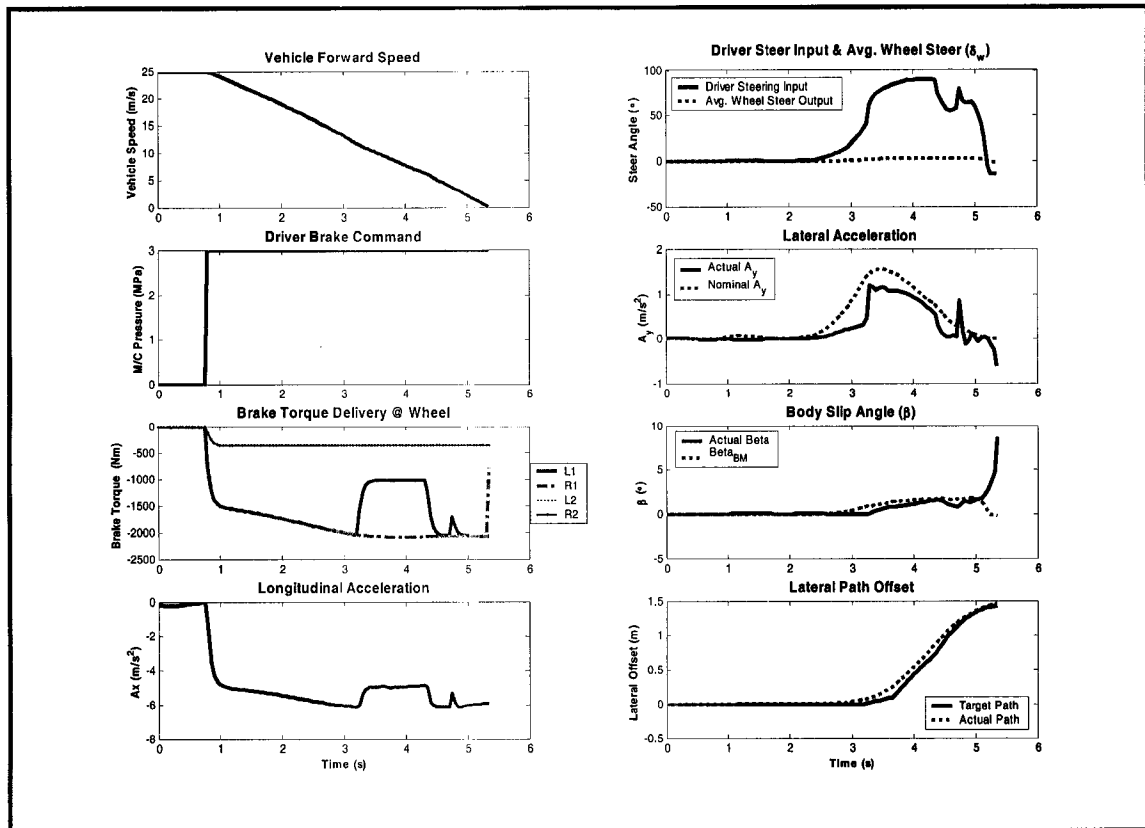
DLX Braking without VDC Control

Figure E.3 DLX braking (REGEN+ABS) without VDC Control @ 90 KPH; μ=0.85

With the additional hydraulic braking torque the vehicle stops much quicker than the case with only regenerative braking. The bicycle model estimates the prototype response very closely.
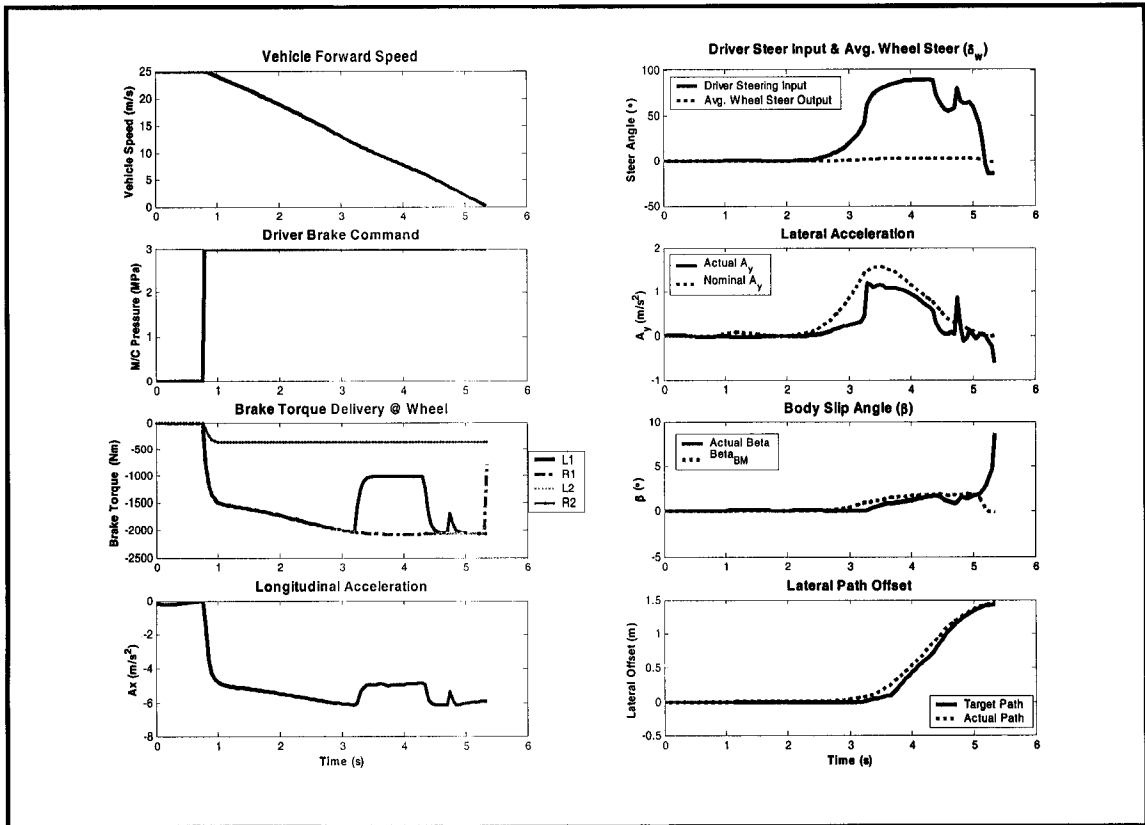
140

DLX Braking with VDC Control

Figure E.4 DLX braking (REGEN+ABS) with VDC Control @ 90 KPH; μ=0.85

No VDC control is provided in this operation since the vehicle response is stable for the

bicycle model estimation which is close to the actual prototype vehicle response.

141

VITA AUCTORIS

Name: Edward Won Kyun Oh

Date of Birth: May 6, 1978

Place of Birth: Nairobi Hospital, Nairobi, Kenya

Education:

2003 – 2005 University of Windsor; Windsor, Ontario, Canada

Master of Applied Science in Mechanical Engineering

1998 - 2002 Queen's University; Kingston, Ontario, Canada

Bachelor of Science in Mechanical Engineering

1994 – 1998 Bayview Secondary School; Richmond Hill, Ontario, Canada

1994 Yong San High School; Seoul, Korea

1991 – 1994 Dae Chung Middle School; Seoul, Korea

1985 – 1991 Sang Myung Elementary School; Seoul, Korea

Employment:

2002 – 2003 Halla Climate Control Canada Inc.; Belleville, Ontario, Canada

Product Development Engineer